ABSTRACT

BOOSTED SPATIAL AND TEMPORAL PRECISION IN FUNCTIONAL BRAIN IMAGING VIA MULTIMODAL ANALYSIS

by
Yaroslav Halchenko

Localizing neuronal activity in the brain, both in time and in space, is a central challenge to progress in understanding brain function. Non-invasive functional brain imaging has become an important tool used by neurophysiologists, cognitive psychologists, cognitive scientists, and other researchers interested in brain function. In the last five decades the technology of non-invasive functional imaging has flowered, and researchers today can choose from EEG, MEG, PET, SPECT, MRI, and fMRI. Each method has its own strengths and weaknesses, and no single method is best suited for all experimental or clinical conditions. EEG and MEG each provide data with high temporal resolution (measured in milliseconds), but limited spatial resolution. In contrast, fMRI provides good spatial but relatively poor temporal resolution.

Because of the inadequacies of individual techniques, there is increased interest in finding ways to combine existing techniques in order to synthesize the strengths inherent in each. Number of techniques refining EEG and MEG analysis by exploring the data from MR modalities (MRI, fMRI) has been developed in order to increase localization *precision*. Demonstrated localization *accuracy* remains a distant goal confounded by the lack of ground truth in any realistic experimental multimodal protocol and the lack of a complete model of the BOLD signal.

The goal of this dissertation is to show that it is possible to obtain reliable estimates of neuronal activity at superior spatio-temporal resolution by combining EEG/MEG with fMRI data whenever forward models of the signals are appropriate to describe the data in terms of underlying neuronal processes. The proposal surveys various aspects of uni- and multimodal imaging, discusses obstacles confronted with on the way to reliable multimodal methods, proposes novel approaches for multimodal imaging, describes a chosen neuroimaging problem to persuade with the suggested methods, and, finally, presents preliminary results on the simulated data.

BOOSTED SPATIAL AND TEMPORAL PRECISION IN FUNCTIONAL BRAIN IMAGING VIA MULTIMODAL ANALYSIS

by
Yaroslav Halchenko

A Dissertation Proposal
Presented to the Faculty of
New Jersey Institute of Technology and
Rutgers, The State University of New Jersey – Newark
in Partial Fulfillment of the Requirements for the Degree of
Doctor of Philosophy in Computer Science

Department of Computer Science

September 2005

APPROVAL PAGE

BOOSTED SPATIAL AND TEMPORAL PRECISION IN FUNCTIONAL BRAIN IMAGING VIA MULTIMODAL ANALYSIS

Yaroslav Halchenko

Dr. Jason T. L. Wang, Dissertation Advisor — Date
Professor, Computer Science Department, NJIT

Dr. Stephen J. Hanson, Committee Member — Date
Professor and Chair of Psychology Department, Rutgers-Newark

Dr. Eliza Michalopoulou, Committee Member — Date
Associate Professor, Mathematical Sciences and Electrical and Computer Engineering Departments, NJIT

Dr. David Nassimi, Committee Member — Date
Associate Professor, Computer Science Department, NJIT

Dr. Chengjun Liu, Committee Member — Date
Assistant Professor, Computer Science Department, NJIT

BIOGRAPHICAL SKETCH

Author: Yaroslav Halchenko

Date: September 2005

Date of Birth: August 13, 1977

Place of Birth: Omsk, Russian Federation

Undergraduate and Graduate Education:

- Master of Science in Computer Science,
  University of New Mexico, Albuquerque, NM, USA, 2002
- Master of Science in Laser and Optoelectronic Engineering,
  Vinnytsya State University, Vinnytsya, Ukraine, 1999
- Bachelor's Degree in Laser and Optoelectronic Engineering,
  Vinnytsya State University, Vinnytsya, Ukraine, 1998

Major: Computer Science

Presentations and Publications:

[1] Yaroslav O. Halchenko, Stephen José Hanson, and Barak A. Pearlmutter. *Advanced Image Processing in Magnetic Resonance Imaging*, chapter Multimodal Integration: fMRI, MRI, EEG, MEG. Dekker, 2005. In Press.

[2] Stephen José Hanson, T. Matsuka, C. Hanson, D. Rebbechi, Yaroslav O. Halchenko, A. Zaimi, and Barak A. Pearlmutter. Structural equation modeling of neuroimaging data: Exhaustive search and markov chain monte carlo. In *Human Brain Mapping*, 2004.

[3] Yaroslav O. Halchenko, Stephen José Hanson, and Barak A. Pearlmutter. Fusion of functional brain imaging modalities using l-norms signal reconstruction. In *Proceedings of the Annual Meeting of the Cognitive Neuroscience Society*, San Francisco, CA, 2004.

[4] Yaroslav O. Halchenko, Barak A. Pearlmutter, Stephen José Hanson, and Adi Zaimi. Fusion of functional brain imaging modalities via linear programming. *Biomedizinische Technik (Biomedical Engineering)*, 48(2):102–104, 2004.

[5] Leonid I. Timchenko, Yuri F. Kutaev, Alexander A. Gertsiy, Yaroslav O. Halchenko, Lubov V. Zahoruiko, and Tamer Mansur. Method for image coordinate definition on extended laser paths. volume 4148, pages 19–26. SPIE, 2000.

[6] Leonid I. Timchenko, Yuri F. Kutaev, Alexander A. Gertsiy, Lubov V. Zahoruiko, Yaroslav O. Halchenko, and Tamer Mansur. Approach to parallel-hierarchical network learning for real-time image sequence recognition. volume 3836, pages 71–81. SPIE, 1999.

[7] Leonid I. Timchenko, A. A. Gertsiy, L. V. Zahoruiko, Y. F. Kutaev, and Yaroslav O. Halchenko. Pre-processing of extended laser path images. In *Industrial Lasers and Inspection: Diagnostic Imaging Technologies and Industrial Applications*, Munich, Germany, June 1999. EOS/SPIE International Symposium. [3827-26].

[8] Leonid I. Tymchenko, Janina Scorukova, Serhij Markov, and Yaroslav O. Halchenko. Image segmentation on the basis of spatial connected features. In *Visnyk VSTU*, volume 4, pages 39–43. VSTU University Press, Vinnytsya, Ukraine, 1998. in Ukrainian.

[9] T. B. Martinyuk, A. V. Kogemiako, and Yaroslav O. Halchenko. The model of associative processor for numerical data sorting. In *Visnyk VSTU*, volume 2, pages 19–23. VSTU University Press, Vinnytsya, Ukraine, 1997. in Ukrainian.

[10] Leonid I. Tymchenko, Janina Scorukova, Jurij Kutaev, Serhij Markov, Tatiana Martynuk, and Yaroslav O. Halchenko. Method spatial connected segmentation of images. In *The Third All-Ukrainian International Conference Ukrobraz*, Kijiv, Ukraine, November 1996. in Ukrainian.

LIST OF SYMBOLS

Abbreviations

Abbreviation	Meaning
BEM	Boundary Elements Method
BMA	Bayesian Model Averaging
BOLD	Blood Oxygenation Level Dependent
DC	Direct Current
DECD	Distributed ECD
ECD	Equivalent Current Dipole
EEG	ElectroEncephaloGraphy
EIT	Electrical Impedance Tomography
EMF	ElectroMotive Force
E/MEG	EEG and/or MEG
EM	Expectation Maximization
EMSI	ElectroMagnetic Source Imaging
EPI	Echo Planar Imaging
ERF	Event Related Field
ERP	Event Related Potential
FDM	Finite Difference Method
FEM	Finite Elements Method
FMRI	Functional MRI
HR	Hemodynamic Response
HRF	HR Function
ICA	Independent Component Analysis
LCMV	Linearly Constrained Minimum Variance
LP	Linear Programming
LTIS	Linear Time Invariant System
MAP	Maximum a Posteriori
MCMC	Monte Carlo Markov Chain
MEG	MagnetoEncephaloGraphy
MR	Magnetic Resonance
MRI	MR Imaging
NIRS	Near-infrared Spectroscopy
NMR	Nuclear Magnetic Resonance
PCA	Principal Component Analysis
PD	Proton Density Imaging
PDF	Probability Density Function
PET	Positron Emission Tomography
PLS	Partial Least-Squares
ROI	Region of Interest
SNR	Signal-to-Noise Ratio
SOBI	Second Order Blind Identification
SPECT	Single Photon Emission Computed Tomography
SQUID	Superconducting QUantum Interference Device

NOTATION AND TERMINOLOGY (Continued)

Symbols

Symbol	Meaning
K	Number of simultaneously active voxels
N	Number of voxels, *i.e.* spatial resolution of high spatial resolution modality (fMRI)
M	Number of EEG/MEG sensors, *i.e.* spatial resolution of low spatial resolution modality
T	Number of time points of high temporal resolution modality (EEG, MEG)
U	Number of time points of low temporal resolution modality (fMRI)
L	Number of orthogonal axes for dipole moment components, $L \in \{1, 2, 3\}$
$\mathbf{I}_n$	Identity matrix ($n \times n$)
$\mathbf{0}$	Zero matrix of appropriate dimensionality
$\mathbf{X}$	General E/MEG data matrix; can contain EEG or/and MEG data ($M \times T$)
$\mathbf{F}$	BOLD fMRI data matrix ($N \times U$)
$\mathbf{Q}$	General dipole sources matrix ($LN \times T$)
$\tilde{\mathbf{Q}}$	Dipole sources strength matrix ($N \times T$)
$\mathbf{\Theta}$	Dipole sources orientation matrix ($LN \times T$)
$\mathbf{X}_{\cdot,i}$	i-th column of $\mathbf{X}$
$\mathbf{X}_{i,\cdot}$	i-th row of $\mathbf{X}$
$\mathcal{G}$	General E/MEG lead function, incorporating information for EEG or/and MEG
$\mathbf{G}$	General E/MEG lead matrix
$\mathbf{F}^i$	Spatial filter matrix for the i-th dipole ($M \times L$)
ν	Variance
σ	Deviation
$\mathbf{C}$	Covariance matrix
$\mathbf{K}$	Matrix of correlation coefficients

Functions

Symbol	Meaning
$\mathbf{M}^\top$	Matrix transpose
$\mathbf{M}^+$	Generalized matrix inverse (pseudo-inverse)
$\operatorname{null}\mathbf{M}$	The *null space* of $\mathbf{M}$, the set of vectors $\{\mathbf{x} \mid \mathbf{M}\mathbf{x} = 0\}$
$\operatorname{diag}\mathbf{M}$	The diagonal matrix with the same diagonal elements as $\mathbf{M}$
$\operatorname{sign}(x)$	Sign of x: -1 for negative values, 1 otherwise
$\otimes$	Kronecker product, $\mathbf{A} \otimes \mathbf{B} \equiv \begin{bmatrix} a_{00}B & \dots \\ \vdots & \ddots \end{bmatrix}$

TABLE OF CONTENTS

TABLE OF CONTENTS
(Continued)

LIST OF FIGURES

INTRODUCTION

A great challenge in any research of brain functioning is to have non-invasive[1] means to asses the characteristics of neuro-physiological processes inside the brain at a fine temporal and spatial resolution. Miscellaneous assumptions of the nature of neuronal signals let neuronal activity to be measured and modeled as biomedical signals which can be registered by several types of non-invasive brain imaging techniques such as electroencephalography (EEG), magnetoencephalography (MEG), nuclear magnetic resonance (NMR) imaging (MRI)[2], positron emission tomography (PET), near-infrared spectroscopy (NIRS), and others.

All of the mentioned modalities could be brought into two categories: passive and active. Passive methods (EEG and MEG) try to register changes in the ambient environment which are caused by neuronal processes inside the brain. Active methods (such as MRI, PET and NIRS) create a controllable environment which changes under underlying neuronal and possibly other related physiological processes. Therefore most of the time they do not capture results of neuronal activity directly, but rather register changes caused by it, *e.g.* consumption of the contrast agents, blood oxygenation or change of blood flow. Captured brain signals by either passive or active modalities are usually non-stationary signals distorted by noise and interferences. Moreover they possess characteristics specific to the technique (modality) used to acquire it, so it is crucial to have a clear understanding of their nature to perform advanced signal analysis.

EEG has been widely used in research and clinical studies since the mid-twentieth century. Although Richard Caton (1842–1926) is believed to have been the first to record the spontaneous electrical activity of the brain, the term EEG first appeared in 1929 when Hans Berger, a psychiatrist working in Jena, Germany, announced to the world that “it was possible to record the feeble electric currents generated on the brain, without opening the skull, and to depict them graphically onto a strip of paper.” The first SQUID-based MEG experiment with a human subject was conducted at MIT by Cohen [31] after his successful application of Zimmerman’s SQUID sensors to acquire a magneto-cardiogram in 1969. EEG and MEG are closely related due to electro-magnetic coupling, and term E/MEG will be used to refer generically to either EEG, MEG, or both altogether. Although EEG and MEG are related, there are

[1] From WordNet (r) 2.0 (August 2003) [wn]: noninvasive adj : relating to a technique that does not involve puncturing the skin or entering a body cavity [ant: invasive]

[2] The term MRI generally substituted NMR so that the public could more easily adopt a term for an imaging modality without the word ”nuclear” in it

some subtle differences which will be outlined further in the text. Both E/MEG provide high temporal resolution (measured in milliseconds) but have a major limitation: the location of neuronal activity can be hard to pin-point with confidence. That is because such modalities acquire data which is created as a super-imposition of electromagnetic fields outside of the head which were caused by the brain signals; therefore in order to obtain characteristics of the original neuronal activations the inverse problem has to be solved. Localization of neural activity from E/MEG data is usually called as *electromagnetic source imaging* (EMSI) and has been a challenging area of research for the last couple decades.

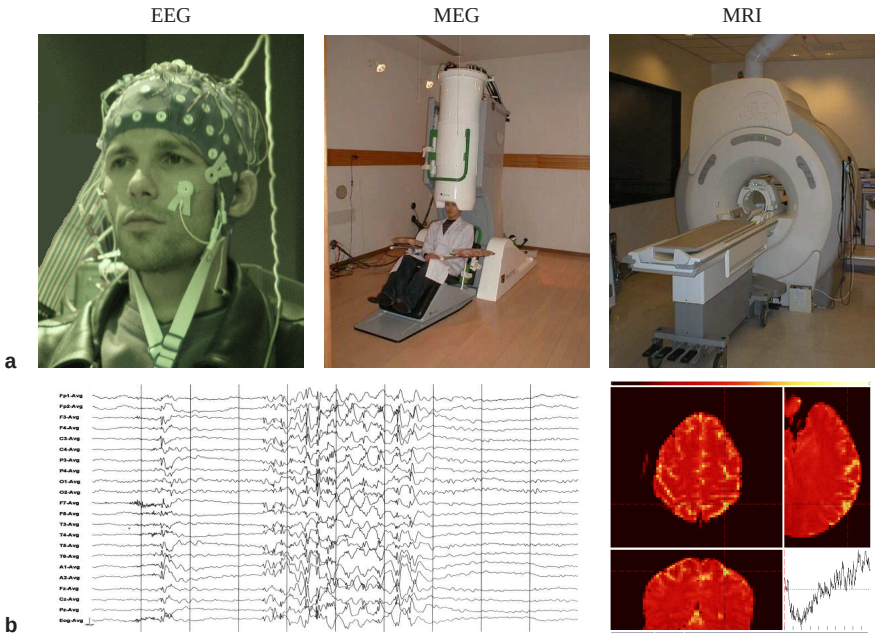

Figure 1 Non-invasive functional brain imaging equipment: from simple EEG to expensive MR. **a.** Equipment **b.** Typical Data

Opposed to E/MEG, MRI modality has a natural capability to provide *in vivo* view on brain structure and function. Nuclear Magnetic Resonance (NMR) was independently discovered by Felix Bloch and Edward Purcell in 1946, so they both received a Nobel Prize in Physics in 1952. Only in 1970, Raymond Damidian discovered that the structure and abundance of water in the human body is the key to MR imaging (MRI). It was Paul Lauterbur in 1973, however, who implemented the concept of tri-plane

gradients used for exciting selective areas of the body (Gx, Gy, and Gz). P. Lauterbur along with Peter Mansfield were awarded a Nobel Prize in Physiology or Medicine in 2003 for the invention of MRI, which made a huge impact on medical imaging.

Since the invention time, MRI techniques evolved. Nowadays image intensity observed in MR images can be determined by various tissue contrast mechanisms such as proton density, T1 and T2 relaxation rates, diffusive processes of proton spin dephasing, loss of proton phase coherence due to tissue magnetic susceptibility variations. Although MRI is capable of detecting transient or subtle changes in the magnetic field in the cortical tissue caused by neuronal activation [19, 196], direct application of MRI to capture functional activity remains limited due to a very low signal-to-noise ratio (SNR) which is why MRI is often labelled *anatomical*. Its applicability for functional studies was not revealed for a while.

It was toward the end of the 19th century, when Charles Roy and Charles Sherrington [151] provided the first evidence supporting the connection between neuronal activity and cerebral blood flow. In 100 years, after MRI technique had received much of appreciation for anatomical studies, Ogawa et al. [136] showed that MRI can reflect blood deoxygenation using T2*contrast. Such finding laid down a framework for functional brain imaging using MRI [17, 137, 150] by capturing blood oxygenation level-dependent (BOLD) signal without necessity to use any reactive agents, thus making functional MRI (fMRI) the first truly non-invasive functional brain imaging modality which bears rich spatial information. Due to the deliberateness of the hemodynamics in comparison to the neuronal activation time course, BOLD fMRI time resolution is coarse but acceptable for many types of studies.

Problem Statement

Any single technology mentioned above is yet to become the best choice for all functional brain imaging necessities. High temporal resolution of E/MEG modalities is crucial in many event-related experiments and it cannot be achieved using BOLD fMRI, which delivers superior spatial resolution, which, in turn, cannot be reliably achieved using E/MEG. Therefore it is beneficial to have methodology that consolidate the information obtained from different brain imaging modalities. Such information integration is hoped to provide consistent and reliable localization of the neuronal activity with higher spatial and temporal precision that cannot be achieved using any of the existing modalities alone.

The main obstacle in the development of multimodal methods involving fMRI nowadays seems to be the absence of a universal model for hemodynamics, where the neuronal activation is the primary

input factor. Simplistic models can be used in particular instances of multimodal analysis where they are supported by the empirical evidence from simple experiments.

Due to the difficulties in assessing ground truth of a combined signal in any realistic experiment—a difficulty further confounded by lack of accurate biophysical models of BOLD signal, any fusion problem has to be tackled with caution. Reported progress on simple experiments where there is a small number of isolated focal sources of activity which are consistently present in all relevant modalities, and phantom studies can already provide basic test-ground to check the validity of the developed fusion methods.

To summarize, now it seems to be the right time for the development of fusion methods which are comprising empirically supported models or are flexible enough to incorporate future elaborated models of the BOLD response. A convincing demonstration of increased accuracy using multimodal integration for a complex protocol would constitute a major success in the field.

Objectives and Scope of the Work

The current work addresses the problem stated: development and validation of a multimodal functional brain imaging technique to gain intrinsic advantages of each used modality. Brain imaging experiment (motor somatotopy) is chosen to comply with the requirements for multimodal analysis which is formalized in the thesis. In the present work few different means to perform multidimensional regression to merge signals from E/MEG and fMRI are approached (non-linear optimization, Linear Programming, Sylvester equation solvers). Further, the technical and methodological difficulties of fusing heterogeneous signals are highlighted and explored. At the end, the hope is that *correct fusion* of multimodal data will allow previously inaccessible spatiotemporal structures to be visualized and formalized and thus eventually become a useful tool in brain imaging research.

Organization

Due to the fact, that source localization techniques used in EMSI served as a starting point for subsequent multimodal analysis, the initial focus concerns reviewing mathematical approaches for solving the localization problem in E/MEG. Thus, Chapter 1 highlights popular methods, formulates canonical problems of E/MEG source localization, and describes how they have been attacked by various researchers.

In order to obtain multimodal data, is it important to keep in mind obstacles on the way to perform truly multimodal experiment. Chapter 2 addresses the problems which are inherent in concurrent multimodal experiments due to the interference between signal acquisition technologies used in E/MEG and MRI.

Chapter 3 covers existing brain imaging techniques which employ multiple modalities. The review starts with the description of benefits achieved by using anatomical MR modalities which do not carry any functional (temporal) information but nevertheless crucial in the fusion process due to their high spatial resolution. In particular, it is discussed how anatomical MRI can be combined with existing EMSI techniques in order to increase the localization *precision* without introducing any additional functional information. Then, the most recent and promising ways in which these signals can be combined with fMRI are documented. Specifically, attention is paid to correlative analysis, decomposition techniques, equivalent dipole fitting, distributed sources modeling, beamforming, and Bayesian methods.

Limited knowledge of BOLD fMRI signal restricts the set of brain imaging experiments which can be successfully and reliably analyzed using multimodal methods. Chapter 4 motivates and presents the choice of suitable brain imaging experiment, which is suggested to be used as a validation of the introduced multimodal methods, which are presented in Chapter 5. To verify plausibility of the new suggested methods, they are probated on the simulated data with known characteristics. Chapter 6 overviews details of the simulated dataset generation and discusses analysis results using new and some existing multimodal imaging methods.

Finally, Chapter 7 gives a brief conclusion and drafts a plan of future research to further support the thesis and complete this dissertation. Throughout the manuscript a consistent and complete set of mathematical formulations that are stand alone is provided, together with appropriate context for this notation into existing literature.

CHAPTER 1

UNIMODAL SOURCE LOCALIZATION

The goal of physicists is to find a use for every branch of mathematics. The goal of mathematicians is to invent a new field of mathematics that has absolutely no practical use

– Unknown Professor

fMRI became a very popular tool for brain imaging due to its high spatial resolution. A vast amount of methods has been developed to achieve reliable spatial localization of neuronal activity, or to be exact, of its secondary effects such as blood flow (perfusion) or oxygenation (see [98] for the review of existing methods). In turn, E/MEG signals have no definite solution to gain reliable spatial localization. Therefore following section covers the specifics of E/MEG signals, the premises for conjoint E/MEG analysis, and the EMSI techniques which have been adopted later for use in multimodal analysis with fMRI data.

1.1 EEG and MEG: Specifics

The theory of electromagnetism and Maxwell's equations, under the assumption of quasi-stationarity[1], theoretically defines the relationship between observed magnetic and electric fields induced by the ionic currents generated inside the brain (see [113, 127, 138] for more information about the biophysics of E/MEG signals).

The similar nature of the EEG and MEG signals means that many methods of data analysis are applicable to both E/MEG modalities. Although the SNR of E/MEG signals have improved with technological advances, and some basic analysis has been performed by experts on raw E/MEG data via visual inspection of spatial signal patterns outside of the brain, more advanced methods are required to use data efficiently. During the last two decades many E/MEG signal analysis techniques [121] have been developed in order to provide insights on different levels of perceptual and cognitive processing of human brain: ERP (event related potential) in EEG and ERF (event related field) in MEG, components analysis (PCA, ICA, *etc.*), frequency domain analysis, pattern analysis, and single-trial analysis to name the few [83, 173, 175], *etc.* Source localization techniques were first developed for MEG because the head model

[1] A signal is quasistatic if it does not change its parameters in time. The non-stationary term present in the E/MEG physical model is relatively small and can be considered zero in the range of signal frequencies which are captured by E/MEG. See [64] for a more detailed description.

required for forward modeling of magnetic field is relatively simple. Source localization using an EEG signal has been difficult to perform since the forward propagation of the electric potentials is more complicated. However, recent advances in automatic MRI segmentation methods together with advances in forward and inverse EEG modeling, have made EEG source localization plausible.

The theory of electromagnetism also explains why EEG and MEG signals can be considered complementary, in that they provide different views on often the same physiological phenomenon [32, 64, 113, 194]. On one hand, often accented difference is that MEG is not capable of registering the magnetic field generated by the sources that are oriented radially to the skull surface in the case of spherical conductor geometry. On the other hand, MEG has the advantage over EEG in that the local variations in conductivity of different brain matter (*e.g.* white matter, gray matter) do not attenuate the MEG signal much, whereas the EEG signal is strongly influenced by the variations in conductivities of different types of brain matter and of the skull in particular [138]. The orientation selectivity, combined with the higher depth precision due to homogeneity, make MEG optimal for detecting activity in sulci (brain fissures) rather than in gyri (brain ridges). In contrast, a registered EEG signal is dominated by the gyral sources close to the skull and therefore more radial to its surface. Yet another crucial difference is dictated by basic physics. The orthogonality of magnetic and electrical fields leads to orthogonal maps of the magnetic field and electrical potential on the scalp surface. This orthogonality means that an orthogonal localization direction is the best localization direction for both modalities [32, 114]. These complementary features of the EEG and MEG signals are what make them good candidates for integration [12, 38]. The conjoint E/MEG analysis has improved the fidelity of EMSI localization, but has not entirely solved the problem of source localization ambiguity. It is the reduction of this remaining ambiguity where information from other brain imaging modalities may play a valuable role.

It is worth noting another purely technical advantage of MEG over EEG: MEG provides a reference-free recording of the actual magnetic field. Whenever EEG sensors capture scalp potentials, a reference electrode must be used as a ground to derive the signal of interest. A reference signal chosen in such a way can be arbitrarily biased relative to the EEG signal observed even when no neuronal sources are active. The unknown in an MEG signal obtained using SQUID sensors, is just a constant in time offset—the DC baseline. This baseline depends on the nearest flux quantum for which the flux-locked loop acquired lock [187, pg. 265]. Although the choice of a reference value in EEG and the DC line in MEG do not influence the analysis of potential/field topographic maps, they do impact inverse solution algorithms which assume

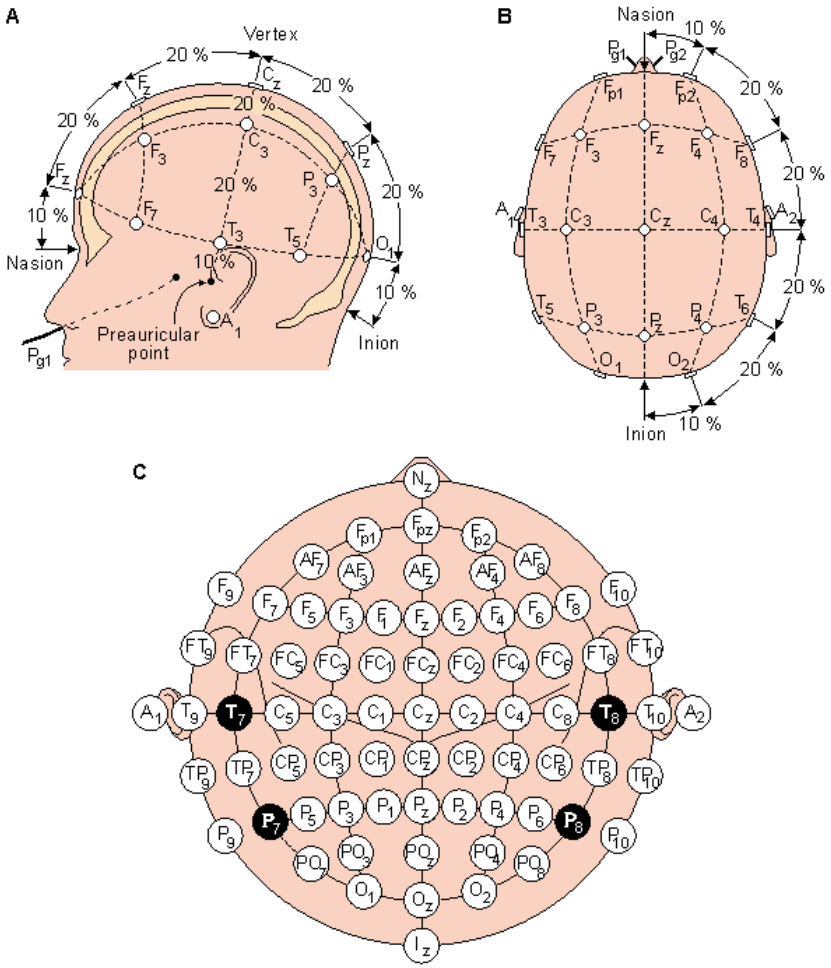

Figure 1.1 The international 10-20 EEG system seen from (A) left and (B) above the head. A = Ear lobe, C = central, Pg = nasopharyngeal, P = parietal, F = frontal, Fp = frontal polar, O = occipital. (C) Location and nomenclature of the intermediate 10% electrodes, as standardized by the American Electroencephalographic Society. (Borrowed with permission from [113])

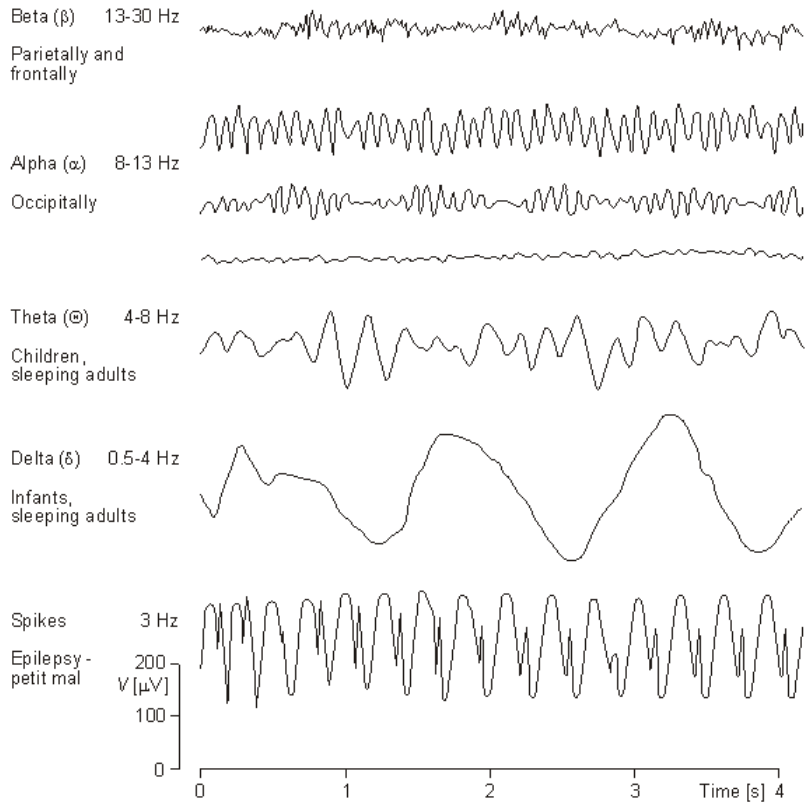

Figure 1.2 From the EEG signal it is possible to differentiate alpha (a), beta (b), delta (d), and theta (Q) waves as well as spikes associated with epilepsy. (Borrowed with permission from [113])

zero net source in the head, *i.e.* zero baseline. In general, the simple average reference across the electrodes is used and it has been shown to be a good approximation to the true reference signal [121, sec. 2.2].

Even if the reference value (baseline) is chosen correctly, both conventional EEG and MEG face obstacles in measuring the slowly changing DC component of the signal in the low frequency range ($f < 0.1\,\mathrm{Hz}$). In the case of EEG the problem is due to the often used coupling of the electrodes via capacitors, so that any DC component (slowly changing bias) of the EEG signal is filtered out. That leaves the researcher with non-zero frequency components of the signal, which often correspond to the most informative part of the signal as in the case of conventional ERP or frequency domain analysis. The DC-EEG component can be registered by using sensors with direct coupling and special scalp electrodes that are gel filled to eliminate changes of electrical impedance at the electrode-skin interface which can cause low frequency noise in the EEG signal. Although the MEG system does not require direct contact between sensors and skin, it is nevertheless subject to $1/f$ sensor noise which interferes with the measurement of the neuronal DC fields. In the last decade DC-MEG has been methodically refined by employing controlled brain-to-sensor modulation allowing the monitoring of low-frequency magnetic fields. Formalized DC-E/MEG techniques make it possible to perform E/MEG studies, which rely on the shift of DC and low frequency components of the signal; components that occur, for example, during epileptic seizures, hyperventilation, changes in vigilance states, cognitive or motor tasks.

1.2 Forward Modeling

The analysis of E/MEG signals often relies on the solution of two related problems. The *forward problem* concerns the calculation of scalp potentials (EEG) or magnetic fields near the scalp (MEG) given the neuronal currents in the brain, whereas the *inverse problem* involves estimating neuronal currents from the observed E/MEG data. The difficulty of solving the forward problem is reflected in the diversity of approaches that have been tried (see [125] for an overview and unified analysis of different methods).

The basic question posed by both the inverse and forward problems is how to model any neuronal activation so that the source of the electromagnetic field can be mapped onto the observed E/MEG signal. Assuming that localized and synchronized primary currents are the generators of the observed E/MEG signals, the most successful approach is to model the i-th source with a simple Equivalent Current Dipole (ECD) $\mathbf{q}_i$ [24], uniquely defined by three factors: location represented by the vector $\mathbf{r}_i$, strength q_i, and orientation coefficients θ_i. The orientation coefficient is defined by projections of the vector $\mathbf{q}_i$ into

L orthogonal Cartesian axes: $\theta_i = \mathbf{q}_i/q_i$. However, the orientation coefficient may be expressed by projections in two axes in the case of a MEG spherical model where the silent radial to the skull component has been removed, or even, just in a single axis if normality to the cortical surface is assumed. The ECD model made it possible to derive a tractable physical model linking neuronal activation and observed E/MEG signals. In case of K simultaneously active sources at time t the observed E/MEG signal at the sensor $\mathbf{x}_j$ positioned at $\mathbf{p}_j$ can be modeled as

$$\hat{\mathbf{x}}_j(\mathbf{r}_i, \mathbf{q}_i, t) = \sum_{i}^{K} \mathcal{G}(\mathbf{r}_i(t), \mathbf{p}_j) \cdot \mathbf{q}_i(t) + \epsilon, \tag{1.1}$$

where $\mathcal{G}$ is a *lead field* function which relates the i-th dipole and the potential (EEG) or magnetic field (MEG) observed at the j-th sensor; and ϵ is the sensor noise. In the given formulation, function $\mathcal{G}(\mathbf{r}_i(t), \mathbf{p}_j)$ returns a vector, where each element corresponds to the lead coefficient at the location $\mathbf{p}_j$ generated by a unit-strength dipole at position $\mathbf{r}_i(t)$ with the same orientation as the corresponding projection axis of θ_i. The inner-product between the returned vector and dipole strength projections on the same coordinate axes yields a j-th sensor the measurement generated by the i-th dipole.

The forward model (1.1) can be solved at substantial computational expense using available numerical methods [147] in combination with realistic structural information obtained from the MRI data (see Section 3.1). This high computational cost is acceptable when the forward model has to be computed once per subject and for a fixed number of dipole locations, but it can be prohibitive for dipole fitting, which requires a recomputation of the forward model for each step of non-linear optimization. For this reason, rough approximations of the head geometry and structure are often used: *e.g.* best-fit single sphere model which has a direct analytical solution [199] or the multiple spheres model to accommodate for the difference in conductivity parameters across different tissues. Recently proposed MEG forward modeling methods for realistic isotropic volume conductors [132, 133] are more accurate and faster than BEM, and hence may be useful substitutes for both crude analytical methods and computationally intensive finite-element numeric approximations. Generally, the solution of the forward problem is crucial for performing source localization using E/MEG, which is the main topic of the next section.

1.3 The Inverse Problem

1.3.1 Equivalent Current Dipole Models

The E/MEG inverse problem is very challenging (see [13, 64] for an overview of methods.) First, it relies on the solution of the forward problem, which can be computationally expensive, especially in the case of realistic head modeling. Second, the lead-field function $\mathcal{G}$ from (1.1) is non-linear in $\mathbf{r}_i$, so that the forward model depends non-linearly on the locations of activations. It is because of this nonlinearity that the inverse problem is generally treated by non-linear optimization methods, which can lead to solutions being trapped in local minima. In case of Gaussian sensor noise, the best estimator for the reconstruction quality of the signal is the squared error between the obtained and modeled E/MEG data:

$$\mathcal{E}(\mathbf{r},\mathbf{q}) = \sum_{i}^{K}\sum_{t=t_1}^{t_2}\sum_{j}^{M}\big(\mathbf{x}_j(t) - \hat{\mathbf{x}}_j(\mathbf{r}_i,\mathbf{q}_i,t)\big)^2 + \lambda\mathcal{C}(\mathbf{r},\mathbf{q}), \tag{1.2}$$

where $\mathcal{C}(\mathbf{r},\mathbf{q}) > 0$ is often introduced to regularize the solution, *i.e.* to obtain the desired features of the estimated signal (*e.g.* smoothness in time, or in space, lowest energy or dispersion), and $\lambda > 0$ is used to vary the trade-off between the goodness of fit and the regularization term.

This least-squares model can be applied to the individual time-points ($t_1 = t_2$) ("moving dipole" model) or to a block ($t_1 < t_2$) of data points. If the sources are assumed not to change during the block (t_1,t_2), then the solution with time constant $\mathbf{q}_i(t) = \mathbf{q}_i$ is the target.

Other features derived from the data besides pure E/MEG signals as the argument $\mathbf{x}$ of (1.1) and (1.2) are often used: *e.g.* ERP/ERF waveforms which represent averaged E/MEG signals across multiple trials, mean map in the case of stable potential/field topography during some period of time, or signal frequency components to localize the sources of the oscillations of interest.

Depending on the treatment of (1.2), the inverse problem can be presented in a couple of different ways. The brute-force minimization of (1.2) in respect to both parameters $\mathbf{r}$ and $\mathbf{q}$, and the consideration of different K neuronal sources, is generally called *ECD fitting*. Because of non-linear optimization, this approach works only for cases where there is a relatively small number of sources K, and therefore the inverse problem formulation is over-determined, *i.e.* (1.1) cannot be solved exactly ($\mathcal{E}(\mathbf{r},\mathbf{q}) > 0$). If fixed time locations of the target dipoles can be assumed, the search space of non-linear optimization is reduced and the optimization can be split into two steps: (a) non-linear optimization to find locations of the dipoles, and then (b) analysis to determine the strength of the dipoles. This assumption constitutes the so-called *spatiotemporal ECD model*.

Two other frameworks have been suggested as means of avoiding the pitfalls associated with non-linear optimization: Distributed ECD (DECD) and beamforming. These two approaches are presented in detail in the next sections.

1.3.2 Linear Inverse Methods: Distributed ECD

In case of multiple simultaneously active sources, an alternative to solving the inverse problem by ECD fitting is a distributed source model. The label Distributed ECD (DECD) will be used further in the text to refer to this type of model. The DECD is based on a spatial sampling of the brain volume and distributing the dipoles across all plausible and spatially small areas, which could be a source of neuronal activation. In such cases, fixed locations ($\mathbf{r}_i$) are available for each source/dipole, removing the necessity of non-linear optimization as in the case of the ECD fitting. The forward model (1.1) can be presented for a noiseless case in the matrix form

$$\mathbf{X} = \mathbf{G}\mathbf{Q}, \tag{1.3}$$

where $\mathbf{G}$, $M\times LN$ *lead field* matrix, is assumed to be static in time. The j,i-th entry of $\mathbf{G}$ describes how much a sensor j is influenced by a dipole i, where j varies over all sensors while i varies over every possible source, or to be more specific, every axis-aligned component of every possible source: $g_{j\bar{\imath}} = \mathcal{G}(\mathbf{r}_i,\mathbf{p}_j)$. The vector $\bar{\imath}$ contains indices of L such projections, *i.e.* $\bar{\imath} = [i, i+N, i+2N]$ when $L = 3$, and $\bar{\imath} = i$ when the dipole has a fixed known orientation. Using this notation, $\mathbf{G}_{\cdot,\bar{\imath}}$ corresponds to the lead matrix for a single dipole $\mathbf{q}_i$. The $M\times T$ matrix $\mathbf{X}$ holds the E/MEG data, while the $LN\times T$ matrix $\mathbf{Q}$ (note that $\mathbf{Q}_{\bar{\imath}t} = \mathbf{q}_i(t)$) corresponds to the projections of the ECD's moment onto L orthogonal axes.

The solution of (1.3) relies on finding an inverse $\mathbf{G}^+$ of the matrix $\mathbf{G}$ to express the estimate $\hat{\mathbf{Q}}$ in terms of $\mathbf{X}$

$$\hat{\mathbf{Q}} = \mathbf{G}^+\mathbf{X}, \tag{1.4}$$

and will produce a linear map $\mathbf{X} \longmapsto \hat{\mathbf{Q}}$. Other than being computationally convenient, there is not much reason to take this approach. The task is to minimize the error function (1.2), which can be generalized by the weighting of the data to account for the sensor noise and its covariance structure:

$$\mathcal{E}(\mathbf{Q}) = \mathrm{tr}\big((\mathbf{X}-\mathbf{G}\mathbf{Q})^\top\mathbf{W}_{\mathbf{X}}^{-1}(\mathbf{X}-\mathbf{G}\mathbf{Q})\big), \tag{1.5}$$

where $\mathbf{W}_{\mathbf{X}}^{-1}$ is a weighting matrix in sensor space.

A zero-mean Gaussian signal can be characterized by the single covariance matrix $\mathbf{C}_\epsilon$. In case of a non-singular $\mathbf{C}_\epsilon$ the most simple weighting scheme $\mathbf{W}_\mathbf{X} = \mathbf{C}_\epsilon$ can be used to account for non-uniform and possibly correlated sensor noise.

Such a brute-force approach solves some problems of ECD modeling, specifically the requirement for a non-linear optimization, but, unfortunately, it introduces another problem: the linear system (1.3) is ill-posed and under-determined because the number of sampled possible source locations is much higher than the dimensionality of the input data space (which cannot exceed the number of sensors), *i.e.* $N \gg M$. Thus, there is an infinite number of solutions for the linear system because any combination of terms from the null space of $\mathbf{G}$ will satisfy equation (1.4) and fit the sensor noise perfectly. In other words, many different arrangements of the sources of neural activation within the brain can produce any given MEG or EEG map. To overcome such ambiguity, a regularization term is introduced into the error measure

$$\mathcal{E}_r(\mathbf{Q}) = \mathcal{E}(\mathbf{Q}) + \lambda \mathcal{C}(\mathbf{Q}), \tag{1.6}$$

where $\lambda \geq 0$ controls the trade-off between the goodness of fit and the regularization term $\mathcal{C}(\mathbf{Q})$.

The equation (1.6) can have different interpretations depending on the approach used to derive it and the meaning given to the regularization term $\mathcal{C}(\mathbf{Q})$. All of the following methods provide the same result under specific conditions [13, 67]: Bayesian methodology to maximize the posterior $p(\mathbf{Q}|\mathbf{X})$ assuming Gaussian prior on $\mathbf{Q}$ [11], Wiener estimator with proper $\mathbf{C}_\epsilon$ and $\mathbf{C}_S$, Tikhonov regularization to trade-off the goodness of fit (1.5) and the regularization term $\mathcal{C}(\mathbf{Q}) = \mathrm{tr}(\mathbf{Q}^\top \mathbf{W}_\mathbf{Q}^{-1} \mathbf{Q})$ which attempts to find the solution with weighted by $\mathbf{W}_\mathbf{Q}^{-1}$ minimal 2nd norm. All the frameworks lead to the solution of the next general form

$$\mathbf{G}^+ = (\mathbf{G}^\top \mathbf{W}_\mathbf{X}^{-1} \mathbf{G} + \lambda \mathbf{W}_\mathbf{Q}^{-1})^{-1} \mathbf{G}^\top \mathbf{W}_\mathbf{X}^{-1}. \tag{1.7}$$

If and only if $\mathbf{W}_\mathbf{Q}$ and $\mathbf{W}_\mathbf{X}$ are positive definite [62] (1.7) is equivalent to

$$\mathbf{G}^+ = \mathbf{W}_\mathbf{Q} \mathbf{G}^\top (\mathbf{G} \mathbf{W}_\mathbf{Q} \mathbf{G}^\top + \lambda \mathbf{W}_\mathbf{X})^{-1}. \tag{1.8}$$

In case when viable prior information about the source distribution is available $\mathbf{Q}_p$, it is easy to account for it by minimizing the deviation of the solution not from $\mathbf{0}$ (which constitutes the minimal 2nd norm solution $\mathbf{G}^+$), but from the prior $\mathbf{Q}_p$, *i.e.* $\mathcal{C}(\mathbf{Q}) = \mathrm{tr}\big((\mathbf{Q} - \mathbf{Q}_p)^\top \mathbf{W}_\mathbf{Q}^{-1} (\mathbf{Q} - \mathbf{Q}_p)\big)$. Then (1.6) will be

minimized at

$$\hat{\mathbf{Q}} = \mathbf{G}^+ \mathbf{X} + (\mathbf{I} - \mathbf{G}^+ \mathbf{G}) \mathbf{Q}_p = \mathbf{Q}_p + \mathbf{G}^+ (\mathbf{X} - \mathbf{G} \mathbf{Q}_p). \tag{1.9}$$

For the noiseless case, with a weighted L_2-norm regularizer, the Moore-Penrose pseudo-inverse gives the inverse $\mathbf{G}^+ = \mathbf{G}^\dagger$ by avoiding the null space projections of $\mathbf{G}$ in the solution, thus providing a unique solution with a minimal second norm $\mathbf{G}^\dagger = \mathbf{W}_\mathbf{Q} \mathbf{G}^\top (\mathbf{G} \mathbf{W}_\mathbf{Q} \mathbf{G}^\top)^{-1}$.

Taking $\mathbf{W}_\mathbf{Q} = \mathbf{I}_N, \mathbf{W}_\mathbf{X} = \mathbf{I}_M$ and $\mathbf{Q}_p = \mathbf{0}$ constitutes the simplest regularized minimum norm solution (Tikhonov regularization). Classically, λ is found using cross-validation [57] or L-curve [66] techniques, to decide how much of the noise power should be brought into the solution. Phillips et al. [145] suggested iterative method ReML where the conditional expectation of the source distribution and the regularization parameters are estimated jointly. Additional constraints can be added to impose an additional regularization: for instance temporal smoothness [25].

As presented in (1.8), $\mathbf{G}^+$ can account for different features of the source or data space by incorporating them correspondingly into $\mathbf{W}_\mathbf{Q}$ and $\mathbf{W}_\mathbf{X}$. Next data-driven features are commonly used in EMSI

- $\mathbf{W}_\mathbf{X} = \mathbf{C}_\epsilon$ accounts for any possible noise covariance structure or, if $\mathbf{C}_\epsilon$ is diagonal, will scale the error terms according to the noise level of each sensor;
- $\mathbf{W}_\mathbf{Q} = \mathbf{W}_{\mathbf{C}_S} = \mathbf{C}_S$ accounts for prior knowledge of the sources covariance structure.

$\mathbf{W}_\mathbf{Q}$ can also account for different spatial features

- $\mathbf{W}_\mathbf{Q} = \mathbf{W}_\mathrm{n} = \big(\mathrm{diag}\,(\mathbf{G}^\top \mathbf{G})\big)^{-1}$ normalizes the columns of the matrix $\mathbf{G}$ to account for deep sources by penalizing voxels too close to the sensors [78, 103];
- $\mathbf{W}_\mathbf{Q} = \mathbf{W}_\mathrm{gm}$, where the i-th diagonal element incorporates the gray matter content in the area of the i-th dipole [144], *i.e.* the probability of having a large population of neurons capable of creating the detected E/MEG signal;
- $\mathbf{W}_\mathbf{Q} = (\mathbf{W}_a{}^\top \mathbf{W}_a)^{-1}$, where rows of $\mathbf{W}_a$ represent averaging coefficients for each source [10]. So far only geometrical [61] or biophysical averaging matrices [62] were suggested;
- $\mathbf{W}_\mathbf{Q}$ incorporates the first-order spatial derivative of the image [190] or Laplacian form [140].

Features defined by the diagonal matrices (*e.g.* $\mathbf{W}_{\text{n}}$ and $\mathbf{W}_{\text{gm}}$) can be combined through the simple matrix product. An alternative approach is to present $\mathbf{W_Q}$ in terms of a linear basis set of the individual $\mathbf{W_Q}$ factors, *i.e.* $\mathbf{W_Q} = \mu_1\mathbf{W}_{\text{n}} + \mu_2\mathbf{W}_{\text{gm}} + \cdots$, with later optimization of μ_i via the EM algorithm [144].

To better condition the under-determined linear inverse problem (1.4), Phillips et al. [144] suggested to perform the inverse operation in the space of the largest eigenvectors of the $\mathbf{W_Q}$. Such preprocessing can also be done in the temporal domain, when a similar sub-space selection is performed using prior temporal covariance matrix, thus effectively selecting the frequency power spectrum of the estimated sources.

Careful selection of the described features of data and source spaces helps to improve the fidelity of the DECD solution. Nevertheless, the inherent ambiguity of the inverse solution precludes achieving a high degree of localization precision. It is for this reason that additional spatial information about the source space, readily available from other functional modalities such as fMRI and PET, can help to condition the DECD solution (Section 3.3.4).

1.3.3 Beamforming

Beamforming (sometimes called a spatial filter or a virtual sensor) is another way to solve the inverse problem, which actually does not directly minimize (1.2). A beamformer attempts to find a linear combination of the input data $\hat{\mathbf{q}}_i = \mathbf{F}^i\mathbf{x}$, which represents the neuronal activity of each dipole $\mathbf{q}_i$ in the best possible way one at a given time. As in DECD methods, the search space is sampled, but, in contrast to the DECD approach, the beamformer does not try to fit all the observed data at once.

The linearly constrained minimum variance (LCMV) beamformer [181] looks for a spatial filter defined as $\mathbf{F}^i$ of size $M \times L$ minimizing the output energy ${\mathbf{F}^i}^\top \mathbf{C}_X \mathbf{F}^i$ under the constraint that only $\mathbf{q}_i$ is active at that time, *i.e.* that there is no attenuation of the signal of interest: $\mathbf{F}^k\mathbf{G}_{\cdot,\bar{\imath}} = \delta_{ki}\mathbf{I}_L$, where the Kronecker delta $\delta_{ki} = 1$ only if $k = i$ and 0 otherwise. Because the beamforming filter $\mathbf{F}^i$ for the i-th dipole is defined independently from the other possible dipoles, index i will be dropped from the derived results for the clarity of presentation.

The constrained minimization, solved using Lagrange multipliers, yields

$$\mathbf{F} = ({\mathbf{G}_{\cdot,\bar{\imath}}}^\top \mathbf{C}_X^{-1} \mathbf{G}_{\cdot,\bar{\imath}})^{-1} {\mathbf{G}_{\cdot,\bar{\imath}}}^\top \mathbf{C}_X^{-1} \tag{1.10}$$

This solution is equivalent to (1.7), when applied to a single dipole with the regularization term omitted. Source localization is performed using (1.10) to compute the variance of every dipole $\mathbf{q}$, which, in the case of uncorrelated dipole moments, is

$$\nu_{\mathbf{q}} = \operatorname{tr}\big(({\mathbf{G}_{\cdot,\bar{\imath}}}^\top \mathbf{C}_X^{-1} \mathbf{G}_{\cdot,\bar{\imath}})^{-1}\big). \tag{1.11}$$

The noise-sensitivity of (1.11) can be reduced by using the noise variance of each dipole as normalizing factor $\nu_\epsilon = \operatorname{tr}\big(({\mathbf{G}_{\cdot,\bar{\imath}}}^\top \mathbf{C}_\epsilon^{-1} \mathbf{G}_{\cdot,\bar{\imath}})^{-1}\big)$. This produces the so-called *neural activity index*

$$z = \frac{\nu_{\mathbf{q}}}{\nu_\epsilon}. \tag{1.12}$$

An alternative beamformer, *synthetic aperture magnetometry* or SAM [149], is similar to the LCMV if the orientation of the dipole is defined, but it is quite different in the case of a dipole with an arbitrary orientation. A vector of lead coefficients $\mathbf{g}_i(\theta)$ is defined as a function of the dipole orientation. This returns a single vector for the orientation θ of the i-th dipole, as opposed to the earlier formulation in which the L columns of $\mathbf{G}_{\cdot,\bar{\imath}}$ played a similar role. With this new formulation, the spatial filter is constructed

$$\mathbf{f}(\theta) = \frac{1}{\mathbf{g}_i(\theta)^\top \mathbf{C}_X^{-1} \mathbf{g}_i(\theta)} \mathbf{g}_i(\theta)^\top (\mathbf{C}_X + \lambda \mathbf{C}_\epsilon)^{-1} \tag{1.13}$$

which, under standard assumptions, is an optimal linear estimator of the time course of the i-th dipole. The variance of the dipole, accordingly, is also a function of θ, specifically $\nu_{\mathbf{q}}(\theta) = 1/\big(\mathbf{g}_i(\theta)^\top \mathbf{C}_X^{-1} \mathbf{g}_i(\theta)\big)$. To compute the neuronal activity index the original SAM formulation uses a slightly different normalization factor $\nu_\epsilon(\theta) = \mathbf{f}(\theta)^\top \mathbf{C}_\epsilon \mathbf{f}(\theta)$, which yields a different result if the noise variance in $\mathbf{C}_\epsilon$ is not equal across the sensors.

The unknown value of θ is found via a non-linear optimization of the neuronal activity index for the dipole:

$$\theta = \arg\max_{\vartheta} \frac{\nu_{\mathbf{q}}(\vartheta)}{\nu_\epsilon(\vartheta)}.$$

Despite the pitfalls of non-linear optimization, SAM filtering provides a higher SNR to LCMV by bringing less than half of the noise power into the solution. In addition, SAM filtering results in sharper peaks of the distribution of neuronal activity index over the volume [186].

Having computed $\nu_{\mathbf{q}}$ and ν_{ϵ} using SAM or LCMV for the two experimental conditions: passive (p) and active (a), it is possible to compute a pseudo-t value $\hat{t}$ for each location across the two conditions

$$\hat{t} = \frac{\nu_{\mathbf{q}}^{(a)} - \nu_{\mathbf{q}}^{(p)}}{\nu_{\epsilon}^{(a)} + \nu_{\epsilon}^{(p)}}. \tag{1.14}$$

Such an approach provides the possibility of considering experimental design in the analysis of E/MEG localization.

Unlike ECD, beamforming does not require prior knowledge of the number of sources, nor does it search for a solution in an underdetermined linear system as does DECD. For these reasons, beamforming remains the favorite method of many researchers in EMSI and has been suggested for use in the integrative analysis of E/MEG and fMRI which is covered in Section 3.3.5.

CHAPTER 2

MULTIMODAL EXPERIMENT PRACTICES

When you build bridges you can keep crossing them

– Rick Pitino

Obtaining non-corrupted simultaneous recordings of EEG and fMRI is a difficult task due to interference between the strong MR field and the EEG acquisition system. Because of this limitation, a concurrent EEG/fMRI experiment requires specialized design and preprocessing techniques to prepare the data for the analysis. The instrumental approaches described in this section are specific to collecting concurrent EEG and fMRI data. For obvious reasons MEG and fMRI data must be acquired separately in two sessions. However, even when MR and MEG are used sequentially, there is the possibility of contamination from the magnetization of a subject's metallic implants which can potentially disturb MEG acquisition if it is performed shortly after the MR experiment.

2.1 Measuring EEG During MRI: Challenges and Approaches

Developing methods for the integrative analysis of EEG and fMRI data is difficult for several reasons, not the least of which is the concurrent acquisition of EEG and fMRI itself has proved challenging. The nature of the problem is expressed by Faraday's law of induction: a time varying magnetic field in a wire loop induces an electromotive force (EMF) proportional in strength to the area of the wire loop and to the rate of change of the magnetic field component orthogonal to the area. When EEG electrodes are placed in a strong ambient magnetic field resulting in the EMF effect several undesirable complications arise:

- Rapidly changing MR gradient fields and RF pulses may induce voltages in the EEG leads placed inside the MR scanner. Introduced potentials may greatly obscure the EEG signal [77]. This kind of artifact is a real concern for concurrent EEG/MRI acquisition. Due to the deterministic nature of MR interference, hardware and algorithmic solutions may be able to unmask the EEG signal from MR disturbances. For example, Allen et al. [4] suggested an average waveform subtraction method to remove MR artifacts which is effective in case of deterministic generative process of a signal [155]. However, it is important to note that time variations of the MR artifact waveform can reduce the success of this method [34, 35]. The problem can be resolved through hardware modification that

increases the precision of the synchronization of MR and EEG systems [5] or during post-processing by using precise timings of the MR pulses during EEG waveform averaging [35]. Other techniques that have been proposed to reduce MR and ballistocardiographic artifacts include spectral domain filtering, spatial Laplacian filtering, PCA (Fig. 2.1), and ICA [see 20, 49, 128, 164, 171]

- Even a slight motion of the EEG electrodes within the strong static field of the magnet can induce significant EMF [68, 94]. For instance, native pulsatile motion related to a heart beat yields a ballistocardiographic artifact in the EEG that can be roughly the same magnitude as the EEG signals themselves [55, 77]. Usually such artifacts are removed by the same average waveform subtraction method, where the waveform is an averaged response to each heartbeat.

- Induced electric currents can heat up the electrode leads to painful or even potentially dangerous levels, such as to the point of burning the subject [107]. Current-limiting electric components (resistors, JFET transistors, *etc.*) are usually necessary to prevent the development of nuisance currents which can have direct contact with subject's scalp. Simulations show the safe power range that should be used for some coil/power/sensors configuration to comply with FDA guidelines [6].

Another concern is the impact of EEG electrodes on the quality of MR images. The introduction of EEG equipment into the scanner can potentially disturb the homogeneity of the magnetic field and distort the resulting MR images [77, 105]. Recent investigations show that such artifacts can be effectively avoided [89] by using specially designed EEG equipment [55]: specialized geometries, and new "MR-safe" materials (carbon fiber, plastic) for the leads. To test the influence of a given EEG system on fMRI data, a comparison of the data collected both with and without the EEG system being present, should be conducted. Analysis of such data usually demonstrates the same activation patterns in two conditions [105], although a general decrease in fMRI SNR is observed when EEG is present in the magnet. A correction to the brain matter conductivities (which are used for forward E/MEG modeling) for the Hall effect finds the following first-order correction to be negligible: $\sigma_H = 4.1 \times 10^{-8}\sigma$ for $B = 1.5\,\mathrm{T}$ [21].

2.2 Experimental Design Limitations

There are two ways of avoiding the difficulties associated with collecting EEG data in the magnet: (1) collect EEG and MRI data separately, or (2) use an experimental paradigm that can work around the potential contamination between the two modalities. The decision between these two alternatives will

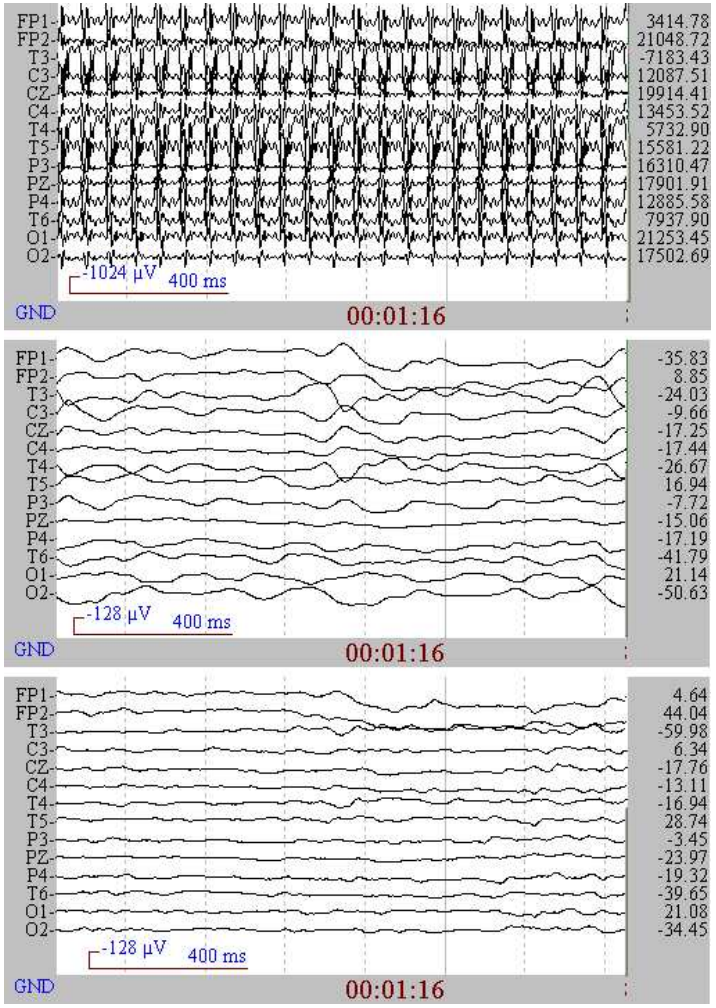

Figure 2.1 EEG MR artifact removal using PCA. EEG taken inside the magnet (top); EEG after PCA-based artifact removal but with ballistocardiographic artifacts present (center); EEG with all artifacts removed (bottom). After artifact removal it can be seen that the subject closed his eyes at time 75.9 s. (Courtesy of M. Negishi and colleagues, Yale University School of Medicine.)

depend on the constraints associated with research goals and methodology. For example, if an experiment can be repeated more than once with a high degree of reliability of the data, separate E/MEG and fMRI acquisition may be appropriate [73, 74, 120, 158]. In cases when simultaneous measurements are essential for the experimental objective (e.g., cognitive experiments where a subject's state might influence the results as in monitoring of spontaneous activity or sleep state changes), one of the following protocols can be chosen:

Triggered fMRI: detected EEG activity of interest (epileptic discharge, *etc.*) triggers MRI acquisition [90, 104, 161, 191]. Due to the slowness of the HR, relevant changes in the BOLD signal can be registered 4–8 s after the event. The EEG signal can settle quickly after the end of the previous MRI block [55], so it is acquired without artifacts caused by RF pulses or gradient fields that are present only during the MRI acquisition block. Note that ballistocardiographic and motion-caused artifacts still can be present and will require post-processing in order to be eliminated. Although this is an elegant solution and has been used with some success in the localization of epileptic seizures, this protocol does have drawbacks. Specifically, it imposes a limitation on the amount of subsequent EEG activity that can be monitored if the EEG high-pass filters do not settle down soon after the MR sequence is terminated [75]. In this case, EEG hardware that does not have a long relaxation period must be used. Another drawback with this approach is that it requires online EEG signal monitoring to trigger the fMRI acquisition in case of spontaneous activity. Often experiments of this kind are called *EEG-correlated fMRI* due to the fact that offline fMRI data time analysis implicitly uses EEG triggers as the event onsets [155];

Interleaved EEG/fMRI: the experiment protocol consists of time blocks and only a single modality is acquired during each time-block [21, 112]. This means that every stimulus has to be presented at least once per modality. To analyze ERP and fMRI activations, the triggered fMRI protocol can be used with every stimulus presentation so that EEG and MR are sequentially acquired in order to capture a clean E/MEG signal followed by the delayed HR [170];

Simultaneous fMRI/EEG: pre-processing of the EEG signal mentioned in Section 2.1 is used to remove the MR-caused artifacts and to obtain an estimate of the true EEG signal. However, neither of the existing artifact removing methods is proved to be general enough to work for every type of EEG experiment and analysis. It is especially difficult to use such an acquisition scheme for

cognitive experiments in which the EEG evoked responses of interest can be of small amplitude and completely overwhelmed by the MR noise [157].

CHAPTER 3

CONVENTIONAL MULTIMODAL ANALYSIS

The average Ph.D. thesis is nothing but the transference of bones from one graveyard to another.

– Frank J. Dobie *"A Texan in England"*, 1945

There is an increasing number of reported E/MEG/fMRI conjoint studies, which attempt to gain the advantages of a multimodal analysis for experiments involving perceptual and cognitive processes: visual perception [105, 166, 170, 183] and motor activation [105], somatosensory mapping [87, 158], fMRI correlates of EEG rhythms [35, 56, 101, 112, 123], arousal and attention interaction [44], auditory oddball tasks [23, 74], passive frequency oddball [109], illusory figures in visual oddball tasks [93], target detection [120, 126], face perception [73], sleep [75], language tasks [166, 185], and epilepsy [90–92, 100, 108, 161, 189, 191].

This section starts with an explanation of the role of anatomical MRI in multimodal experiments followed by a description of multimodal analysis methods used in the above mentioned studies or test-driven on the simulated data.

3.1 Using Anatomical MRI

The difference in captured MRI contrasts (proton densities (PD) or T1, T2 relaxation times) for different types of organic tissue makes possible the non-invasive collection of information about the structural organization of the brain. In addition, a regular gradient or spin echo EPI sequence is capable of detecting transient or subtle changes of the magnetic field in cortical tissue caused by neuronal activation [19, 196]. However, direct application of MRI to capture functional activity remains limited due to a low signal-to-noise ratio (SNR) which is why MRI is often labelled *anatomical*. The next section briefly describes the analysis of acquired high-resolution 3D images of the brain and how obtained structural information can be used to analyze data collected from other modalities (for other reviews see [51, 52, 135, 154]).

3.1.1 Registration of EEG and MEG to MRI

If an EEG experiment is performed inside the magnet, it is possible to "mark" [95] the location of the EEG sensors to make them distinguishable on the anatomical MRI. Coordinates for these locations can then be

found either manually or automatically [165] and will lie in MRI coordinate system. In case when MR and E/MEG data are acquired in separate sessions, spatial registration between E/MEG and MRI coordinate systems must be performed before any anatomical information can be introduced into the analysis of E/MEG data. There are two general possible ways for performing registration between MRI and E/MEG data: (a) registering a limited set of fiducial points or (b) aligning scalp surfaces obtained during MRI with a digitization of the scalp during E/MEG. Methods based on the alignment of the scalp surfaces (or points clouds) considered to perform better than those using fiducial-points [76, 88, 97, 159], but are more computationally demanding and rely on iterative optimization. In addition, it can be time consuming to obtain the dense digitization of the subject's head using a single point 3D digitizer. For these reasons the fiducial points approach remains the preferred E/MEG/MRI registration method [for instance 95, 176]. The fiducial points method involves the alignment of a limited set of points, which have a strict known correspondence between the two spaces, so that each fiducial point in E/MEG space with coordinates ($\mathbf{x}_i^E$) has a corresponding known point ($\mathbf{x}_i^M$) in MRI space. Such coupling removes the possibility of being trapped in the local minima of the iterative surface aligning methods and makes registration simple and fast. The precision of the derived transformation can be increased by adding more pairs of corresponding E/MEG and MRI points. A more detailed description of the registration method using fiducial points follows.

Locations of the fiducial points (*e.g.* anatomical points: nasion, inion, pre-auricular points or tragus of the left and right earlobes, vertex; MRI-visible capsules or even bite-bar points [1, 167]) are captured together with the locations of E/MEG sensors using a 3D digitizer and then matched to the locations of corresponding fiducial points obtained from the analysis of the MRI for the same subject. A 3D rigid transformation of the points from the E/MEG ($\mathbf{x}^E$) to the MRI coordinate system ($\mathbf{x}^{E\to M}$) can be defined by the rotation matrix $\mathbf{R}$ and translation vector $\mathbf{v}$, so that $\mathbf{x}^{E\to M} = \mathbf{R}\mathbf{x}_i^E + \mathbf{v}$. Commonly, the quadratic mis-registration error measure is the subject to minimization $\varepsilon(\mathbf{R}, \mathbf{v}) = \sum_i^P (\mathbf{x}_i^M - \mathbf{x}^{E\to M})^2$, where P is the number of the points. Solutions can be found with simplified geometrical formulations [193], or iterative search optimization using Powell's algorithm [167]. Such simplifications or complications are not necessary because the analytical form solutions have been derived in other fields [71, 72], and they are often used in the surface matching methods earlier discussed. For instance, quaternions (vectors in L_4) can be natively used to describe a rotation in 3D space leading to a straightforward solution of the registration problem [71] (see Appendix C). This method is simple to implement. Its precision rapidly

increases with the number of fiducial points, reaching the performance of surface matching algorithms cheaply and efficiently.

3.1.2 Segmentation and Tessellation

PD or T1/T2 3D MR images can be used to segment different brain tissues (white matter, gray matter, cerebrospinal fluid (CSF), skull, scalp) as well as abnormal formations (tumors) [38, 131]. Different kinds of MR contrasts are optimal for the segmentation of the different kinds of head and brain structures. For instance, PD-weighted MRI yields superior segmentation of the inner and outer skull surfaces because bones have much smaller water content than brain tissue, making the skull easily distinguishable on PD images. On the other hand, exploiting T1 and T2 relaxation time differences between various sorts of brain tissue leads to higher quality segmentation of structures within the brain.

Using triangulation (tessellation) and interpolation it is possible to create fine-grained smooth mesh representations or tetrahedral assemblies of the segmented tissues [36, 146, 163]. Obtained 3D mesh of the cortical surface alone brings valuable information to the analysis of E/MEG signals [28]: the physiology of the neuronal generators can be considered, allowing one to limit the search space for activated sources to the gray matter regions and oriented orthogonally or nearly so to the cortical surface [38, 134].

Monte Carlo studies [110] tested the influence of the orientation constraint in the case of the DECD model and showed that such constraint leads to much better conditioning of the inverse problem while still being robust to the error of the assumed cortical surface: random deviation of the orientation in 30° range leads to just a slight increase of distortion, thus not significantly affecting the accuracy of the localization procedure. Anatomical constraints improve the localization and contrast of beamforming imaging methods as well, but the use of anatomical constraints found to be advantageous only in case of good MRI/E/MEG coregistration [69].

3.1.3 Forward Modeling of EEG and MEG

Volumetric structures derived from the tessellation procedure are used to create a realistic geometry of the head, which is crucial for the forward modeling of E/MEG fields. Previously, rough approximations based on best-fit single/multiple sphere models were developed to overcome the burden of creating realistic head geometry, but they became less favorable as the increased availability of powerful computational resources made more realistic modeling possible. Spatial information is especially important for EEG

forward modeling due to the fact that it is more strongly affected by the conductivities of the skull and the scalp than the MEG forward model. Such inhomogeneities do not affect the magnetic field at all in case of a spherical head model, when only the inner skull surface is of the main concern for the forward modeling.

There are four numerical methods available to solve the E/MEG modeling problem, and the Boundary Elements Method (BEM) [65] is the most commonly used when isotropy (direction independence) of the matters is assumed, so that only boundary meshes obtained by the tessellation process are required. It was shown, however, that anisotropy of the skull [115] and white-matter [195] can bias EEG and MEG forward models. To solve the forward problem in the case of an anisotropic medium, the head volume is presented by a large assembly of small homogeneous tetrahedrons, and a Finite Elements Method (FEM) [122] is used to approximate the solution. Another possible way is to use the Finite Difference Method (FDM) on a regular computational mesh [153]. Table A lists some publicly available software which can help performing the forward E/MEG modeling. Forward modeling of E/MEG signal rely on the knowledge of matter conductivities. Common values of conductivities for different tissues can be found in the literature [50], or can be estimated on a per-subject basis using Electrical Impedance Tomography (EIT) [58] or Diffusion Tensor (DT) [179] MRI.

3.2 Forward Modeling of BOLD Signal

The successful analysis of the results of a multimodal experiment remains problematic. The main problem of multimodal analysis is the absence of a general unifying account of the BOLD fMRI signal in terms of the characteristics of a neuronal response. Various models have been suggested, on one hand they include naive modeling of BOLD signal in the context of a Linear Time Invariant System (LTIS). On the other hand there are general models of the BOLD signal in terms of detailed biophysical processes (*Balloon* [26] or *Vein and Capillary* [162] models). The naive models are not general enough to explain the variability of the BOLD signal, whereas complex parametric models that rely heavily on a prior knowledge of nuisance parameters (due to biophysical details), almost never do not have a reliable and straightforward means of estimation. This fact makes it unlikely to use such comprehensive models as reliable generative models of the BOLD signal. Research continues in attempts to derive novel suitable models to support data obtained in different modalities based on originating them neuronal signal. Interesting *heuristic model* of neuronal activation and its influence on BOLD and EEG signals was recently suggested by Kilner, et al. [85]. Suggested model relates BOLD signal to the changes in spectral characteristics of the EEG signal during

activation. Proposed model formulation agrees well with the results of many multimodal experiments which used other methods of multimodal analysis. Thus this model sounds promising and it might reveal reliable interdependencies between different brain imaging modalities. The following section describes modeling issues in greater detail to further underline the limited applicability of many multimodal analysis methods covered in Section 3.3.

3.2.1 Convolutional Model of BOLD Signal

Various experimenters had originally focused on simple contrast designs such as block design paradigms in order to exploit the presumed linearity between their design parameters and the HR. This assumption depends critically on the ability of the block design to amplify the SNR and the implicit belief that the HR possess more temporal resolution than indicated by the TR.

In order to account for the present autocorrelation of the HR caused by its temporal dispersive nature, Friston et al. [47] suggested to model HR with a LTIS. To describe the output of such a system, a convolution of an input (joint intrinsic and evoked neuronal activity $q(t)$) with a hemodynamic response function (HRF) $h(t)$ is used to model the HR

$$f(t) = (h * q)(t). \tag{3.1}$$

Localized neuronal activity itself is not readily available via means of non-invasive imaging, therefore it is more appropriate to verify LTIS modeling on real data as a function of parameters of the presented stimuli (*i.e.* duration, contrast).

The convolutional model was used on real data to demonstrate linearity between the BOLD response and the parameters of presented stimuli [22, 33]. In fact, many experimenters have shown apparent agreement between LTIS modeling and real data. Specificly it has been possible to model responses to longer stimuli durations by constructing them using the responses to shorter duration stimuli, which is consistent with LTIS modeling. Because of the predictive success, its relative simplicity of application and resulting ignorance of biophysical details this modeling approach became widely accepted. Unfortunately LTIS as a modeling constraint is very weak therefore allowing an arbitrary choice of parametric HRF based only on preference and familiarity.

Over the years multiple models for the HRF have been suggested. The most popular and widely used up until now is a single probability density function (PDF) of Gamma distribution by [99]. It was

elaborated by Glover [54] to perform the deconvolution of the HR signal, and the nuisance parameters $(n_1, t_1, n_2, t_2, a_2)$ of the next HRF were estimated for motor and auditory areas

$$h(t) = \frac{1}{c_1}\, t^{n_1}\, e^{-t/t_1} - \frac{a_2}{c_2}\, t^{n_2}\, e^{-t/t_2} \qquad \text{where} \qquad c_i = \max_t t^{n_i}\, e^{-t/t_i} = \left(\frac{e}{n_i t_i}\right)^{-n_i} \tag{3.2}$$

which can be described as the sum of two unscaled PDFs of Gamma distribution. The first term captures the positive BOLD HR and the second term is to capture the overshoot often observed in the BOLD signal. Many other simple and as well as more sophisticated models of HRF were suggested: Poisson PDF [47], Gaussians [148], Bayesian derivations [29, 53, 116] and others. The particular choice of any of them was primarily dictated by some other than bio-physics motivation: easy Fourier transformation, presence of post-response dip or “best-fit” properties.

Since the suggestion of the convolutional model describing BOLD response, different aspects of HR linearity became an actively debated question. If HR is linear, then what features of the stimulus (*e.g.* duration, intensity) or neuronal activation (*e.g.* firing frequency, field potentials, frequency power) does it vary linearly with? As the first approximation, it is important to define the ranges of the above mentioned parameters in which HR was found to behave linearly. For example, early linearity tests [54] showed the difficulty in predicting long duration stimuli based on an estimated HR from shorter duration stimuli. [169] reviewed existing papers describing different aspects of non-linearity in BOLD HR and attempted to determine the ranges of linearity in respect to stimuli duration in three cortical areas: motor, visual and auditory complex. The results of these analyses have shown that although there is a strong non-linearity observed on small stimuli durations, long stimuli durations show higher degree of linearity.

It appears that a simple convolutional model generally is not capable of describing the BOLD responses in terms of the experimental design parameters if such are varying in a wide range during the experiment. Nevertheless LTIS might be more appropriate to model BOLD response in terms of neuronal activation if most of the non-linearity in the experimental design can be explained by the non-linearity of the neuronal activation itself.

3.2.2 Neurophysiologic Constraints

In the previous section the subject of linearity between the experimental design parameters and the observed BOLD signal was explored. For the purpose of this review it may be more interesting to explore the relation between neuronal activity and HR.

It is known that E/MEG signals are produced by large-scale synchronous neuronal activity, whereas the nature of the BOLD signal is not clearly understood. The BOLD signal does not correspond to the neural activity that consumes the most energy [8], as early researchers believed. Furthermore, the transformation between the electrophysiological indicators of neuronal activity and the BOLD signal cannot be linear for the entire dynamic range, under all experimental conditions and across all the brain areas. Generally, a transformation function cannot be linear since the BOLD signal is driven by a number of "nuisance" physiologic processes such as cerebral metabolic oxygen consumption ($CMRO_2$), cerebral blood flow (CBF) and cerebral blood volume (CBV) as suggested by the *Balloon model* [26], which are not generally linear.

Due to the indirect nature of the BOLD signal as a tool to measure neuronal activity, in many multimodal experiments a preliminary comparative study is done first in order to assess the localization disagreement across different modalities. Spatial displacement is often found to be very consistent across multiple runs or experiments (see Section 3.3.3 for an example). Specifically, observed differences can potentially be caused by the variability in the cell types and neuronal activities producing each particular signal of interest Nunez and Silberstein [135]. That is why it is important first to discover the types of neuronal activations that are primary sources of the BOLD signal. Some progress on this issue has been made. A series of papers generated by a project to cast light on the relationship between the BOLD signal and neurophysiology, have argued that local field potentials (LFP) serve a primary role in predicting BOLD signal [111, and references 27, 29, 54, 55 and 81 therein]. This work countered the common belief that spiking activity was the source of the BOLD signal [for example 7] by demonstrating a closer relation of the observed visually evoked HR to the local field potentials (LFP) of neurons than to the spiking activity. This result places most of the reported non-linearity between experimental design and observed HR into the non-linearity of the neural response, which would benefit a multimodal analysis.

Note that the extracellular recordings experiments described above, were carried out over a small ROIs, therefore they inherit the parameters of underlying hemodynamic processes for the given limited area. Thus, even if LFP is taken as the primary electrophysiological indicator of the neuronal activity causing BOLD signal, the relationship between the neuronal activity and the hemodynamic processes on a larger scale remains an open question.

Since near-infrared optical imaging (NIOI) is capable of capturing the individual characteristics of cerebral hemodynamics such as total, oxy-, and deoxy-hemoglobin content, some researchers tried to use

NIOI to reveal the nature of the BOLD signal. Rat studies using 2D optical imaging [41] showed the non-linear mapping between the neuronal activity and evoked hemodynamic processes. This result should be a red flag for those who try to define the general relation between neuronal activation and BOLD signal as mostly linear. The conjoint analysis of BOLD and NIOI signals revealed the silent BOLD signal during present neural activation registered by E/MEG modalities [162]. This mismatch between E/MEG and fMRI results is known as the *sensory motor paradox* [141]. To explain this effect, the *Vein and Capillary* model was used to describe the BOLD signal in terms of hemodynamic parameters [162]. The suggested model permits the existence of silent and negative BOLD responses during positive neuronal activation. This fact, together with an increasing number of studies [172] confirming that sustained negative BOLD HR is a primary indicator of decreased neuronal activation, provide yet more evidence that the BOLD HR generally is not a simple linear function of neuronal activation but at best is a monotone function which has close to linear behavior in a wide range of nuisance neurophysiologic parameters. This section concludes by noting that the absence of a generative model of the BOLD response prevents the development of universal methods of multimodal analysis. Nevertheless, as discussed in this section and is shown by the results presented in the next section, there are specific ranges of applications where the linearity between BOLD and neuronal activation can be assumed. Such simplistic model can be voted for by the supported of *Occam's razor* principle which is to prefer simple models capable of describing the data of interest.

3.3 Analysis Methods

Whenever applicable, a simple comparative analysis of the results obtained from the conventional unimodal analyses together with findings reported elsewhere, can be considered as the first confirmatory level of a multimodal analysis. This type of analysis is very flexible, as long as the researcher knows how to interpret the results and to draw useful conclusions, especially whenever the results of comparison reveal commonalities and differences between the two [185]. On the other hand, by default a unimodal analysis makes limited use of the data from the modalities, and encourages researchers to look for analysis methods which would incorporate the advantages of each single modality. Nevertheless, simple inspection is helpful for drawing preliminary conclusions on the plausibility to perform any conjoint analysis using one of the methods described in this section, including correlative analysis which might be considered an initial approach to try.

3.3.1 Correlative Analysis of EEG and MEG with fMRI

In some experiments, the E/MEG signal can serve as the detector of spontaneous neuronal activity (*e.g.* epileptic discharges) or changes in the processing states (*e.g.* vigilance states). The time onsets derived from E/MEG are alone valuable for further fMRI analysis, where the BOLD signal often cannot provide such timing information. For instance, such use of EEG data is characteristic for the experiments performed via a *Triggered fMRI* acquisition scheme (Section 2.2).

Correlative E/MEG/fMRI analysis becomes more intriguing if there is a stronger belief in the linear dependency between the BOLD response and features of E/MEG signal (*e.g.* amplitudes of ERP peaks, powers of frequency components), than between the hemodynamics of the brain and the corresponding parameter of the design (*e.g.* frequency of stimulus presentation or level of stimulus degradation). Then E/MEG/fMRI analysis effectively reduces the inherent bias present in the conventional fMRI analysis methods by removing the possible non-linearity between the design parameter and the evoked neuronal response.

The correlative analysis relies on the preprocessing of E/MEG data to extract the features of interest to be compared with the fMRI time course. The obtained E/MEG features first get convolved with a hypothetical HRF (Section 3.2.1) to accommodate for the HR sloppiness and are then subsampled to fit the temporal resolution of fMRI. The analysis of fMRI signal correlation with amplitudes of selected peaks of ERPs revealed sets of voxels which have a close to linear dependency between the BOLD response and amplitude of the selected ERP peak (N170 in [73], P300 in [74], and amplitude of mismatch negativity (MMN) [109]), thus providing a strong correlation ($P < 0.001$ [73]). A parametric experimental design with different noise levels introduced for the stimulus degradation [73, 109] or different levels of sound frequency deviant [109] helped to extend the range of detected ERP and fMRI activations, thus effectively increasing the significance of the results found. To support the suggested connection between the specific ERP peak and fMRI activated area, the correlation of the same BOLD signal with the other ERP peaks must be lower if any at all [73]. As a consequence, such analysis cannot prove that any specific peak of EEG is produced by the neurons located in the fMRI detected areas alone but it definitely shows that they are connected in the specific paradigm.

The search for the covariates between the BOLD signal and wide-spread neuronal signals, such as the alpha rhythm, remains a more difficult problem due to the ambiguity of the underlying process, since there are many possible generators of alpha rhythms corresponding to various functions [130].

As an example, Goldman et al. [56] and Laufs et al. [101] were looking for the dependency between fMRI signal and EEG alpha rhythm power during interleaved and simultaneous EEG/fMRI acquisition correspondingly. They report similar (negative correlation in parietal and frontal cortical activity), as well as contradictory (positive correlation) findings, which can be explained by the variations in the experimental setup [102] or by the heterogeneous coupling between the alpha rhythm and the BOLD response [101]. Despite the obvious simplification of the correlative methods, they may still have a role to play in constraining and revealing the definitive forward model in multimodal applications.

3.3.2 Decomposition Techniques

The common drawback of the presented correlative analyses techniques is that they are based on the selection of the specific feature of the E/MEG signal to be correlated with the fMRI time trends, which are not so perfectly conditioned to be characterized primarily by the feature of interest. The variance of the background processes, which are present in the fMRI data and are possibly explained by the discarded information from the E/MEG data, can reduce the significance of the found correlation. That is why it was suggested [117] to use the entirety of the E/MEG signal, without focusing on its specific frequency band, to derive the E/MEG and fMRI signal components which have the strongest correlation among them. The introduction of decomposition techniques (such as basis pursuit, PCA, ICA, *etc.*) into the multimodal analysis makes this work particularly interesting.

To perform the decomposition [117], Partial Least-Squares (PLS) regression was generalized into the tri-PLS2 model, which represents the E/MEG spectrum as a linear composition of trilinear components. Each component is the product of spatial (among E/MEG sensors), spectral and temporal factors, where the temporal factors have to be maximally correlated with the corresponding temporal component of the similar fMRI signal decomposition into bilinear components: products of the spatial and temporal factors. Analysis using tri-PLS2 modeling on the data from [56] found a decomposition into 3 components corresponding to alpha, theta and gamma bands of the EEG signal. The fMRI components found had a strong correlation only in alpha band component (Pearson correlation 0.83 ($p = 0.005$)), although the theta component also showed a linear correlation of 0.56 ($p = 0.070$). It is interesting to note, that spectral profiles of the trilinear EEG atoms received with and without fMRI influence were almost identical, which can be explained either by the non-influential role of fMRI in tri-PLS2 decomposition of EEG, or just by a

good agreement between the two. On the other hand, EEG definitely guided fMRI decomposition, so that the alpha rhythm spatial fMRI component agreed very well with the previous findings [56].

3.3.3 Equivalent Current Dipole Models

ECD is the most elaborated and widely used technique for source localization in EMSI. It can easily account for activation areas obtained from the fMRI analysis thus giving the necessary fine time-space resolution by minimizing the search space of non-linear optimization to the thresholded fMRI activation map. While being very attractive, such a method bears most of the problems of the ECD method mentioned in Section 1.3, and introduces another possible bias due to the belief in the strong coupling between hemodynamic and electrophysiological activities. For this reason it needs to be approached with caution in order to carefully select the fMRI regions to be used in the ECD/fMRI combined analysis.

Although good correspondence between ECD and fMRI results is often found [3], some studies reported a significant (1–5 cm) displacement between locations obtained from fMRI analysis and ECD modeling [15, 59, 87, 108]. It is interesting to note, that such displacement can be very consistent across the experiments of different researchers using the same paradigm (for instance motor activations [86, 87, 158]). As it was already mentioned, in the first step, a simple comparison of detected activations across the two modalities can be done to increase the reliability of dipole localization alone. Further, additional weighting by the distance from the ECD to the corresponding fMRI activation foci can guide ECD optimization [188] and silent in fMRI activations can be accommodated by introducing free dipoles without the constraint on dipole location.

Auxiliary fMRI results can help to resolve the ambiguity of the inverse E/MEG problem if ECD lies in the neighborhood of multiple fMRI activations. Placing multiple ECDs inside the fMRI foci with successive optimization of ECDs orientations and magnitudes may produce more meaningful results, especially if it better describes the E/MEG signal by the suggested multiple ECDs model.

Due the large number of consistent published fMRI results, it seems viable to perform a pure E/MEG experiment with consequent ECD analysis using known relevant fMRI activation areas found by the other researchers performing the same kind of experiment [45], thus providing the missing temporal explanation to the known fMRI activations.

3.3.4 Linear Inverse Methods

Dale and Sereno [38] formulated a simple but powerful linear framework for the integration of different imaging modalities into the inverse solution of DECD, where the solution was presented as unregularized (just minimum-norm) (1.8) with $\mathbf{W_Q} = \mathbf{C}_S$ and $\lambda\mathbf{W_X} = \mathbf{C}_\epsilon$. The simplest way to account for fMRI data is to use thresholded fMRI activation map as the inverse solution space but this was rejected [51] due to its incapability to account for fMRI silent sources, which is why the idea to incorporate variance information from fMRI into $\mathbf{C}_S$ was further elaborated [110] by the introduction of relative weighting for fMRI activated voxels via constructing a diagonal matrix $\mathbf{W_Q} = \mathbf{W}_{\text{fMRI}} = \{\nu_{ii}\}$, where $\nu_{ii} = 1$ for fMRI activated voxels and $\nu_{ii} = \nu_0 \in [0, 1]$ for voxels which are not revealed by fMRI analysis. A Monte Carlo simulation showed that $\nu_0 = 0.1$ (which corresponds to the 90% relative fMRI weighting) leads to a good compromise with the ability to find activation in the areas which are not found active by fMRI analysis and to detect active fMRI spots (even superficial) in the DECD inverse solution. An alternative formulation of the relative fMRI weighting in the DECD solution can be given using a subspace regularization (SSR) technique [2], in which an E/MEG source estimate is chosen from all possible solutions describing the E/MEG signal, and is such that it minimizes the distance to a subspace defined by the fMRI data (Fig. 3.1). Such formulation helps to understand the mechanism of fMRI influence on the inverse E/MEG solution: SSR biases underdetermined the E/MEG source locations toward the fMRI foci.

The relative fMRI weighting was tested [37] in an MEG experiment and found conjoint fMRI/MEG analysis results similar to the results reported in previous fMRI, PET, MEG and intracranial EEG studies. Babiloni et al. [9] followed Dale et al. [37] in a high resolution EEG and fMRI study to incorporate non-thresholded fMRI activation maps with other factors. First of all, the $\mathbf{W}_{\text{fMRI}}$ was reformulated to $(\mathbf{W}_{\text{fMRI}\prime})_{ii} = \nu_0 + (1 - \nu_0)\Delta_i/\Delta_{\max}$, where Δ_i corresponds to the relative change of the fMRI signal in the i-th voxel, and $\Delta_{\max}$ is the maximal detected change. This way the relative E/MEG/fMRI scheme is preserved and locations of stronger fMRI activations have higher prior variance. Finally the three available weighting factors were combined: fMRI relative weighting, correlation structure obtained from fMRI described by the matrix of correlation coefficients $\mathbf{K}_S$, and the gain normalization weighting matrix $\mathbf{W}_{\text{n}}$ (Section 1.3.2): $\mathbf{W_Q} = \mathbf{W}^{1/2}_{\text{fMRI}\prime}\mathbf{W}^{1/2}_{\text{n}}\mathbf{K}_S\mathbf{W}^{1/2}_{\text{n}}\mathbf{W}^{1/2}_{\text{fMRI}\prime}$. Although $\mathbf{W}_{\text{fMRI}\prime}$ alone had improved EMSI localization, the incorporation of the $\mathbf{K}_S$ lead to finer localization of neuronal activation associated with finger movement.

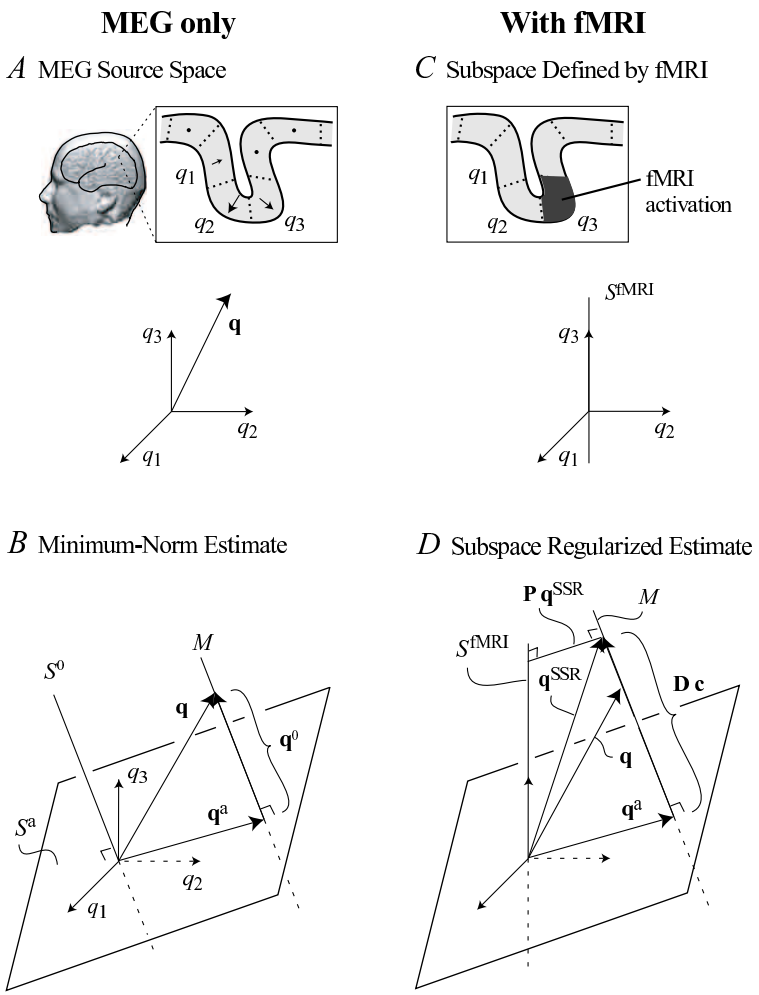

Figure 3.1 Geometrical interpretation of subspace regularization in the MEG/EEG source space. (A) The cerebral cortex is divided into source elements $\mathbf{q}_1, \mathbf{q}_2, \ldots, \mathbf{q}_K$, each representing an ECD with a fixed orientation. All source distributions compose a vector $\mathbf{q}$ in K-dimensional space. (B) The source distribution $\mathbf{q}$ is divided into two components $\mathbf{q}^a \in S^a \equiv \mathrm{range}(\mathbf{G}^\top)$, determined by the sensitivity of MEG sensors and $\mathbf{q}^0 \in \mathrm{null}\,\mathbf{G}$, which does not produce an MEG signal. (C) The fMRI activations define another subspace S^{fMRI}. (D) The subspace-regularized fMRI-guided solution $\mathbf{q}^{\mathrm{SSR}} \in \mathrm{M}$ is closest to S^{fMRI}, minimizing the distance $\|\mathbf{P}\mathbf{q}^{\mathrm{SSR}}\|$, where $\mathbf{P}$ (a $N \times N$ diagonal matrix with $\mathbf{P}_{ii} = 1/0$ when the i-th fMRI voxel is active/inactive) is the projection matrix into the orthogonal complement of S^{fMRI}. (Adapted from [2, Figure 1])

Although most of the previously discussed DECD methods are involved in finding minimal L_2 norm solution, the fMRI conditioned solution with minimal L_1 norm (regularization term in (1.6) $\mathcal{C}(\mathbf{Q}) = \|\mathbf{Q}\|_1$) is shown to provide a sparser activation map [48] with activity focalized to the seeded hotspot locations [188].

An fMRI-conditioned linear inverse is an appealing method due to its simplicity, and rich background of DECD linear inverse methods derived for the analysis of E/MEG signals. Nonetheless, one should approach these methods with extreme caution in a domain where non-linear coupling between BOLD and neural activity is likely to overwhelm any linear approximation [59].

3.3.5 Beamforming

Lahaye et al. [96] suggest an iterative algorithm for conjoint analysis of EEG and fMRI data acquired simultaneously during an event-related experiment. Their method relies on iterated source localization by the LCMV beamformer (1.10), which makes use of both EEG and fMRI data. The covariance $\mathbf{C}_X$ used by the beamformer is calculated anew each time step, using the previously estimated sources and current event responses from both modalities. This way neuronal sites with a good agreement between the BOLD response and EEG beamformer reconstructed source amplitude, benefit most at each iteration. Although the original formulation is cumbersome, this method appears promising as (a) it makes use of both spatial and temporal information available from both modalities, and (b) it can account for silent BOLD sources using an electro-metabolic coupling constant which is estimated for each dipole and defines the influence of the BOLD signal at a given location onto the estimation of $\mathbf{C}_S$ which, in turn, drives the estimate of $\mathbf{C}_X$.

3.3.6 Bayesian Inference

During the last decade, Bayesian methods became dominant in the probabilistic signal analysis. The idea behind them is to use Bayes' rule to derive a *posterior probability* of a given *hypothesis* having observed data $\mathcal{D}$, which serves as *evidence* to support the hypothesis

$$p(\mathcal{H}|\mathcal{D}) = \frac{p(\mathcal{D}|\mathcal{H})\, p(\mathcal{H})}{p(\mathcal{D})}, \tag{3.3}$$

where $p(\mathcal{H})$ and $p(\mathcal{D})$ are prior probabilities of the hypothesis and evidence correspondingly, and the conditional probability $p(\mathcal{D}|\mathcal{H})$ is known as a *likelihood function*. Thus, (3.3) can be viewed as a method

to combine the results of conventional likelihood analyses for multiple hypotheses into the posterior probability of the hypotheses $p(\mathcal{H}|\mathcal{D})$ or some function of it, after been exposed to the data. The derived posterior probability can be used to select the most probable hypothesis, *i.e.* the one with the highest probability

$$\hat{\mathcal{H}}_{|\mathcal{D}} = \arg\max_{\mathcal{H}} p(\mathcal{H}|\mathcal{D}) = \arg\max_{\mathcal{H}} \log p(\mathcal{D}|\mathcal{H}) + \log p(\mathcal{H}) \tag{3.4}$$

leading to the maximum *a posteriori* (MAP) estimate, where the prior data probability $p(\mathcal{D})$ (often called a *partition function*) is omitted because the data does not depend on the choice of the hypothesis and it does not influence the maximization over $\mathcal{H}$.

For the class of problems related to the signal processing, hypothesis $\mathcal{H}$ generally consists of a model $\mathcal{M}$ characterized by a set of nuisance parameters $\boldsymbol{\Theta} = \{\theta_1, \theta_{2\ldots n}\}$. The primary goal usually is to find a MAP estimate of some quantity of interest $\boldsymbol{\Delta}$ or, more generally, its posterior probability distribution $p(\boldsymbol{\Delta}|\mathcal{D}, \mathcal{M}, \boldsymbol{\Theta})$. $\boldsymbol{\Delta}$ can be an arbitrary function of the hypothesis or its components $\boldsymbol{\Delta} = f(\mathcal{H})$, or often just a specific nuisance parameter of the model $\boldsymbol{\Delta} \equiv \theta_1$. To obtain posterior probability of the nuisance parameter, its marginal probability has to be computed by the integration over the rest of the parameters of the model

$$p(\theta_1|\mathcal{D}, \mathcal{M}) = \int p(\theta_1, \theta_{2\ldots n}|\mathcal{D}, \mathcal{M})\, d\theta_{2\ldots n} = \int p(\theta_1|\theta_{2\ldots n}, \mathcal{D}, \mathcal{M})\, p(\theta_{2\ldots n}|\mathcal{D}, \mathcal{M})\, d\theta_{2\ldots n}. \tag{3.5}$$

Due to the integration operation involved in determination of any marginal probability, Bayesian analysis becomes very computationally intensive if analytical integral solution does not exist. Therefore, sampling techniques (*e.g.* MCMC, Gibbs sampler) are often used to estimate full posterior probability $p(\boldsymbol{\Delta}|\mathcal{D}, \mathcal{M})$, MAP $\hat{\boldsymbol{\Delta}}_{|\mathcal{D},\mathcal{M}} = \arg\max_{\boldsymbol{\Delta}} p(\boldsymbol{\Delta}|\mathcal{D}, \mathcal{M})$, or some statistics such as an expected value $E[\boldsymbol{\Delta}|\mathcal{D}, \mathcal{M}]$ of the quantity of interest.

The Bayesian approach sounds very appealing for the development of multimodal methods. It is inherently able to incorporate all available evidence, which is in our case obtained from the fMRI and E/MEG data ($\mathcal{D} = \{\mathbf{X}, \mathbf{F}\}$) to support the hypothesis on the location of neuronal activations, which is in the case of DECD model is $\mathcal{H} = \{\mathbf{Q}, \mathcal{M}\}$. However, the detailed analysis of (3.3) leads to necessary simplifications and assumptions of the prior probabilities in order to derive a computationally tractable formulation. Therefore it often loses its generality. Thus to derive a MAP estimator for $\hat{\mathbf{Q}}_{|\mathbf{X},\mathbf{B},\mathcal{M}}$ Trujillo-Barreto et al. [178] had to condition the computation by a set of simplifying modeling assumptions

such as: noise is normally distributed, nuisance parameters of forward models have inverse Gamma prior distributions, and neuronal activation is described by a linear function of hemodynamic response. The results on simulated and experimental data from a somatosensory MEG/fMRI experiment confirmed the applicability of Bayesian formalism to the multimodal imaging even under the set of simplifying assumptions mentioned above.

Usually, model $\mathcal{M}$ is not explicitly mentioned in Bayesian formulations (such as (3.5)) because only a single model is considered. For instance, Bayesian formulation of LORETA E/MEG inverse corresponds to a DECD model, where $\boldsymbol{\Theta} = \mathbf{Q}$ is constrained to be smooth (in space), and to cover whole cortex surface. In the case of the *Bayesian Model Averaging* (BMA), the analysis is carried out for different models $\mathcal{M}_i$, which might have different nuisance parameters, *e.g.* E/MEG and BOLD signals forward models, possible spatial locations of the activations, constraints to regularize E/MEG inverse solution. In BMA analysis we combine results obtained using all considered models to compute the posterior distribution of the quantity of interest

$$p(\boldsymbol{\Delta}|\mathcal{D}) = \sum_i p(\boldsymbol{\Delta}|\mathcal{D}, \mathcal{M}_i)\, p(\mathcal{M}_i|\mathcal{D}), \tag{3.6}$$

where the posterior probability $p(\mathcal{M}_i|\mathcal{D})$ of any given model $\mathcal{M}_i$ is computed via Bayes' rule using prior probabilities $p(\mathcal{M}_i)$, $p(\mathcal{D})$ and the likelihood of the data given each model

$$p(\mathcal{D}|\mathcal{M}_i) = \int p(\mathcal{D}|\boldsymbol{\Theta}, \mathcal{M}_i)\, p(\boldsymbol{\Theta}|\mathcal{M}_i)\, d\boldsymbol{\Theta}. \tag{3.7}$$

Initially, BMA was introduced into the E/MEG imaging [177], where Bayesian interpretation of (1.8) was formulated to obtain $p(\mathbf{Q}|\mathbf{X}, \mathbf{F})$ for the case of Gaussian uncorrelated noise ($\mathbf{W}_{\mathbf{X}} = \mathbf{C}_\epsilon = \nu_\epsilon \mathbf{I}$). In order to create a model, the brain volume gets partitioned into a limited set of spatially distinct functional compartments, which are arbitrarily combined to define a $\mathcal{M}_i$, search space for the E/MEG inverse problem.

At the end, different models are sampled from the posterior probability $p(\mathcal{M}_i|\mathbf{X})$ to get the estimate of the expected activity distribution of ECDs over all considered source models

$$E[\mathbf{Q}|\mathbf{X}] = \sum_i E[\mathbf{Q}|\mathbf{X}, \mathcal{M}_i]\, p(\mathcal{M}_i|\mathbf{X})$$

$$\mathrm{Var}[\mathbf{Q}|\mathbf{X}] = \sum_i \mathrm{Var}[\mathbf{Q}|\mathbf{X}, \mathcal{M}_i]\, p(\mathcal{M}_i|\mathbf{X}),$$

where the normalized probability $p(\mathcal{M}_i|\mathbf{X})$, Bayes' Factor B_{i0}, and prior odds α_i, are

$$p(\mathcal{M}_i|\mathbf{X}) = \frac{\alpha_i B_{i0}}{\sum_k \alpha_k B_{k0}} \qquad B_{i0} = \frac{p(\mathbf{X}|\mathcal{M}_i)}{p(\mathbf{X}|\mathcal{M}_0)} \qquad \alpha_i = \frac{p(\mathcal{M}_i)}{p(\mathcal{M}_0)}$$

In the original BMA framework for E/MEG [177] $\alpha_i = 1\,\forall i$, *i.e.* the models had a flat prior PDF because no additional functional information was available at that point. Melie-García et al. [119] suggested to use the significance values of fMRI statistical t-maps to derive $p(\mathcal{M}_i)$ as the mean of all such significance probabilities across the present in $\mathcal{M}_i$ compartments. This strategy causes the models consisting of the compartments with significantly activated voxels get higher prior probabilities in BMA. The introduction of fMRI information as the prior to BMA analysis reduced the ambiguity of the inverse solution, thus leading to better localization performance. Although further analysis is necessary to define the applicability range of the BMA in E/MEG/fMRI fusion, it already looks promising because of the use of fMRI information as an additional evidence factor in E/MEG localization rather than a hard constraint.

Due to the flexibility of Bayesian formalism, various Bayesian methods solving E/MEG inverse problem already can be easily extended to partially accommodate evidence obtained from the analysis of fMRI data. For instance, correlation among different areas obtained from fMRI data analysis can be used as a prior in the Bayesian reconstruction of correlated sources [152]. The development of a neurophysiologic generative model of BOLD signal would allow many Bayesian inference methods (such as [156]) to introduce complete temporal and spatial fMRI information into the analysis of E/MEG data.

CHAPTER 4

MOTIVATIONS FOR FURTHER DEVELOPMENT OF MULTIMODAL METHODS

The only reason some people get lost in thought is because
it's unfamiliar territory

– Paul Fix

As shown above, fMRI BOLD signal is inherently non-linear as a function of neuronal activation. Nevertheless there have been multiple reports of linear dependency between the observed BOLD response and the selected set of E/MEG signal features. In general, such results are not inconsistent with the non-linearity of BOLD, since of course, often a non-linear function can be well approximately linear in the context of a specific experimental design, regions of interest, or dynamic ranges of the selected features of E/MEG signals. Besides dominant LFP/BOLD linearity reported by Logothetis and also confirmed in the specific frequency bands of EEG signal during flashing checkerboard experiment [168], there have been reports of a strong correlation between the BOLD signal amplitude and other features of E/MEG responses.

The exploration of techniques in addition to the ones presented in the Section 3.3, and analysis of the other components contributing to E/MEG signals might bring fruitful results in terms of the conjoint analysis. Next Section 4.1 discusses such possible novel directions before Section 4.2 sketches the motivation, goals and scope of this Ph.D. thesis.

4.1 Alternative Ways to Explore

In the past DC-E/MEG signal component (Section 1.1) has not been of an attention for multimodal integration, despite recent experiments showing the strong correlation between the changes of the observed DC-EEG signal and hemodynamic changes in the human brain [182]. In fact, such DC-E/MEG/BOLD coupling suggests that the integration of fMRI and DC-E/MEG might be a particularly useful way to study the nature of the time variations in HR signal. Such variations are usually observed during fMRI experiments but are not explicitly explained by the experimental design or by the physics of MR acquisition process.

Having selected features of the signals which would be involved in the fusion, many EMSI methods can be naturally extended to account for fMRI data if a generative forward model of BOLD signal is available. For instance, direct universal-approximator inverse methods [79, 80] have been found to be

very effective (fast, robust to noise and to complex forward models) for the E/MEG dipole localization problem, and could be augmented to accept fMRI data if the generative model for it was provided.

FMRI conditioned E/MEG DECD methods have been shown to be relatively simple and mathematically compelling for source imaging when there is a good spatial agreement between E/MEG and fMRI signals. Due to the advantages of these methods, it might be valuable to consider other advanced E/MEG DECD methods such as FOCUSS [60], which is known to bring improvement of estimation of focal sources over simple linear inverse methods [14].

ICA as a signal decomposition technique has been found effective in removing artifacts in E/MEG without degrading neuronal signals [82, 84, 174, 184], moreover it is known to be superior to PCA in the component analysis of E/MEG signals [81]. Initial research using ICA of fMRI in the spatial domain [118] was controversial, however consecutive experiments and generalization of ICA to fMRI in the temporal domain (see [27] for an overview) has increased its normative value. The development of ICA methods for the analysis of multimodal data provides a logical extension of the decomposition techniques covered earlier.

The formulation of a general BOLD signal model capable of describing the desired non-linear dependency in terms of neuronal activation and nuisance physiological parameters would constitute a major step toward the development of the multimodal methods with wider range of application than in the current "linear" domain. Since most of the multimodal methods presented before rely upon the linear dependence between signals, it is also important to analyze, expand and formalize the knowledge about the "linear" case, which is the simplest modeling assumption valid in many instances. Thus it deserves closer attention especially if we follow the notion of *Occam's razor* principle.

4.2 "The Challenge"

As many other attempts to process different brain imaging modalities, this work aims to develop a viable method for multimodal information integration. Such method should make use of the available temporal and spatial information from both functional brain imaging modalities such as fMRI and EEG or MEG. Being said, it is important to emphasize once again, that due to the uncertainty in the amount of synergy which is present between E/MEG and fMRI signals, a general methodology applicable to all brain imaging studies cannot yet to be defined. Nevertheless in the cases where the primary goal of the experiment is to gain a better resolution in the analysis of neuronal activations of the same origin (*e.g.* just motor, or just

visual activations), assumption of linearity might be valid if the experimental design is non-parametric, and activations are known to be reproducible and consistent over time. The assumption that fMRI and E/MEG signals generally correspond to the same neuronal activity taken along with experimental design restrictions, lets us consider simple generative models such as the convolutional model (Section 3.2.1).

The search for an *appropriate* brain imaging experiment converged to an interesting and challenging topic in the brain imaging: mapping of the primary motor cortex (M1) and the higher processing level areas (*e.g.* PMA, SMA, SI), *i.e.* the investigation of the assignment of different body parts motor actions to the responsible locations on the cortex. This type of studies took off more than a century ago with direct cortical stimulation in animals and the known pioneers in human studies were Penfield and Boldrey [142]. They made direct observations by stimulating the human brain with weak electrical shocks in conscious patients who were undergoing surgery. Well-known *homunculus* (Fig. 4.1), a caricature of the human form with body parts drawn in sizes that are proportional to the presumed extent of their representations, was one of the outcomes of their study.

All studies aiming to create a mapping of motor cortex (or also called somatotopy[1]) could be split into 2 major groups: active and passive. In active studies, cortex regions are stimulated either invasively through direct stimulation of the exposed cortex (*i.e.* during neurosurgical procedures) or non-invasively using such tools as TMS. Corresponding elicited motor movements or subject's description of sensation allows to discover the mapping. Safer and more challenging methodology is to register neuronal activation in primary motor (M1) and somato-sensory (S1) cortical areas using non-invasive brain imaging techniques such as E/MEG and fMRI, when subject is either performing some motor task (*e.g.* finger-tapping) or experiencing sensory or nerve stimulation. For instance, MEG experiment allowed to distinguish cubitus from clunis along the somato-sensory cortex (Fig. 4.1) when subjects experienced stimulation of the corresponding body part [43]. Fisher et al. [43] suggested that such kind of study could be used as a benchmark for different localization methods. Their idea supports the challenge present in this task.

Although coarse mapping of body parts is well studied, fine mapping of fingers while performing motor task is difficult to investigate with any non-invasive brain imaging technique [39, 70]. Consequently, some ad-hoc experimental design, thoughtful experimental setup, and advanced statistical processing [39] are required to extract the spatial sequencing between the adjacent fingers. It is even more challenging [70]

[1] *Somatotopic* - organized in a point-to-point representation of the surface of the body

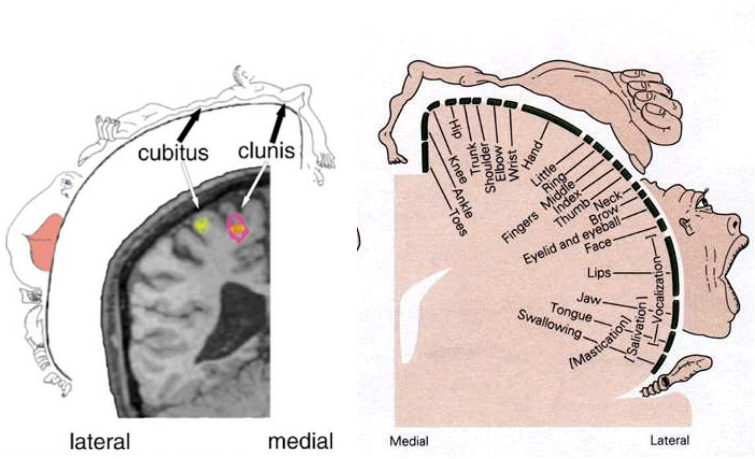

(a) (b)

Figure 4.1 **a** Identified sites of cortical activity, and 95% confidence ellipsoids, corresponding to stimulation of the clunis and cubitus superimposed on a representative magnetic resonance image. The two cortical sites are clearly distinct, with no overlap of the 95% confidence volumes. Furthermore, the data are in good agreement with Penfield's neurosurgically established homunculus. (Borrowed from [43]) **b** Detailed homunculus mapping.

to separate between finger taps sequential in time. After all of the research investigations, fine somatotopy of M1 remains a controversy. There is an emerging evidence from animal studies and fMRI human studies in favor of distributed and overlapping cortical somatotopy representation [39]. Thus a methodology able to resolve the ambiguity in this question, would be a prominent achievement in the field.

Before tackling the problem, it is helpful to highlight obvious problems with the existing studies:

- E/MEG studies investigating M1 somatotopy used single ECD modeling to get focal activation locations. This kind of modeling is unrealistic and very biased if activation is not adequately modeled by an ECD, which is often the case when there are multiple activation sites as it was suggested before. Preliminary localization studies using fMRI conditioned DECD modeling [9] were able to improve DECD localization in such kinds of tasks but they did not aim to discover and analyze the somatotopy;

- observed overlaps in BOLD detected activation sites can be simply due to the spatial spread of BOLD signal. Taking into account vessel structure or using novel protocols such as fCBF [143] might improve spatial resolution of fMRI studies, thus careful analysis of the experimental settings and protocols should be carried out before carrying out the mapping experiment using fMRI;

- poor temporal resolution of BOLD signal does not allow any reliable sub-second temporal separation of the motor events, thus reliable separation between sequential in time (sub-second interval) finger taps cannot be achieved.

Bringing both E/MEG and fMRI modalities together is hoped to provide grater amount of spatio-temporal information about motor activations. Although it is necessary to use highly parameterized models to describe motor activations registered with fMRI [197], they are believed to be consistent and reproducible in time. Consequently they satisfy our restrictions for multimodal analysis stated before. The goal of this Ph.D. project becomes: **to propose multimodal analysis methods and validate them on conjoint EEG/fMRI finger-tapping experiment**.

The methods for conjoint analysis proposed in this dissertation rely on simultaneous fitting of the signals from both given modalities using the models of observed signals at the high temporal and spatial resolution. Such modeling of both signals which are produced by temporal (fMRI) and spatial (E/MEG) filtering of the neuronal activity, implicitly defines regularization for the E/MEG inverse problem, thus making it less ill-conditioned.

It is important first to validate the suggested methods, *i.e.* verify their capabilities and compare to the existing methods. Chapter 6 presents the results and comparisons to the other methods when applied to artificially generated data. While performing such simulations, it would be possible to investigate the ranges of signals and noise characteristics in which suggested methods could be applied to provide reliable results. In order to reach the goal stated above the future thesis work will consist of the experimental design and the analysis of acquired neuroimaging data.

CHAPTER 5

MULTIMODAL IMAGING USING L-NORMS SIGNAL RECONSTRUCTION

First, this chapter introduces a general formulation of the fusion problem. After that, the description of proposed methods to derive the solution under different problem conditions follows: generic formulation in terms of the minimization of the squared sum error (L_2 norm), outliers insensitive formulation using minimization of the absolute error sum (L_1 norm), and the simplifications of the problem in case of fixed source orientation.

5.1 Generalized Problem Formulation

5.1.1 Forward Models

According to DECD model of E/MEG signals (Section 1.3.2) and a simple convolutional model (Section 3.2.1) for BOLD signal, we can summarize performed forward modeling as

Modality	Data Matrix	Size	Model
fMRI	$\mathbf{F}$	$N \times U$	$\hat{\mathbf{F}} = \tilde{\mathbf{Q}}\mathbf{B}$
E/MEG	$\mathbf{X}$	$M \times T$	$\hat{\mathbf{X}} = \mathbf{G}\mathbf{Q}$

$$\mathbf{Q} = \begin{bmatrix} \mathbf{Q}_x \\ \mathbf{Q}_y \\ \mathbf{Q}_z \end{bmatrix},$$

where $\tilde{\mathbf{Q}}(\mathbf{Q})$ ($N \times T$ matrix) represents the strength of the dipoles without orientation information $\tilde{q}_{jt} = \sqrt{q_{xit}^2 + q_{yit}^2 + q_{zit}^2}$; $\mathbf{\Theta}(\mathbf{Q})$ ($3N \times T$ matrix) contains pure orientation as $\Theta_{jt} = q_{jt}/\tilde{q}_{it}$, where $i = j \bmod N$[1]; $\mathbf{B}$ ($T \times U$ matrix) is a circulant matrix which corresponds to the temporal filtering of the neuronal signal amplitude to reconstruct BOLD response using the convolutional model (Section 3.2.1); and $\mathbf{G}$ ($M \times 3N$ matrix) is a lead field matrix for NEM (Section 1.3.2). In the case of fixed known orientations of the dipoles representing neuronal generators, a single projection of the strength to that direction is used, thus $\tilde{\mathbf{Q}} = \mathbf{Q}$.

5.1.2 Objective Function

The objective of the presented multimodal analysis is to estimate a temporally and spatially superior modality $\mathbf{Q}$ which is used to reconstruct both $\hat{\mathbf{X}}$ and $\hat{\mathbf{F}}$ using described forward models. The reconstruction

[1]Here and further we will use $j \in \{1..3N\}$ and corresponding $i \in \{1..N\}$, s.t. $j \in \{i, i+N, i+2N\}$ for the projections of the ith dipole on 3 axis (see Section 1.3.2 for more details)

aims to minimize the residuals between the empirical and reconstructed values: $\hat{\mathbf{X}}(\mathbf{Q}) - \mathbf{X}$ and $\hat{\mathbf{F}}(\mathbf{Q}) - \mathbf{F}$. Because these signals are of different dimensionality, measured in different units and subject to different noise levels, it is appropriate to define scaled residuals $\Delta_{\mathbf{X}}(\mathbf{Q}) = \frac{\hat{\mathbf{X}}(\mathbf{Q}) - \mathbf{X}}{\sqrt{\nu_{\mathbf{X}} MT}}$ and $\Delta_{\mathbf{F}}(\mathbf{Q}) = \frac{\hat{\mathbf{F}}(\mathbf{Q}) - \mathbf{F}}{\sqrt{\nu_{\mathbf{F}} NU}}$, if the noise is uncorrelated and has the same variance across sensors $\nu_{\mathbf{X}}$ and $\nu_{\mathbf{F}}$.

By introducing a *trade-off* parameter α between the quality of fit of two acquired modalities, the *regularization* parameter λ, and regularization function $\mathcal{C}(\mathbf{Q})$, objective function (1.6) can be extended for multimodal case as

$$\mathcal{E}_r(\mathbf{Q}) = \|\Delta_{\mathbf{X}}(\mathbf{Q})\|_l + \alpha \|\Delta_{\mathbf{F}}(\mathbf{Q})\|_l + \lambda \mathcal{C}(\mathbf{Q}) \tag{5.1}$$

where $l \in \{1, 2\}$ is the norm to define specific error cost function and $\mathcal{C}(\mathbf{Q})$ can incorporate some other constraints such as the smoothness of the solution in time or in space, minimal norm of the solution requirement, etc.

5.2 L_2 Error, Variable Orientation – Gradient Descent

In the case of $l = 2$, cost function (5.1) is represented as a sum of squared errors over the residuals. Taking its derivative leads to a simple gradient descent rule

$$\mathbf{Q}_{\tau+1} = \mathbf{Q}_\tau - \eta \frac{\partial \mathcal{E}_r(\mathbf{Q})}{\partial \mathbf{Q}}, \text{where } \eta \text{ is a learning rate.} \tag{5.2}$$

$$\frac{\partial \mathcal{E}_r(\mathbf{Q})}{\partial \mathbf{Q}} = \frac{\partial \Delta_{\mathbf{X}}(\mathbf{Q})}{\partial \mathbf{Q}} + \alpha \frac{\partial \Delta_{\mathbf{F}}(\mathbf{Q})}{\partial \mathbf{Q}} + \lambda \frac{\partial \mathcal{C}(\mathbf{Q})}{\partial \mathbf{Q}} \tag{5.3}$$

$$\frac{\partial \Delta_{\mathbf{X}}(\mathbf{Q})}{\partial \mathbf{Q}} = 2\mathbf{G}^T(\mathbf{X} - \mathbf{G}\mathbf{Q}), \frac{\partial \Delta_{\mathbf{F}}(\mathbf{Q})}{\partial \mathbf{Q}} = 2\mathbf{\Theta} \star \left((\mathbf{F} - \tilde{\mathbf{Q}}\mathbf{B})\mathbf{B}^T\right), \tag{5.4}$$

where $\cdot \star \cdot$ operation corresponds to element-wise product of two matrices.

5.3 L_2 Error, Fixed Orientation

In the case of quadratic error and fixed orientation ($\tilde{\mathbf{Q}} = \mathbf{Q}$) derivative $\frac{\partial \Delta_{\mathbf{F}}(\mathbf{Q})}{\partial \mathbf{Q}}$ simplifies

$$\frac{\partial \Delta_{\mathbf{F}}(\mathbf{Q})}{\partial \mathbf{Q}} = 2\,\mathrm{sign}(\mathbf{Q}) \star \left((\mathbf{F} - \tilde{\mathbf{Q}}\mathbf{B})\mathbf{B}^T\right). \tag{5.5}$$

Instabilities in optimization brought by $\mathrm{sign}(x)$ can be reduced by using some smooth function which approximates it well (*e.g.* squashed hyperbolic tangent function).

It is very appealing to reformulate (5.4) in a presence of constraint $\mathbf{Q} > 0$

$$\frac{\partial \Delta_{\mathbf{X}}(\mathbf{Q})}{\partial \mathbf{Q}} = 2\mathbf{G}^T(\mathbf{X} - \mathbf{G}\mathbf{Q})\,, \frac{\partial \Delta_{\mathbf{F}}(\mathbf{Q})}{\partial \mathbf{Q}} = 2(\mathbf{F} - \mathbf{Q}\mathbf{B})\mathbf{B}^T\,, \tag{5.6}$$

and if no additional constraints are imposed ($\lambda\,\mathcal{C}(\mathbf{Q}) = 0$), then $\mathbf{Q}$ can be found as a solution of

$$\begin{aligned}
\frac{\partial \mathcal{E}_r(\mathbf{Q})}{\partial \mathbf{Q}} &= \frac{\partial \Delta_{\mathbf{X}}(\mathbf{Q})}{\partial \mathbf{Q}} + \alpha \frac{\partial \Delta_{\mathbf{F}}(\mathbf{Q})}{\partial \mathbf{Q}} = 0 \\
\mathbf{G}^T(\mathbf{X} - \mathbf{G}\mathbf{Q}) + \alpha\,(\mathbf{F} - \mathbf{Q}\mathbf{B})\mathbf{B}^T &= 0, \\
\mathbf{G}^T\mathbf{G}\,\mathbf{Q} + \mathbf{Q}\left(\alpha\,\mathbf{B}\mathbf{B}^T\right) - \left(\alpha\,\mathbf{F}\mathbf{B}^T + \mathbf{G}^T\mathbf{X}\right) &= 0,
\end{aligned}$$

known as Sylvester equation, for which efficient solvers exist. But presence of the constraint $\mathbf{Q} > 0$ forbids us from using this simple formulation.

5.4 L_1 Error Minimization - LP Minimization

Using defined abbreviations we formulate an initial LP problem as follows

$$\hat{\mathbf{X}} + \Delta_{\mathbf{X}} = \mathbf{X} \qquad \text{Constraints} \tag{5.7}$$

$$\hat{\mathbf{F}} + \Delta_{\mathbf{F}} = \mathbf{F} \tag{5.8}$$

$$\tilde{q}_{ij} \geq 0 \qquad \text{Region} \tag{5.9}$$

$$\mathcal{E} = \|\Delta_{\mathbf{X}}\|_1 + \alpha\|\Delta_{\mathbf{F}}\|_1 \qquad \text{Objective}\,, \tag{5.10}$$

where α is used to check different trade-offs between two modalities as well as to normalize their influence in the optimization criteria.

Next we redefine each $|x|$, which are present in computation of $\mathcal{E}$ (5.10) and $\tilde{q}_{ij}$ (5.12), in a form suitable for LP as shown in Appendix B. These transformations lead to a side effect, namely minimization of the sum of absolute values $|s_{ij}|$, so we need to add another term $\gamma\|S\|_1$ to the objective function (5.10). This side effect could be considered a desired result - the minimization of L_1 norm of the solution results in its increased sparseness.

Transformation to LP

It is required to agree on the order of how any 2D array is "unfolded" into a 1D sequence. Each unfolded matrix $\mathbf{X}$ is presented as a vector $\bar{\mathbf{X}}$ and it is decomposed row-wise - rows compose unfolded matrix when

taken sequentially. So for $\mathbf{Q}$ $3N\times T$ matrix, which is the argument of optimization we want to obtain, we get vector $\bar{\mathbf{Q}}$ $3NT\times 1$ where the order of dimensions growth within the vector is $t \rightarrow$ *sensor* $\rightarrow$ orientation(*axis*), therefore time is the fastest growing dimension.

E/MEG Equation in LP form

We can represent (5.7) in a form suitable for LP using the Kronecker product

$$(\mathbf{G} \otimes \mathbf{I}_T)\bar{\mathbf{Q}} = \bar{\mathbf{X}} \tag{5.11}$$

where $\mathbf{I}_Z$ is the identity matrix of size $Z\times Z$.

FMRI Equation in LP form

First we need to encode the definition of $\tilde{\mathbf{Q}}$ into an LP constraint matrix using an approximation described in Appendix B.2,

$$\tilde{\mathbf{Q}} = l(|\mathbf{Q}_x|, |\mathbf{Q}_y|, |\mathbf{Q}_z|), \tag{5.12}$$

where $l(\cdot)$ is an LP approximation of the L_2 norm.

In a similar to (5.11) way we represent the product $\tilde{\mathbf{Q}}\mathbf{B}$ in a form suitable for LP

$$\hat{\mathbf{F}} = (\mathbf{I}_N \otimes \mathbf{B}^T)\bar{\tilde{\mathbf{Q}}} \tag{5.13}$$

Final LP form

Finally we group all the constraints and the objective function together into an extended LP canonical form,

$$(\mathbf{G} \otimes \mathbf{I}_T)\bar{\mathbf{Q}} + \Delta_{\bar{\mathbf{X}}} = \bar{\mathbf{X}} \tag{5.14}$$

$$(\mathbf{I}_T \otimes \mathbf{B}^T)\bar{\tilde{\mathbf{Q}}} + \Delta_{\bar{\mathbf{F}}} = \bar{\mathbf{F}} \tag{5.15}$$

$$\tilde{\mathbf{Q}} - l(|\mathbf{Q}_x|, |\mathbf{Q}_y|, |\mathbf{Q}_z|) = 0 \tag{5.16}$$

$$\bar{\tilde{\mathbf{Q}}} \geq 0 \tag{5.17}$$

$$\mathcal{E} = ||\Delta_{\mathbf{X}}||_1 + \alpha||\Delta_{\mathbf{F}}||_1 + \gamma||S||_1 \tag{5.18}$$

5.5 Remarks

It is necessary to list restrictions and omitted factors which have to be considered in the given models when working with real data. Due to the undetermined BOLD fMRI forward model, unknown coupling coefficient ξ to map neuronal activation (dipole strength) to BOLD signal ($\xi = \mathbf{B}_{\cdot,i}/||\mathbf{B}_{\cdot,i}||$) yet to be estimated. Approaches to consider when applying the suggested methods to real data are

- ξ parameter can be naturally included in the L_2 formulation. Then it simply becomes yet another argument for the optimization. For L_1 it is necessary to seek for other means of estimation as following;
- normalization by matching the variances of the produced signals and their fit residuals. This is the simplest approach but the analysis of occurring bias is necessary;
- Bayesian approach: either to find the coefficient having maximal probability (*i.e.* to find MAP), or sample model space and find model average based on different possible values of the coefficient. Bayesian approach requires specification of prior pdf of the coefficient, thus can be arbitrarily biased. Taking uniform probability would lead to a maximum likelihood solution;

CHAPTER 6

MULTIMODAL IMAGING: SIMULATION STUDY

This works every time, provided you're lucky

– Unknown soul-mate

As previously emphasized, any novel methodology has to be validated first on the dataset with known characteristics of the noise and of the signal of interest (*i.e.* of spatio-temporal signals of the neuronal activation in case of neuroimaging). Due to the absence of a realistic phantom study involving covered here brain imaging modalities, it was necessary to simulate the signal and noise conditions. This chapter describes the protocol used to simulate the dataset and provides analysis of the results obtained using different localization methods including the ones presented in the preceding chapter. Results of the analysis using some conventional multimodal methods (*e.g.* fMRI conditioned DECD) and L_2 norm misfit methods presented in the previous chapter follow.

6.1 Simulated Dataset Generation

Simulated dataset consists of an ROI region of the brain uniformly sampled for possible source locations and the corresponding simulated brain imaging signals (EEG, MEG and fMRI). Temporal sampling of the source space $\mathbf{Q}$ was taken to be 16 [Hz], which allowed to represent simulated neuronal activations as truncated Gaussian with the deviation of 50 [ms].

6.1.1 Forward Modeling

In this study, conductivity boundaries and cortical surfaces were determined from MRI anatomy of a template brain [30] (Fig. 6.1). MRI scan, tessellated surfaces, and original E/MEG electrodes locations (181 EEG and 138 MEG electrodes) (Fig. 6.2) were provided along with *Brainstorm* software package [106]. Realistic BEM model with 3 compartments (brain+cerebral fluid, skull, scalp with conductivities 0.33, $.0042$, and 0.33 respectively) was used to approximate the solution of the forward E/MEG problem for the 30 sensors of each E/MEG modality which were located in the vicinity of the ROI.

"Hand area" of M1 is the area of interest for this simulation study. Therefore appropriate region defined by 239 out of $10,000$ vertices of the whole cortical surface was selected (Fig. 6.3). Mean distance between any two sampled source points within selected ROI was $4.3\,\mathrm{mm}$. The furthest distance between

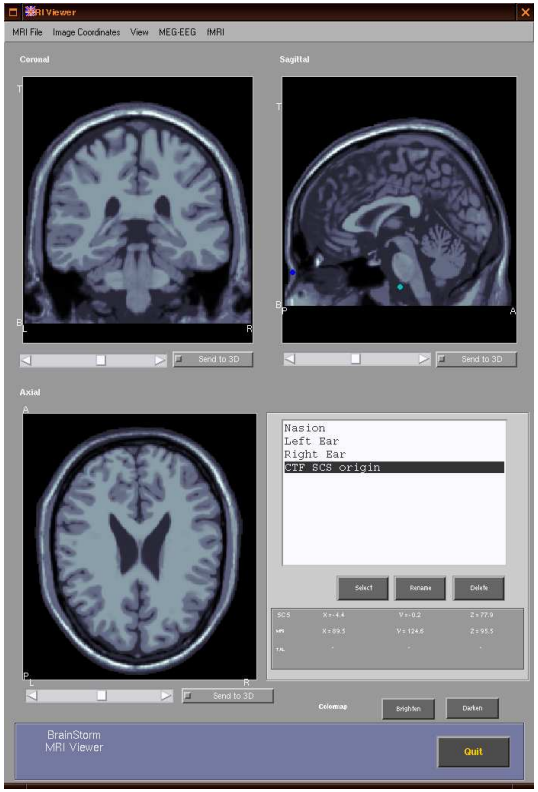

Figure 6.1 3 slices of MRI with marked fiducial points (Screenshort from Brainstorm [106])

any two points within ROI constituted $47.4\,\mathrm{mm}$. Region of interest ("Hand area") was reported to be considerably smaller - up to $18\,\mathrm{mm}$ [39] and lie around the Ω shaped "knob" covered by the selected ROI (Fig. 6.3).

Space around ROI cortical area was sampled with the resolution of 2 [mm] to generate 895 possible source locations, which also constitute a modeling space for fMRI signal (Fig. 6.4) and serve as locations for dipoles generating E/MEG signals.

Each possible source location was characterized with the orientation of a normal of a closest vertex on the surface of ROI. Such orientation was used for forward modeling of E/MEG signals using pre-computed BEM models.

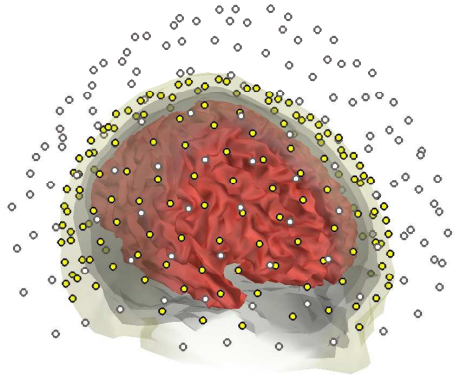

Figure 6.2 MEG (grey) and EEG (yellow) electrodes locations along with tessellated brain volume into 4 boundary structures: (listed from the inside out) white/grey matter boundary (cortex boundary), inner skull, outer skull, and scalp surfaces (Part of the skull and scalp surfaces displayed transparent for visualization purposes. Screenshort from Brainstorm [106])

6.1.2 Additive Noise

Simulation studies often generate additive noise contaminating clean signal using very simplistic models such as Gaussian white noise. Because suggested fusion methodology relies on spatio-temporal analysis of the data, such noise modeling would be overly simplistic for the goals of current study. That is why simple Gaussian noise and realistic noise from experimental data were considered. Realistic noise was obtained from the epochs of EEG, MEG and fMRI datasets collected during "rest" periods of the experiments. Such data were hoped to bear minimal amount of the signals corresponding to spontaneous neuronal activity, nevertheless careful pre-processing was required to eliminate signal components which were caused by muscle artifacts, or had prominent localization, thus unlikely to be a part of instrumental or even neurological noise. The details of carried preprocessing are covered in the Appendix D.

6.1.3 Simulation Protocol

Datasets/Activations: Source space (**Q**) consists of 895 possible source locations during 1 [sec] and at a sampling rate of 16 [Hz]. E/MEG signals were simulated accordingly for a given period of time (*i.e.* 1 [sec]). FMRI signal, due to its time-lagged hemodynamic response was modeled at a temporal sampling rate of 1 [Hz] (TR=1 [sec]) for the duration of 10 [secs].

Totally 5 datasets were generated. First 4 datasets consist of non-overlapping spatially activations,

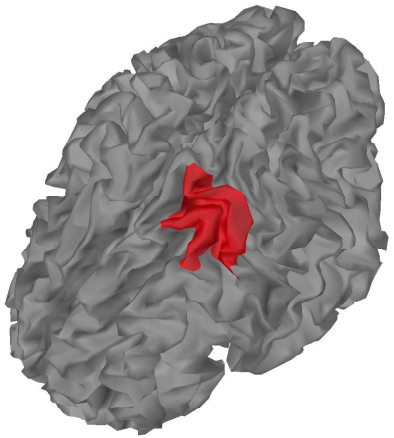

Figure 6.3 Contralateral to the right hand central sulcus along with pre- and post-central gyri (area in red) were selected as the region of simulated neuronal activations faking the response to motor actions. The choice of such region is directed by different imaging studies of detected elicited neuronal responses in response to motor actions of the hand and/or fingers [42, 198]. (Screenshort from Brainstorm [106])

i.e. when only a single activation could appear in a voxel at some random moment in time. These datasets have different number of active sources randomly (spatially and temporally) chosen to be active: $[1,\ 10,\ 100,\ 895]$ sources. The last dataset has 10 randomly activated locations with a following within 100–300 [ms] second activation at the same spatial location[1]. Activations in all cases were modeled by a truncated (at 10% of area) Gaussian with the deviation of 50 [ms]. Each dataset has 30 **epochs**, which differed by the randomly chosen source temporal and spatial locations confirming dataset requirements;

E/MEG type: Both EEG and MEG signals are considered (one at a time) for the fusion with fMRI signal;

Noise Type: Two types of noise are used: empirical (as described in Section 6.1.2) and Gaussian white noise;

Noise Level: Due to the fact that signals of interest are sparse in time, there is no sense to characterize noise level as the ratio between signal power and noise power. Thus the amount of noise added

[1]Datasets were given "codenames" NONOVERLAP1, NONOVERLAP10, NONOVERLAP100, NONOVERLAP895, and OVERLAP10 accordingly

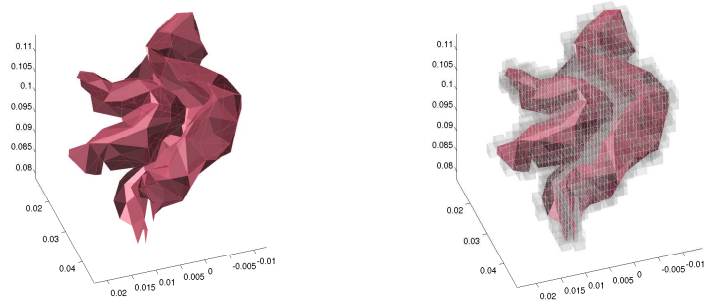

(a) Cortical Mesh (b) Cortical Mesh and Surrounding Voxels

Figure 6.4 Region of interest which includes "hand area" of M1 is a source space for modeled neuronal activations

to a signal is defined in terms of the ratio between noise deviation and maximal signal amplitude: $\varepsilon = \sigma_\epsilon / \max(s)$. Datasets for following noise levels $\varepsilon = [0,\ 0.1,\ 0.2,\ 0.4,\ 0.6]$ were generated;

Trials: For each instance of the signal, noise type, and noise level 30 trials (runs) were generated, so the same underlying signal was contaminated with different noise samples. Further, epochs were averaged. Such transformation reduces noise variance by a factor of $\sqrt{30}$. That was done to boost SNR of the acquired signals – a common practice in neuroimaging. In the future, these simulated trials will be used individually to provide statistical measures for the quality of the solution.

6.1.4 Algorithms Tested

To validate the advantage of the suggested fusion method, it is necessary to compare its performance to other methods established in the field. For this study we tested L_2 norms methods (fixed and variable orientation) against DECD methods (Section 1.3.2) where the solution at any given point in time is

$$\hat{\mathbf{Q}} = \mathbf{G}^{+}\mathbf{X}, \tag{6.1}$$

where

$$\mathbf{G}^{+} = \mathbf{W}_\mathbf{Q}\mathbf{G}^{\top}(\mathbf{G}\mathbf{W}_\mathbf{Q}\mathbf{G}^{\top})^{-1}. \tag{6.2}$$

DECD solutions were conditioned using a combination of the following methods

Conditioning of the Inverse: Truncated SVD was used to find stable inverse of $(\mathbf{G}\mathbf{W}_{\mathbf{Q}}\mathbf{G}^{\top})$. Singular values smaller than the projected noise variance were discarded;

Gain Matrix Normalization: Two possible cases were considered: with and without column normalization (Section 1.3.2): $\mathbf{W}_{\mathbf{Q}} = \mathbf{W}_{\mathrm{n}} = \left(\mathrm{diag}\,(\mathbf{G}^{\top}\mathbf{G})\right)^{-1}$;

Relative FMRI Weighting: Following the ideas described in Section 3.3.4, considered ν_0 values were $[\,1.0,\ 0.5,\ 0.1\,]$ which correspond to 0, 50, and 90% of relative fMRI weighting.

Such range of conditioning was hoped to cover the variability in possible DECD solutions conditioned or not ($\nu_0 = 1.0$) by fMRI. Besides that, DECD solutions with variable and fixed (to original) orientations were considered.

6.1.5 Results

To compare between different methods an error metric had to be chosen. In the current study, quality of the source time line reconstruction is considered to be the primary comparison criterion. Localization comparison is a much wider topic and will be addressed in the future. Quality of the source signal reconstruction is measured with a quadratic error measure $||\hat{\mathbf{Q}} - \mathbf{Q}||_2^2$ over the source locations with present activation. Quadratic error is further normalized by the squared norm of the source $||\mathbf{Q}||_2^2$ to characterize the quality criterion as a relative amount of noise energy brought into the source estimate. To summarize, $E = ||\hat{\mathbf{Q}} - \mathbf{Q}||_2^2 / ||\mathbf{Q}||_2^2$ and thus its minimal value $E = 0$ corresponds to the perfect restoration of the sources time course. For each epoch, best result across differently conditioned (as described in the previous section) DECD solutions was chosen.

Optimization of L_2 cost function (5.4) was carried out via conjugate gradient with a line search, which allows to avoid the use of the Hessian which is of unfeasible dimension size for this task. A set of $\alpha = [\,0.5,\ 1,\ 10\,]$ for a tradeoff between E/MEG and FMRI fit were used. Only the best result is reported in the plots.

Fig. 6.5, Fig. 6.6, Fig. 6.7, Fig. 6.8, and Fig. 6.9 present the comparison between the results achieved using FMRI conditioned DECD methods and L_2 -Fusion method suggested in this work. Plots show mentioned above criterion E for both E/MEG signals separately (each one owns a row) and with different types of the noise used for modeling of the signals. As it is seen from all of the plots, novel method often

outperforms DECD providing higher quality source signal reconstruction with a lighter influence of the noise level. As expected, the increase in the error of reconstruction closely follows the increase in number of activated sources. L_2 method provides much better solution in the case of sources spatially overlapping (Fig. 6.9).

Surprisingly, there is a strong difference between EEG and MEG results. There is a much higher reconstruction error of DECD estimates in case of MEG, especially for high noise values and a large number of activations. Such difference can possible be explained by the fact that a large part of the source space is located on the surface of pre-motor and post-motor gyri, which means that such sources are radially oriented to the skull surface. MEG sensitivity for imaging of such sources is known to be poor even in the cases of realistic head modeling (Section 1.1). Minimum norm solution thus discards such activations in favor of the minimal norm regularization term. L_2 norm method doesn't explicitly suppress such activations if they comply with the reconstruction of fMRI signal. In the future work, regional sensitivity analysis will be carried out to verify such explanations. Additional simulations utilizing higher number of sensors might reveal the other source of such difference.

The nature of the added noise (Empirical vs simulated Gaussian) does not seem to affect the results much. This fact supports the choice of Gaussian distribution for the creation of simulated datasets. Nevertheless it is important to continue comparing results with empirical and simulated noise, because some other performance characteristics (*e.g.* localization quality) might reveal the difference.

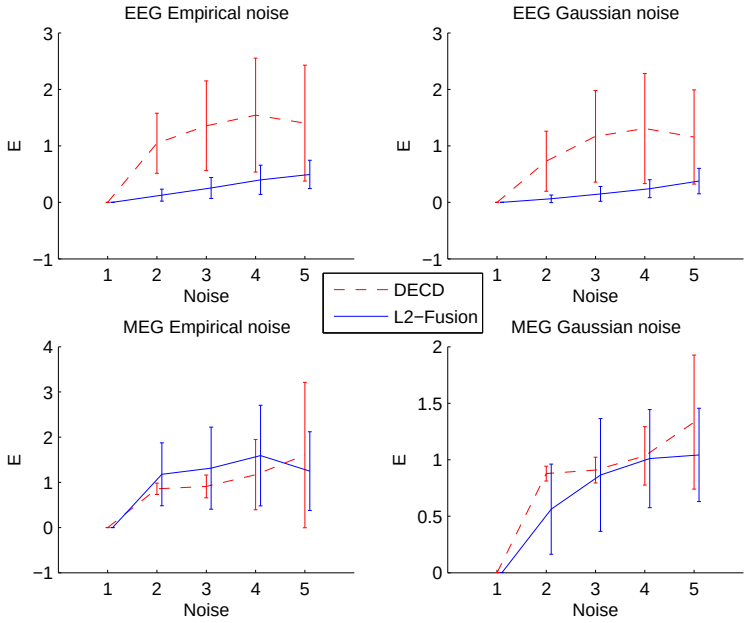

Figure 6.5 Dataset NONOVERLAP1: Solutions comparison. L_2 -Fusion plots are intentionally shifted a fraction for ease of observation.

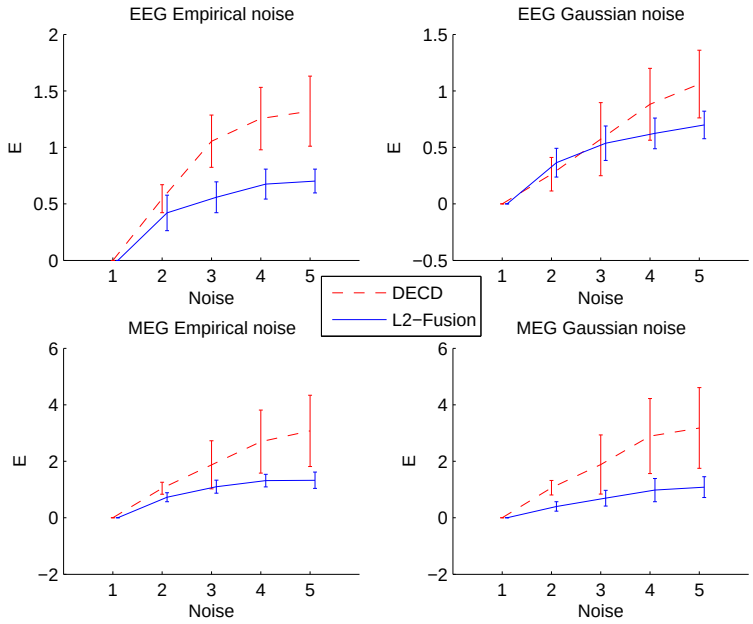

Figure 6.6 Dataset NONOVERLAP10: Solutions comparison.

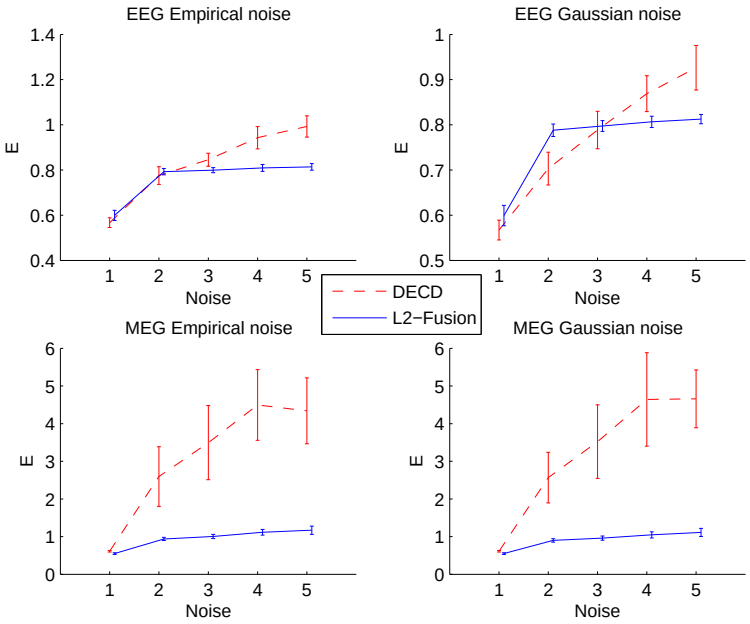

Figure 6.7 Dataset NONOVERLAP100: Solutions comparison.

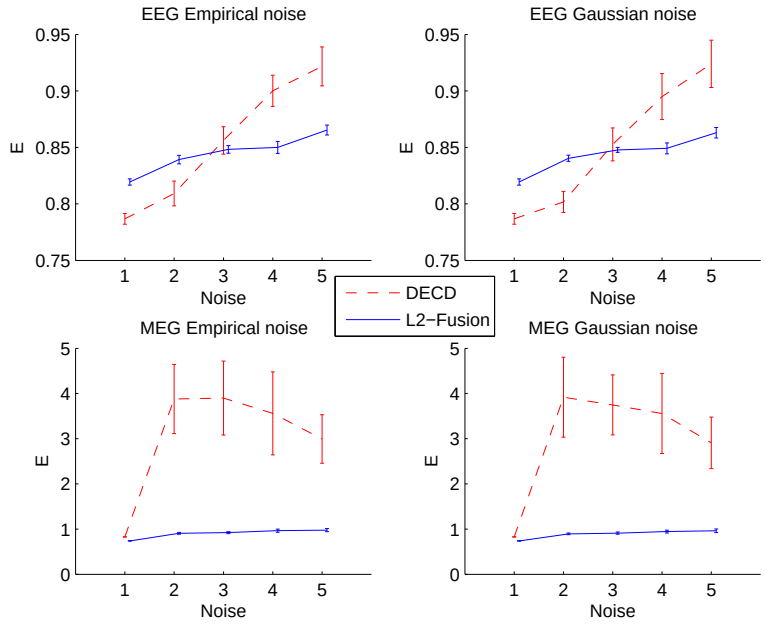

Figure 6.8 Dataset NONOVERLAP895: Solutions comparison.

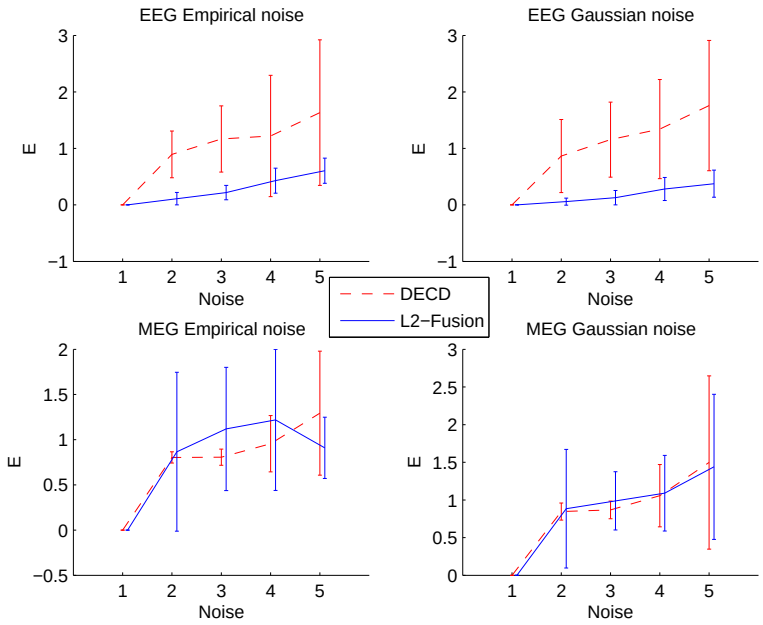

Figure 6.9 Dataset OVERLAP10: Solutions comparison.

CHAPTER 7

FURTHER RESEARCH

There is no such thing as failure, only results, with some more successful than others

– Jeff Keller *Attitude is Everything, Inc.*

Future work requires further analysis of the simulated data to get a better control over the suggested novel methods, and a better understanding of noise and experimental conditions which could provide stable source reconstruction and localization. Future directions include

- Verify L_1 -Fusion method on the simulated datasets. So far only L_2 methods were tested on the somatotopy simulated data (preliminary results of using L_1 -Fusion on other simulations were reported elsewhere [63]);
- Incorporate, and verify advantages of additional constraints (*e.g.* smoothness in time or in space) in the fusion cost function;
- Extend the models to handle cases of a slight spatial misalignment between E/MEG sources and fMRI BOLD signal activations;
- Choose or devise an appropriate localization technique to extract spatio-temporal activation locations from the estimated source time courses;
- Analyze complex activation patterns and cover wider area including SMA, PMA, and SI;
- Verify approaches suggested in Section 5.5 before applying analysis methods to empirical data.

After satisfactory results achieved on the simulated data, it will make it reasonable to apply the suggested methods to the empirical data in attempts to obtain trustworthy results. Thus next coarsely grained research tasks should be taken care of

- Elaborate experiment design and acquisition protocol which would allow high resolution spatio-temporal multimodal analysis;
- Estimate empirical HRF for the activations in the areas of interest;

- Apply suggested multimodal methods to the empirical data to recover fine somatotopy, and to complete the challenge – recover the temporal sequence of activated fingers.

APPENDIX A

FREE SOFTWARE GERMANE TO MULTIMODAL ANALYSIS OF EEG/MEG/FMRI DATA

	Forward						EEG/MEG Inverse			MRI†					fMRI	Environment			
	EEG			MEG															
Package	Spherical	BEM	FEM	Spherical	BEM	FEM	ECD	DECD	Beamforming	Brain Segm.	Skull Segm.	Scalp Segm.	Tessellation	E/MEG Regist.		Matlab	POSIX‡	Mac OS X	MS Windows
Brainstorm [106]	√	√		√	√			√	√				⇅	√		√			
NeuroFEM [129]/Pebbles	√	√	√	√	√	√	√	√					⇅				√	√	
BioPSE [18]/SCIRun [160]	√	√	√				√	√					⇅		√	⇅	√		
Brainvisa/Anatomist [146]										√		√	√		√		√	√	√
FreeSurfer [46]										√		√	√		√		√	√	
Surefit [180]										√		√	√		√		√		
Brainsuite [163]										√	√	√	√						√
EEG/MEG/MRI tlbx* [192]	√			√			√	√		⇅	⇅	⇅	⇅	√	√	√			
MEG tlbx* [124]				√			√	√		√	√	√	√	√	√	√			
EEGLAB/FMRILAB [40]							√								√	√			

†An extensive MR segmentation bibliography is available online [131].

‡POSIX includes all versions of Unix and GNU/Linux. Most POSIX packages listed use X Windows for their graphical output.

*Matlab Toolbox.

APPENDIX B

CANONICAL FORM FOR LP

Above we have freely used the minimum operator in formula like $a = \min(b, c)$, the absolute value function $y = |x|$, and other constructs not allowed in the canonical form of a linear program. In this section we describe a general technique for reducing a system of linear equalities and inequalities which include minimization of the L_1 norm, $|\cdot|$ and $\min(\cdot, \cdot)$ operators, along with a linear objective function, into a linear programming problem in standard canonical form.

B.1 Absolute Value

Commonly accepted way to deal with absolute value function $y = |x|$ in LP is to represent x as a difference of two non-negative numbers, with $|x|$ as their sum. Minimization of the sum would force one of them to become 0, with the other corresponding to $|x|$:

$$x = x^+ - x^- \tag{B.1}$$

$$|x| = x^+ + x^- \tag{B.2}$$

$$x^+ \geq 0 \tag{B.3}$$

$$x^- \geq 0 \tag{B.4}$$

while minimizing $|x|$

B.2 Minimal Value

To obtain $a = \min(b, c)$ we first relax it to

$$a \leq \min(b, c), \tag{B.5}$$

Inclusion of a $-a$ term in the objective function will lead to maximization of a thus achieving the necessary equality. Equality (B.5) can be easily represented in a form suitable for LP

$$a - b \leq 0$$

$$a - c \leq 0$$

Approximation of l_2 norm in LP

The magnitude of a dipole with moment vector $\mathbf{m} = (x, y, z)$ is $||\mathbf{m}|| = \sqrt{x^2 + y^2 + z^2}$. We assume that FMRI readings are related linearly to dipole magnitudes. In order to fit this into an LP framework, we need a way to approximate $e = ||\mathbf{m}||$ within an LP. Our solution is to note that the $\min(\cdot, \cdot)$ and modulus $|\cdot|$ functions can be used freely in a LP and then reduced to canonical form using the transformation described below. For our method, let $\{\mathbf{R}_i\}$ be a set of rotation matrices. To approximate $||\mathbf{m}||$ we let

$$e_i = ||\mathbf{R}_i\mathbf{m}||_1 \qquad e = \min_i e_i \tag{B.6}$$

where $||\cdot||_1$ denotes the l_1 norm. These can simply be added to the linear programming problem, enforcing the relation $e \approx ||\mathbf{m}||$. We can increase the number of matrices in the set to improve the accuracy of this approximation, at the expense of computational efficiency.

APPENDIX C

3D RIGID TRANSFORMATION VIA QUATERNIONS

To find the minimum of the squared error function $\varepsilon(\mathbf{R}, \mathbf{v}) = \sum_{i}^{P} (\mathbf{x}_i^M - \mathbf{x}^{E \to M})^2$ (Section 3.1.1), it is necessary to calculate a principal eigenvector

$$\mathbf{r} = \max\_\text{eigenvector} \begin{bmatrix} \text{tr}(\mathbf{\Sigma}) & \mathbf{\Delta}^\top \\ \mathbf{\Delta} & \mathbf{\Sigma} + \mathbf{\Sigma}^\top - \text{tr}(\mathbf{\Sigma})\mathbf{I}_3 \end{bmatrix},$$

where

$$\bar{\mathbf{x}} = \frac{1}{P} \sum_{i}^{P} \mathbf{x}_i \qquad \mathbf{\Sigma} = \frac{1}{P} \sum_{i}^{P} (\mathbf{x}_i^E - \bar{\mathbf{x}}^E)(\mathbf{x}_i^M - \bar{\mathbf{x}}^M)^\top \qquad \mathbf{\Delta} = \begin{bmatrix} (\mathbf{\Sigma} - \mathbf{\Sigma}^\top)_{23} \\ (\mathbf{\Sigma} - \mathbf{\Sigma}^\top)_{31} \\ (\mathbf{\Sigma} - \mathbf{\Sigma}^\top)_{12} \end{bmatrix}.$$

The eigenvector $\mathbf{r}$ can be assumed to be normalized (unit length). Regarded as a quaternion, $\mathbf{r} = [r_0, r_1, r_2, r_3]^\top$ uniquely defines the rotation. This can be converted into a conventional rotation matrix

$$\mathbf{R} = \begin{bmatrix} r_0^2 + r_1^2 - r_2^2 - r_3^2 & 2(r_1 r_2 - r_0 r_3) & 2(r_1 r_3 + r_0 r_2) \\ 2(r_1 r_2 + r_0 r_3) & r_0^2 + r_2^2 - r_1^2 - r_3^2 & 2(r_2 r_3 - r_0 r_1) \\ 2(r_1 r_3 - r_0 r_2) & 2(r_2 r_3 + r_0 r_1) & r_0^2 + r_3^2 - r_1^2 - r_2^2 \end{bmatrix}.$$

The translation vector is then $\mathbf{v} = \bar{\mathbf{x}}^M - \mathbf{R}\bar{\mathbf{x}}^E$.

APPENDIX D

DATA PREPROCESSING TO OBTAIN EMPIRICAL NOISE SAMPLES

Raw EEG and fMRI data collected during rest periods had to be pre-processed before being added to the generated signal. MEG noise signal was taken from the phantom study, thus by definition it didn't contain any artifacts and only instrumental noise. That gives MEG additional advantage and first two steps of preprocessing were omitted for MEG signal. The following processing took place:

Filtering To prepare E/MEG signals for the next preprocessing stage, raw E/MEG (Fig. D.1) data was filtered using bandpass filter to allow only $0.2 - 30\,\text{Hz}$ frequency components. Similar signal preprocessing is usually carried in conventional brain imaging data analysis to eliminate frequencies irrelevant to the design and to the expected neuronal response (*e.g.* DC components, slow drifts, power-line background).

Irrelevant features removal ICA (Infomax [16]) has been applied [139] to E/MEG data to extract the sources which are different from simple noisy components and rather correspond to some electro-physiological activity (*e.g.* muscle noise, eye movements) which is not of interest of the given study. Visual inspection of the components time courses (Fig. D.3) and projected topographies (Fig. D.4) allows to identify the components which are artifacts due to electro-physiological activity (components 1, 4), relevant for the events of the experiment (components 8, 9, 20, 22) or just sharply localized (components 11, 19), thus they are highly unprobable to be noise components for our purpose;

Downsampling To prepare E/MEG noise signals for down-sampling, E/MEG time-trends were filtered using bad-pass filter to permit only $0.5 - 8\,\text{Hz}$ frequency components. Upper limit of $8\,\text{Hz}$ was set to match the temporal resolution of the modeling environment ($16\,\text{samples/sec}$). fMRI time series was high pass filtered $> 0.1\,\text{Hz}$ to remove present time trends;

Normalization To gain control of the amount of noise added to the simulated signals, all noise signals were normalized to have unit variance (Fig. D.5). Although extracted E/MEG noise signal indeed has distribution close to Gaussian (Fig. D.6), its temporal characteristics show a prevalence of lower

frequency components (Fig. D.7). To reduce impact of correlations across channels, noise samples were taken with arbitrary temporal delay varying across sensors.

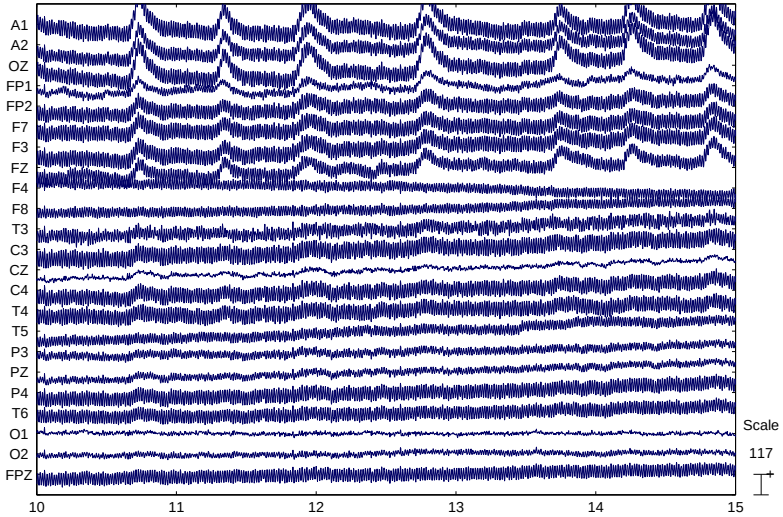

Figure D.1 Raw EEG signal shows a lot of present high frequency noise, low frequency trends and artifacts present in the signal.

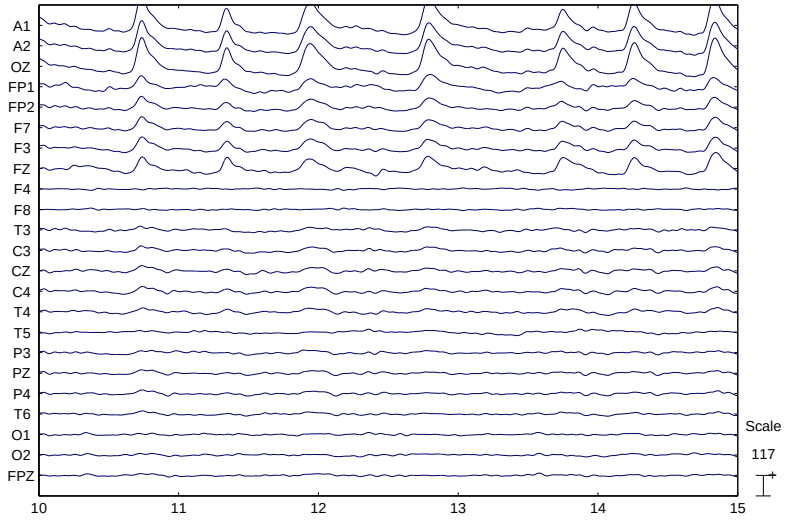

Figure D.2 Before any processing raw EEG signal is bandpass filtered.

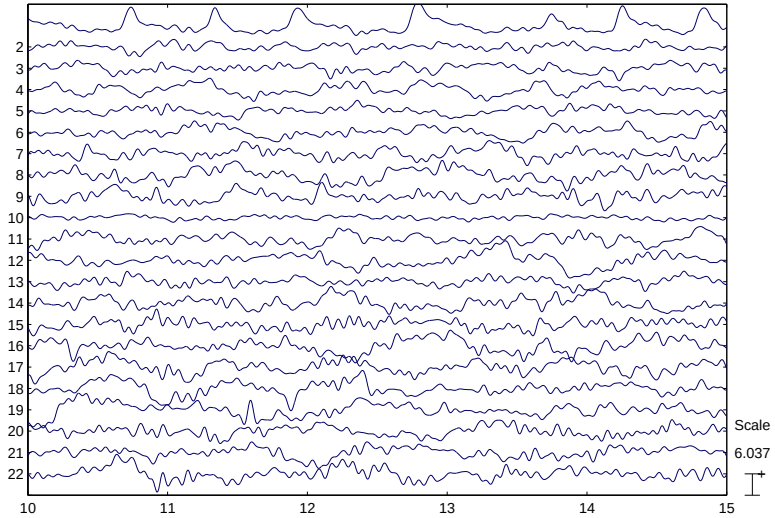

Figure D.3 ICA analysis allows to separate the multichannel signal into the components such as muscle artifacts (top component), electrical line noise, slow trends, etc.

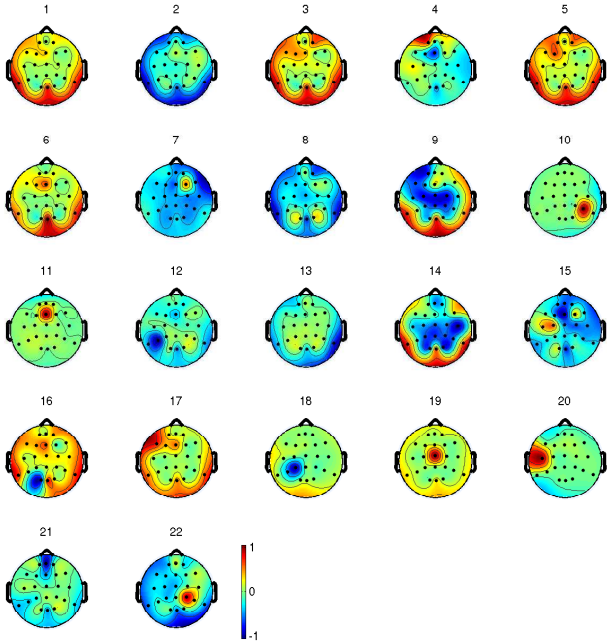

Figure D.4 Using the separation matrix obtained during ICA it is possible to visualize influence of each component on each sensor, thus creating topographic maps.

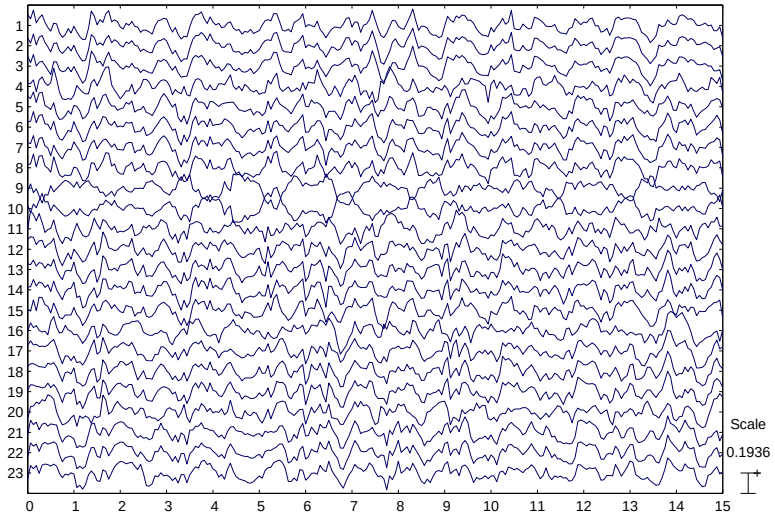

Figure D.5 Empirical EEG noise samples after all preprocessing stages.

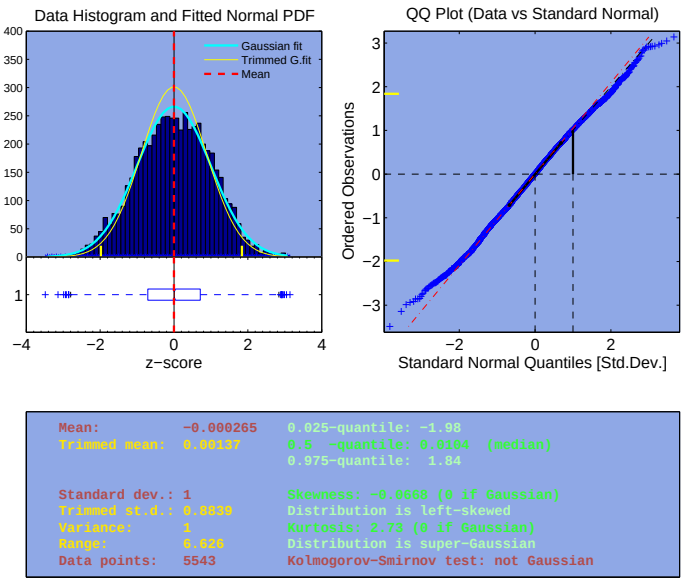

Figure D.6 Data histogram (top left), QQ plot to the matching Gaussian (top right) and statistics (bottom) of the noise components extracted from the empirical EEG data.

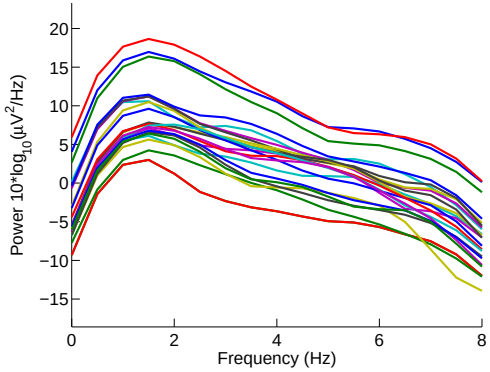

Figure D.7 Power spectrum of extracted empirical noise shows present correlations at lower frequencies

BIBLIOGRAPHY

[1] P. Adjamian, G. R. Barnes, A. Hillebrand, I. E. Holliday, K. D. Singh, P. L. Furlong, E. Harrington, C. W. Barclay, and P. J. Route. Co-registration of magnetoencephalography with magnetic resonance imaging using bite-bar-based fiducials and surface-matching. *Clin Neurophysiol*, 115 (3):691–698, 2004.

[2] S. P. Ahlfors and G. V. Simpson. Geometrical interpretation of fMRI-guided MEG/EEG inverse estimates. *NeuroImage*, 22(1):323–332, 2004.

[3] S. P. Ahlfors, G. V. Simpson, A. M. Dale, J. W. Belliveau, A. K. Liu, A. Korvenoja, J. Virtanen, M. Huotilainen, R. B. Tootell, H. J. Aronen, and R. J. Ilmoniemi. Spatiotemporal activity of a cortical network for processing visual motion revealed by MEG and fMRI. *J Neurophysiol*, 82(5): 2545–2555, 1999.

[4] P. J. Allen, O. Josephs, and R. Turner. A method for removing imaging artifact from continuous EEG recorded during functional MRI. *NeuroImage*, 12(2):230–239, 2000.

[5] K. Anami, T. Mori, F. Tanaka, Y. Kawagoe, J. Okamoto, M. Yarita, T. Ohnishi, M. Yumoto, H. Matsuda, and O. Saitoh. Stepping stone sampling for retrieving artifact-free electroencephalogram during functional magnetic resonance imaging. *NeuroImage*, 19(2.1): 281–295, 2003.

[6] L. M. Angelone, A. Potthast, F. Segonne, S. Iwaki, J. W. Belliveau, and G. Bonmassar. Metallic electrodes and leads in simultaneous EEG-MRI: specific absorption rate (SAR) simulation studies. *Bioelectromagnetics*, 25(4):285–295, 2004.

[7] O. J. Arthurs and S. Boniface. How well do we understand the neural origins of the fMRI BOLD signal? *Trends Neurosci*, 25(1):27–31, 2002.

[8] D. Attwell and C. Iadecola. The neural basis of functional brain imaging signals. *Trends Neurosci*, 25(12):621–625, 2002.

[9] F. Babiloni, C. Babiloni, F. Carducci, L. Angelone, C. Del-Gratta, G. L. Romani, P. M. Rossini, and F. Cincotti. Linear inverse estimation of cortical sources by using high resolution EEG and fMRI priors. *Int J of Bioelectromag*, 3(1), 2001. URL http://www.ijbem.org/volume3/number1/babilioni/i/index.htm.

[10] G. Backus and F. Gilbert. The resolving power of gross Earth data. *Geophys J R Astron Soc*, 16: 169–205, 1968.

[11] S. Baillet and L. Garnero. A bayesian approach to introducing anatomo-functional priors in the EEG/MEG inverse problem. *IEEE Trans Biomed Eng*, 44(5):374–385, May 1997.

[12] S. Baillet, L. Garnero, G. Marin, and J. P. Hugonin. Combined MEG and EEG source imaging by minimization of mutual information. *IEEE Transactions on Biomedical Engineering*, 46(5): 522–534, 1999.

[13] S. Baillet, J. C. Mosher, and M. Leahy. Electromagnetic brain mapping. *IEEE Sig Proc Mag*, 18 (6):14–30, Nov. 2001.

[14] S. Baillet, J. Riera, G. Marin, J. Mangin, J. Aubert, and L. Garnero. Evaluation of inverse methods and head models for EEG source localization using a human skull phantom. *Phys Med Biol*, 46(1): 77–96, 2001.

[15] R. Beisteiner, M. Erdler, C. Teichtmeister, M. Diemling, E. Moser, V. Edward, and L. Deecke. Magnetoencephalography may help to improve functional MRI brain mapping. *Eur J Neurosci*, 9 (5):1072–1077, 1997.

[16] A. J. Bell and T. J. Sejnowski. An information-maximization approach to blind separation and blind deconvolution. *Neural Comput*, 7(6):1129–1159, 1995.

[17] J. Belliveau, D. Kennedy, Jr, R. McKinstry, B. Buchbinder, R. Weisskoff, M. Cohen, J. Vevea, T. Brady, and B. Rosen. Functional mapping of the human visual cortex by magnetic resonance imaging. *Science*, 254(5032):716–719, 1991.

[18] BioPSE. Problem solving environment for modeling, simulation, and visualization of bioelectric fields, 2002. URL http://software.sci.utah.edu/biopse.html. Scientific Computing and Imaging Institute (SCI).

[19] J. Bodurka and P. A. Bandettini. Toward direct mapping of neuronal activity: MRI detection of ultraweak, transient magnetic field changes. *Magn Reson Med*, 47(6):1052–1058, 2002.

[20] G. Bonmassar, P. L. Purdon, I. P. Jaaskelainen, K. Chiappa, V. Solo, E. N. Brown, and J. W. Belliveau. Motion and ballistocardiogram artifact removal for interleaved recording of EEG and EPs during MRI. *NeuroImage*, 16(4):1127–1141, 2002.

[21] G. Bonmassar, D. P. Schwartz, A. K. Liu, K. K. Kwong, A. M. Dale, and J. W. Belliveau. Spatiotemporal brain imaging of visual-evoked activity using interleaved EEG and fMRI recordings. *NeuroImage*, 13(6.1):1035–1043, 2001.

[22] G. M. Boynton, S. A. Engel, G. H. Glover, and D. J. Heeger. Linear systems analysis of functional magnetic resonance imaging in human V1. *J Neurosci*, 16(13):4207–4221, 1996.

[23] M. Brazdil, M. Dobsik, M. Mikl, P. Hlustik, P. Daniel, M. Pazourkova, P. Krupa, and I. Rektor. Combined event-related fMRI and intracerebral ERP study of an auditory oddball task. *Neuroimage*, 26(1):285–93, 2005. URL http://eutils.ncbi.nlm.nih.gov/entrez/eutils/elink.fcgi?cmd=prlinks\&db%from=pubmed\&retmode=ref\&id=15862229. Enter text here.

[24] M. A. B. Brazier. A study of the electric field at the surface of the head. *Electroencephalogr Clin Neurophysiol*, 2:38–52, 1949.

[25] D. H. Brooks, G. F. Ahmad, R. S. MacLeod, and G. M. Maratos. Inverse electrocardiography by simultaneous imposition of multiple constraints. *IEEE Trans Biomed Eng*, 46(1):3–18, 1999.

[26] R. B. Buxton and L. R. Frank. A model for the coupling between cerebral blood flow and oxygen metabolism during neural stimulation. *J Cereb Blood Flow Metab*, 17(1):64–72, 1997.

[27] V. D. Calhoun, T. Adali, L. K. Hansen, J. Larsen, and J. J. Pekar. ICA of functional MRI data: An overview. In *Fourth International Symposium on Independent Component Analysis and Blind Source Separation*, pages 281–288, Nara, Japan, Apr. 2003. URL http://www.imm.dtu.dk/pubdb/p.php?1669. Invited Paper.

[28] S. A. Castellano. *The Folding of the Human Brain: From Shape to Function*. PhD thesis, University of London, Division of Radiological Sciences and Medical Engineering, King's College London, Sept. 1999.

[29] P. Ciuciu, J. B. Poline, G. Marrelec, J. Idier, C. Pallier, and H. Benali. Unsupervised robust nonparametric estimation of the hemodynamic response function for any fMRI experiment. *IEEE Trans Med Imaging*, 22(10):1235–1251, 2003.

[30] C. A. Cocosco, V. Kollokian, R.-S. Kwan, and A. C. Evans. Brainweb: Online interface to a 3d mri simulated brain database. *NeuroImage*, 5(4), May 1997.

[31] D. Cohen. Magnetoencephalography: detection of the brain's electrical activity with a superconducting magnetometer. *Science*, 175:664–666, 1972.

[32] D. Cohen and E. Halgren. Magnetoencephalography (neuromagnetism). In *Encyclopedia of Neuroscience*, pages 1–7. Elsevier, 3rd edition, 2003.

[33] M. S. Cohen. Parametric analysis of fMRI data using linear systems methods. *NeuroImage*, 6(2): 93–103, 1997.

[34] M. S. Cohen. Method and apparatus for reducing contamination of an electrical signal. United States Patent application 0040097802, 2004.

[35] M. S. Cohen, R. I. Goldman, J. Stern, and J. Engel, Jr. Simultaneous EEG and fMRI made easy. *NeuroImage*, 13(6 Supp.1):S6, Jan. 2001.

[36] A. M. Dale, B. Fischl, and M. I. Sereno. Cortical surface-based analysis. I. Segmentation and surface reconstruction. *NeuroImage*, 9(2):179–194, 1999.

[37] A. M. Dale, A. K. Liu, B. Fischl, J. D. Lewine, R. L. Buckner, J. W. Belliveau, and E. Halgren. Dynamic statistical parameter mapping: combining fMRI and MEG to produce high resolution imaging of cortical activity. *Neuron*, 26:55–67, 2000.

[38] A. M. Dale and M. I. Sereno. Improved localization of cortical activity by combining EEG and MEG with MRI cortical surface reconstruction: A linear approach. *J of Cog Neurosci*, 5(2):162–176, 1993.

[39] P. Dechent and J. Frahm. Functional somatotopy of finger representations in human primary motor cortex. *Hum Brain Mapp*, 18(4):272–283, 2003.

[40] A. Delorme and S. Makeig. EEGLAB: an open source toolbox for analysis of single-trial EEG dynamics including independent component analysis. *J Neurosci Methods*, 134(1):9–21, 2004.

[41] A. Devor, A. K. Dunn, M. L. Andermann, I. Ulbert, D. A. Boas, and A. M. Dale. Coupling of total hemoglobin concentration, oxygenation, and neural activity in rat somatosensory cortex. *Neuron*, 39(2):353–359, 2003.

[42] E. Disbrow, T. Roberts, and L. Krubitzer. Somatotopic organization of cortical fields in the lateral sulcus of Homo sapiens: evidence for SII and PV. *J Comp Neurol*, 418(1):1–21, 2000.

[43] A. Fisher, G. Barnes, A. Hillebrand, C. Burrow, P. Furlong, and I. Holliday. Can you tell your clunis from your cubitus? A benchmark for functional imaging. *BMJ*, 329(7480):1492–3, 2004.

[44] J. Foucher, H. Otzenberger, and D. Gounot. Where arousal meets attention: a simultaneous fMRI and EEG recording study. *Neuroimage*, 22(2):688–697, 2004.

[45] J. J. Foxe, M. E. McCourt, and D. C. Javitt. Right hemisphere control of visuospatial attention: line-bisection judgments evaluated with high-density electrical mapping and source analysis. *NeuroImage*, 19(3):710–726, 2003.

[46] FreeSurfer. FreeSurfer, 2004. URL http://surfer.nmr.mgh.harvard.edu/. CorTechs and the Athinoula A. Martinos Center for Biomedical Imaging.

[47] K. J. Friston, P. Jezzard, and R. Turner. Analysis of functional MRI time-series. *Hum Brain Mapp*, 1:153–171, 1994.

[48] M. Fuchs, M. Wagner, T. Kohler, and H. Wischmann. Linear and nonlinear current density reconstructions. *J Clin Neurophysiol*, 16(3):267–295, 1999.

[49] G. Garreffa, M. Carni, G. Gualniera, G. B. Ricci, L. Bozzao, D. De Carli, P. Morasso, P. Pantano, C. Colonnese, V. Roma, and B. Maraviglia. Real-time MR artifacts filtering during continuous EEG/fMRI acquisition. *Magn Reson Imaging*, 21(10):1175–1189, 2003.

[50] L. A. Geddes and L. E. Baker. The specific resistance of biological material–a compendium of data for the biomedical engineer and physiologist. *Med Biol Eng*, 5(3):271–293, 1967.

[51] J. S. George, C. J. Aine, J. C. Mosher, D. M. Schmidt, D. M. Ranken, H. A. Schlitt, C. C. Wood, J. D. Lewine, J. A. Sanders, and J. W. Belliveau. Mapping function in the human brain with magnetoencephalography, anatomical magnetic-resonance-imaging, and functional magnetic-resonance-imaging. *J of Clin Neurophysiol*, 12(5):406–431, 1995.

[52] J. S. George, D. M. Schmidt, D. M. Rector, and C. C. Wood. *Functional MRI: An Introduction to Methods*, chapter 19. Dynamic functional neuroimaging intergratin multiple modalities, pages 353–382. Oxford University Press, 2002.

[53] D. R. Gitelman, W. D. Penny, J. Ashburner, and K. J. Friston. Modeling regional and psychophysiologic interactions in fMRI: the importance of hemodynamic deconvolution. *NeuroImage*, 19(1):200–207, 2003.

[54] G. H. Glover. Deconvolution of impulse response in event-related BOLD fMRI. *NeuroImage*, 9(4): 416–429, 1999.

[55] R. I. Goldman, J. M. Stern, J. Engel, Jr, and M. S. Cohen. Acquiring simultaneous EEG and functional MRI. *Clin Neurophysiol*, 111(11):1974–1980, 2000.

[56] R. I. Goldman, J. M. Stern, J. Engel, Jr, and M. S. Cohen. Simultaneous EEG and fMRI of the alpha rhythm. *Neuroreport*, 13(18):2487–2492, 2002.

[57] G. Golub, M. Heath, and G. Wahba. Generalized cross-validation as a method for choosing a good ridge parameter. *Technometrics*, 21:215–223, 1979.

[58] S. I. Goncalves, J. C. de Munck, J. P. Verbunt, F. Bijma, R. M. Heethaar, and F. Lopes da Silva. In vivo measurement of the brain and skull resistivities using an EIT-based method and realistic models for the head. *IEEE Trans Biomed Eng*, 50(6):754–767, 2003.

[59] S. L. Gonzalez Andino, O. Blanke, G. Lantz, G. Thut, and R. Grave de Peralta Menendez. The use of functional constraints for the neuroelectromagnetic inverse problem: Alternatives and caveats. *Int J of Bioelectromag*, 3(1), 2001. URL http://www.ijbem.org/volume3/number1/gravedeperalta/index.htm.

[60] I. F. Gorodnitsky and B. D. Rao. Sparse signal reconstruction from limited data using FOCUSS: A re-weighted minimum norm algorithm. *IEEE Trans Signal Proccessing*, 45(3):600–616, 1997.

[61] R. Grave de Peralta Menendez and S. L. Gonzalez Andino. A critical analysis of linear inverse solutions to the neuroelectromagnetic inverse problem. *IEEE Trans Biomed Eng*, pages 440–448, 1998.

[62] R. Grave de Peralta Menendez, M. M. Murray, C. M. Michel, R. Martuzzi, and S. L. Gonzalez Andino. Electrical neuroimaging based on biophysical constraints. *NeuroImage*, 21 (2):527–539, 2004.

[63] Y. O. Halchenko, B. A. Pearlmutter, S. J. Hanson, and A. Zaimi. Fusion of functional brain imaging modalities via linear programming. In *NFSI*, Chiety, Italy, 2003.

[64] M. Hämäläinen, R. Hari, R. J. Ilmoniemi, J. Knuutila, and O. V. Lounasmaa. Magnetoencephalography—theory, instrumentation, and applications to noninvasive studies of the working human brain. *Rev. Modern Physics*, 65(2):413–497, 1993.

[65] M. S. Hamalainen and J. Sarvas. Realistic conductivity geometry model of the human head for interpretation of neuromagnetic data. *IEEE Trans Biomed Eng*, 36(2):165–171, 1989.

[66] P. C. Hansen. Analysis of discrete ill-posed problems by means of the L-curve. In *SIAM Review*, volume 34, pages 561–580. Society for Industrial and Applied Mathematics, Philadelphia, PA, USA, 1992.

[67] O. Hauk. Keep it simple: a case for using classical minimum norm estimation in the analysis of EEG and MEG data. *NeuroImage*, 21(4):1612–1621, 2004.

[68] R. A. Hill, K. H. Chiappa, F. Huang-Hellinger, and B. G. Jenkins. EEG during MR imaging: differentiation of movement artifact from paroxysmal cortical activity. *Neurology*, 45(10):1942–1943, 1995.

[69] A. Hillebrand and G. R. Barnes. The use of anatomical constraints with MEG beamformers. *NeuroImage*, 20(4):2302–2313, 2003.

[70] P. Hlustik, A. Solodkin, R. Gullapalli, D. Noll, and S. Small. Somatotopy in human primary motor and somatosensory hand representations revisited. *Cereb Cortex*, 11(4):312–21, 2001.

[71] B. K. P. Horn. Closed-form solution of absolute orientation using unit quaternions. *J of Opt Soc Amer*, 4(4):629–642, Apr. 1987.

[72] B. K. P. Horn, H. Hilden, and S. Negahdaripour. Closed-form solution of absolute orientation using orthonormal matrices. *J of Opt Soc Amer*, 5(7):1127–1135, July 1988.

[73] S. G. Horovitz, B. Rossion, P. Skudlarski, and J. C. Gore. Parametric design and correlational analyses help integrating fMRI and electrophysiological data during face processing. *NeuroImage*, 22(4):1587–1595, 2004.

[74] S. G. Horovitz, P. Skudlarski, and J. C. Gore. Correlations and dissociations between BOLD signal and P300 amplitude in an auditory oddball task: a parametric approach to combining fMRI and ERP. *Magn Reson Imaging*, 20(4):319–325, 2002.

[75] F. R. Huang-Hellinger, H. C. Breiter, G. McCormack, M. S. Cohen, K. K. Kwong, J. P. Sutton, R. L. Savoy, R. M. Weisskoff, T. L. Davis, J. R. Baker, J. W. Belliveau, and B. R. Rosen. Simultaneous functional magnetic resonance imaging and electrophysiological recording. *Hum Brain Mapp*, 3: 13–25, 1995.

[76] H. J. Huppertz, M. Otte, C. Grimm, R. Kristeva-Feige, T. Mergner, and C. H. Lucking. Estimation of the accuracy of a surface matching technique for registration of EEG and MRI data. *Electroencephalogr Clin Neurophysiol*, 106(5):409–415, 1998.

[77] J. R. Ives, S. Warach, F. Schmitt, R. R. Edelman, and D. L. Schomer. Monitoring the patient's EEG during echo planar MRI. *Electroencephalogr Clin Neurophysiol*, 87(6):417–420, 1993.

[78] B. Jeffs, R. Leahy, and M. Singh. An evaluation of methods for neuromagnetic image reconstruction. *IEEE Trans Biomed Eng*, 34(9):713–723, 1987.

[79] S. C. Jun and B. A. Pearlmutter. Fast robust subject-independent magnetoencephalographic source localization using an artificial neural network. *Human Brain Mapping*, 24(1):21–34, 2005.

[80] S. C. Jun, B. A. Pearlmutter, and G. Nolte. MEG source localization using a MLP with a distributed output representation. *IEEE Trans Biomed Eng*, 50(6):786–789, June 2003.

[81] T.-P. Jung, C. Humphries, T.-W. Lee, S. Makeig, M. J. McKeown, V. Iragui, and T. J. Sejnowski. Removing electroencephalographic artifacts: comparison between ICA and PCA. In *Neural Networks for Signal Processing VIII*. IEEE Press, 1999.

[82] T.-P. Jung, C. Humphries, T.-W. Lee, M. J. McKeown, V. Iragui, S. Makeig, and T. J. Sejnowski. Removing electroencephalographic artifacts by blind source separation. *Psychophysiology*, 37: 163–178, 2000.

[83] T.-P. Jung, S. Makeig, M. Westerfield, J. Townsend, E. Courchesne, and T. J. Sejnowski. Analyzing and visualizing single-trial event-related potentials. In *Advances in Neural Info Proc Sys 11*, pages 118–124. MIT Press, 1999.

[84] T.-P. Jung, S. Makeig, M. Westerfield, J. Townsend, E. Courchesne, and T. J. Sejnowski. Removal of eye activity artifacts from visual event-related potentials in normal and clinical subjects. *Clinical Neurophysiology*, 111(10):1745–1758, 2000.

[85] J. Kilner,, J. Mattout,, R. Henson,, and K. Friston,.

[86] H. Kober, C. Nimsky, M. Moller, P. Hastreiter, R. Fahlbusch, and O. Ganslandt. Correlation of sensorimotor activation with functional magnetic resonance imaging and magnetoencephalography in presurgical functional imaging: a spatial analysis. *NeuroImage*, 14(5):1214–1228, 2001.

[87] A. Korvenoja, J. Huttunen, E. Salli, H. Pohjonen, S. Martinkauppi, J. M. Palva, L. Lauronen, J. Virtanen, R. J. Ilmoniemi, and H. J. Aronen. Activation of multiple cortical areas in response to somatosensory stimulation: combined magnetoencephalographic and functional magnetic resonance imaging. *Hum Brain Mapp*, 8(1):13–27, 1999.

[88] D. Kozinska, F. Carducci, and K. Nowinski. Automatic alignment of EEG/MEG and MRI data sets. *Clin Neurophysiol*, 112(8):1553–1561, 2001.

[89] K. Krakow, P. J. Allen, M. R. Symms, L. Lemieux, O. Josephs, and D. R. Fish. EEG recording during fMRI experiments: image quality. *Hum Brain Mapp*, 10(1):10–15, 2000.

[90] K. Krakow, L. Lemieux, D. Messina, C. A. Scott, M. R. Symms, J. S. Duncan, and D. R. Fish. Spatio-temporal imaging of focal interictal epileptiform activity using EEG-triggered functional MRI. *Epileptic Disord*, 3(2):67–74, 2001.

[91] K. Krakow, U. C. Wieshmann, F. G. Woermann, M. R. Symms, M. A. McLean, L. Lemieux, P. J. Allen, G. J. Barker, D. R. Fish, and J. S. Duncan. Multimodal MR imaging: functional, diffusion tensor, and chemical shift imaging in a patient with localization-related epilepsy. *Epilepsia*, 40(10): 1459–1462, 1999.

[92] K. Krakow, F. G. Woermann, M. R. Symms, P. J. Allen, L. Lemieux, G. J. Barker, J. S. Duncan, and D. R. Fish. EEG-triggered functional MRI of interictal epileptiform activity in patients with partial seizures. *Brain*, 122(9):1679–1688, 1999.

[93] F. Kruggel, C. S. Herrmann, C. J. Wiggins, and D. Y. von Cramon. Hemodynamic and electroencephalographic responses to illusory figures: recording of the evoked potentials during functional MRI. *NeuroImage*, 14(6):1327–1336, 2001.

[94] F. Kruggel, C. J. Wiggins, C. S. Herrmann, and D. Y. von Cramon. Recording of the event-related potentials during functional MRI at 3.0 Tesla field strength. *Magn Reson Med*, 44(2):277–282, 2000.

[95] T. D. Lagerlund, F. W. Sharbrough, C. R. Jack, Jr, B. J. Erickson, D. C. Strelow, K. M. Cicora, and N. E. Busacker. Determination of 10-20 system electrode locations using magnetic resonance image scanning with markers. *Electroencephalogr Clin Neurophysiol*, 86(1):7–14, 1993.

[96] P.-J. Lahaye, S. Baillet, J.-B. Poline, and L. Garnero. Fusion of simultaneous fMRI/EEG data based on the electro-metabolic coupling. pages 864–867, Arlington, Virginia, Apr. 2004.

[97] C. Lamm, C. Windischberger, U. Leodolter, E. Moser, and H. Bauer. Co-registration of EEG and MRI data using matching of spline interpolated and MRI-segmented reconstructions of the scalp surface. *Brain Topogr*, 14(2):93–100, 2001.

[98] L. Landini, editor. Signal Processing and Communications. Dekker, 2005. In press.

[99] N. Lange and S. L. Zeger. Non-linear fourier time series analysis for human brain mapping by functional magnetic resonance imaging. *Appl Stat*, 46(1):1–29, 1997.

[100] G. Lantz, L. Spinelli, R. G. Menendez, M. Seeck, and C. M. Michel. Localization of distributed sources and comparison with functional MRI. *Epileptic Disord*, Special Issue:45–58, 2001.

[101] H. Laufs, A. Kleinschmidt, A. Beyerle, E. Eger, A. Salek-Haddadi, C. Preibisch, and K. Krakow. EEG-correlated fMRI of human alpha activity. *NeuroImage*, 19(4):1463–1476, 2003.

[102] H. Laufs, K. Krakow, P. Sterzer, E. Eger, A. Beyerle, A. Salek-Haddadi, and A. Kleinschmidt. Electroencephalographic signatures of attentional and cognitive default modes in spontaneous brain activity fluctuations at rest. *Proc Natl Acad Sci U S A*, 100(19):11053–11058, 2003.

[103] C. L. Lawson and R. J. Hanson. *Solving Least Squares Problems*. Series in Automatic Computation. Prentice-Hall, Englewood Cliffs, NJ 07632, USA, 1974. ISBN 0-13-822585-0.

[104] F. Lazeyras, O. Blanke, S. Perrig, I. Zimine, X. Golay, J. Delavelle, C. M. Michel, N. de Tribolet, J. G. Villemure, and M. Seeck. EEG-triggered functional MRI in patients with pharmacoresistant epilepsy. *J Magn Reson Imaging*, 12(1):177–185, 2000.

[105] F. Lazeyras, I. Zimine, O. Blanke, S. H. Perrig, and M. Seeck. Functional MRI with simultaneous EEG recording: feasibility and application to motor and visual activation. *J Magn Reson Imaging*, 13(6):943–948, 2001.

[106] R. M. Leahy, S. Baillet, and J. C. Mosher. Integrated matlab toolbox dedicated to magnetoencephalography (MEG) and electroencephalography (EEG) data visualization and processing, 2004. URL http://neuroimage.usc.edu/brainstorm/.

[107] L. Lemieux, P. J. Allen, F. Franconi, M. R. Symms, and D. R. Fish. Recording of EEG during fMRI experiments: patient safety. *Magn Reson Med*, 38(6):943–952, 1997.

[108] L. Lemieux, K. Krakow, and D. R. Fish. Comparison of spike-triggered functional MRI BOLD activation and EEG dipole model localization. *NeuroImage*, 14(5):1097–1104, 2001.

[109] E. Liebenthal, M. L. Ellingson, M. V. Spanaki, T. E. Prieto, K. M. Ropella, and J. R. Binder. Simultaneous ERP and fMRI of the auditory cortex in a passive oddball paradigm. *NeuroImage*, 19 (4):1395–1404, 2003.

[110] A. K. Liu, J. W. Belliveau, and A. M. Dale. Spatiotemporal imaging of human brain activity using functional MRI constrained magnetoencephalography data: Monte Carlo simulations. *Proc Natl Acad Sci U S A*, 95(15):8945–8950, 1998.

[111] N. K. Logothetis and B. A. Wandell. Interpreting the BOLD signal. *Annu Rev Physiol*, 66:735–769, 2004.

[112] M. J. Makiranta, J. Ruohonen, K. Suominen, E. Sonkajarvi, T. Salomaki, V. Kiviniemi, T. Seppanen, S. Alahuhta, V. Jantti, and O. Tervonen. BOLD-contrast functional MRI signal changes related to intermittent rhythmic delta activity in EEG during voluntary hyperventilation-simultaneous EEG and fMRI study. *NeuroImage*, 22(1):222–231, 2004.

[113] J. Malmivuo and R. Plonsey. *Bioelectromagnetism—Principles and Applications of Bioelectric and Biomagnetic Fields*. Oxford University Press, New York, 1995, 1995. URL http://butler.cc.tut.fi/~malmivuo/bem/bembook/index.htm.

[114] J. Malmivuo, V. Suihko, and H. Eskola. Sensitivity distributions of EEG and MEG measurements. *IEEE Trans Biomed Eng*, 44(3):196–208, 1997.

[115] G. Marin, C. Guerin, S. Baillet, L. Garnero, and G. Meunier. Influence of skull anisotropy for the forward and inverse problems in EEG: simulation studies using FEM on realistic head models. *Hum Brain Mapp*, 6:250–269, 1998.

[116] G. Marrelec, H. Benali, P. Ciuciu, M. Pelegrini-Issac, and J. B. Poline. Robust Bayesian estimation of the hemodynamic response function in event-related BOLD fMRI using basic physiological information. *Hum Brain Mapp*, 19(1):1–17, 2003.

[117] E. Martinez-Montes, P. A. Valdes-Sosa, F. Miwakeichi, R. I. Goldman, and M. S. Cohen. Concurrent EEG/fMRI analysis by multiway Partial Least Squares. *NeuroImage*, 22(3):1023–1034, 2004.

[118] M. J. McKeown, S. Makeig, G. G. Brown, T.-P. Jung, S. S. Kindermann, A. J. Bell, and T. J. Sejnowski. Analysis of fMRI data by blind separation into independent spatial components. *Human Brain Mapping*, 6:160–188, 1998.

[119] L. Melie-García, N. J. Trujillo-Barreto, E. Martínez-Montes, T. Koenig, and P. A. Valdés-Sosa. EEG imaging via BMA with fMRI pre-defined prior model probabilities. In *Hum Brain Mapp*, Budapest, Hungary, June 2004.

[120] V. Menon, J. M. Ford, K. O. Lim, G. H. Glover, and A. Pfefferbaum. Combined event-related fMRI and EEG evidence for temporal-parietal cortex activation during target detection. *Neuroreport*, 8 (14):3029–3037, 1997.

[121] C. M. Michel, M. M. Murray, G. Lantz, S. Gonzalez, L. Spinelli, and R. Grave De Peralta. EEG source imaging. *Clin Neurophysiol*, 115(10):2195–2222, 2004.

[122] C. E. Miller and C. S. Henriquez. Finite element analysis of bioelectric phenomena. *Crit Rev Biomed Eng*, 18(3):207–233, 1990.

[123] M. Moosmann, P. Ritter, I. Krastel, A. Brink, S. Thees, F. Blankenburg, B. Taskin, H. Obrig, and A. Villringer. Correlates of alpha rhythm in functional magnetic resonance imaging and near infrared spectroscopy. *NeuroImage*, 20(1):145–158, 2003.

[124] J. E. Moran. MEG tools for Matlab software, 2005. URL http://rambutan.phy.oakland.edu/~meg/.

[125] J. C. Mosher, R. M. Leahy, and P. S. Lewis. EEG and MEG: Forward solutions for inverse methods. *IEEE Trans Biomed Eng*, 46(3):245–260, Mar. 1999.

[126] C. Mulert, L. Jager, R. Schmitt, P. Bussfeld, O. Pogarell, H. J. Moller, G. Juckel, and U. Hegerl. Integration of fMRI and simultaneous EEG: towards a comprehensive understanding of localization and time-course of brain activity in target detection. *NeuroImage*, 22(1):83–94, 2004.

[127] S. Murakami, A. Hirose, and Y. Okada. Contribution of ionic currents to magnetoencephalography (MEG) and electroencephalography (EEG) signals generated by guinea-pig CA3 slices. *J Physiol*, 553(Pt 3):975–985, 2003.

[128] M. Negishi, M. Abildgaard, T. Nixon, and R. Todd Constable. Removal of time-varying gradient artifacts from EEG data acquired during continuous fMRI. *Clin Neurophysiol*, 115(9):2181–2192, 2004.

[129] NeuroFEM. Finite element software for fast computation of the forward solution in EEG/MEG source localisation, 2005. URL http://www.neurofem.com/. Max Planck Institute for Human Cognitive and Brain Sciences.

[130] E. Niedermeyer. Alpha rhythms as physiological and abnormal phenomena. *Int J Psychophysiol*, 26(1-3):31–49, 1997.

[131] F. Å. Nielsen. Bibliography of segmentation in neuroimaging, 2001. URL http://www.imm.dtu.dk/~fn/bib/Nielsen2001BibSegmentation/.

[132] G. Nolte. The magnetic lead field theorem in the quasi-static approximation and its use for magnetoencephalography forward calculation in realistic volume conductors. *Phys. Med. Biol.*, 48:3637–3652, Nov. 2003. URL http://stacks.iop.org/PMB/48/3637.

[133] G. Nolte. The magnetic lead field theorem in the quasi-static approximation and its use for MEG forward calculation in realistic volume conductors. *Physics in Medicine and Biology*, 48(22):3637–3652, 2004.

[134] P. L. Nunez. *Electric Fields of the Brain: The Neurophysics of EEG*. New York: Oxford University Press, 1981.

[135] P. L. Nunez and R. B. Silberstein. On the relationship of synaptic activity to macroscopic measurements: does co-registration of EEG with fMRI make sense? *Brain Topogr*, 13(2):79–96, 2000.

[136] S. Ogawa, T. Lee, A. Nayak, and P. Glynn. Oxygenation-sensitive contrast in magnetic resonance image of rodent brain at high magnetic fields. *Magn Reson Med*, 14(1):68–78, 1990.

[137] S. Ogawa, T. M. Lee, A. R. Kay, and D. W. Tank. Brain magnetic resonance imaging with contrast dependent on blood oxygenation. *Proc Natl Acad Sci U S A*, 87(24):9868–9872, 1990.

[138] Y. Okada, A. Lahteenmaki, and C. Xu. Comparison of MEG and EEG on the basis of somatic evoked responses elicited by stimulation of the snout in the juvenile swine. *Clin Neurophysiol*, 110 (2):214–229, 1999.

[139] L. Parra, C. Alvino, A. Tang, B. Pearlmutter, N. Yeung, A. Osman, and P. Sajda. Linear spatial integration for single-trial detection in encephalography. *Neuroimage*, 17(1):223–230, Sept. 2002.

[140] R. D. Pascual-Marqui, C. M. Michel, and D. Lehman. Low resolution electromagnetic tomography: A new method for localizing electrical activity of the brain. *Int J of Psychophysiol*, 18:49–65, 1994.

[141] R. S. Paulesu, R. S. J. Frackowiak, and G. Bottini. Maps of somatosensory systems. In R. S. J. Frackowiak, editor, *Human brain function*, page 528. Academic Press, San Diego, CA, 1997.

[142] W. Penfield and E. Boldrey. Somatic motor and sensory representation in the cerebral cortex of man as studies by electrical stimulation. *Brain*, 60:389–443, 1937.

[143] J. Pfeuffer, H. Merkle, and N. Logothetis. Perfusion-based high-resolution fmri in the primate brain using a novel vertical large-bore 7 tesla setup. page 1392, 2005.

[144] C. Phillips, M. D. Rugg, and K. J. Friston. Anatomically informed basis functions for EEG source localization: combining functional and anatomical constraints. *NeuroImage*, 16(3.1):678–695, 2002.

[145] C. Phillips, M. D. Rugg, and K. J. Friston. Systematic regularization of linear inverse solutions of the EEG source localization problem. *NeuroImage*, 17(1):287–301, 2002.

[146] F. Poupon. *Parcellisation systématique du cerveau en volumes d'intérêt. Le cas des structures profondes*. Phd thesis, INSA Lyon, Lyon, France, Dec. 1999. URL ftp://ftp.cea.fr/pub/dsv/anatomist/papers/fpoupon-thesis99.pdf.

[147] G. W. Pruis, B. H. Gilding, and M. J. Peters. A comparison of different numerical methods for solving the forward problem in EEG and MEG. *Physiol Meas*, 14 Suppl 4A:A1–9, 1993.

[148] J. C. Rajapakse, F. Kruggel, J. M. Maisog, and D. Y. von Cramon. Modeling hemodynamic response for analysis of functional MRI time-series. *Hum Brain Mapp*, 6(4):283–300, 1998.

[149] S. E. Robinson and J. Vrba. Functional neuroimaging by syntheticaperture magnetometry (SAM). In T. Yoshimoto, M. Kotani, S. Kuriki, H. Karibe, and N. Nakasato, editors, *Recent Advances in Biomagnetism*, pages 302–305, Sendai, Japan, 1999. Tohoku Univ. Press.

[150] B. Rosen, J. Belliveau, H. Aronen, D. Kennedy, B. Buchbinder, A. Fischman, M. Gruber, J. Glas, R. Weisskoff, M. Cohen, and et al. Susceptibility contrast imaging of cerebral blood volume: human experience. *Magn Reson Med*, 22(2):293–9; discussion 300–3, 1991.

[151] C. S. Roy and C. S. Sherrington. On the regulation of the blood-supply of the brain. *J of Physiol (London)*, 11:85–108, 1890.

[152] M. Sahani and S. S. Nagarajan. Reconstructing MEG sources with unknown correlations. In *Advances in Neural Info Proc Sys 16*. MIT Press, 2004.

[153] H. I. Saleheen and K. T. Ng. New finite difference formulations for general inhomogeneous anisotropic bioelectric problems. *IEEE Trans Biomed Eng*, 44(9):800–809, 1997.

[154] A. Salek-Haddadi, K. J. Friston, L. Lemieux, and D. R. Fish. Studying spontaneous EEG activity with fMRI. *Brain Res Brain Res Rev*, 43(1):110–133, 2003.

[155] A. Salek-Haddadi, M. Merschhemke, L. Lemieux, and D. R. Fish. Simultaneous EEG-Correlated Ictal fMRI. *NeuroImage*, 16(1):32–40, 2002.

[156] D. M. Schmidt, J. S. George, and C. C. Wood. Bayesian inference applied to the electromagnetic inverse problem. *Hum Brain Mapp*, 7(3):195–212, 1999.

[157] D. L. Schomer, G. Bonmassar, F. Lazeyras, M. Seeck, A. Blum, K. Anami, D. Schwartz, J. W. Belliveau, and J. Ives. EEG-Linked functional magnetic resonance imaging in epilepsy and cognitive neurophysiology. *J Clin Neurophysiol*, 17(1):43–58, 2000.

[158] M. Schulz, W. Chau, S. J. Graham, A. R. McIntosh, B. Ross, R. Ishii, and C. Pantev. An integrative MEG-fMRI study of the primary somatosensory cortex using cross-modal correspondence analysis. *NeuroImage*, 22(1):120–133, 2004.

[159] D. P. Schwartz, E. Poiseau, D. Lemoine, and C. Barillot. Registration of MEG/EEG data with 3D MRI: Methodology and precision issues. *Brain Topogr*, 9(1):101–116, Winter 1996.

[160] SCIRun. SCIRun: a scientific computing problem solving environment, 2002. URL http://software.sci.utah.edu/scirun.html. Scientific Computing and Imaging Institute (SCI).

[161] M. Seeck, F. Lazeyras, C. M. Michel, O. Blanke, C. A. Gericke, J. Ives, J. Delavelle, X. Golay, C. A. Haenggeli, N. de Tribolet, and T. Landis. Non-invasive epileptic focus localization using EEG-triggered functional MRI and electromagnetic tomography. *Electroencephalogr Clin Neurophysiol*, 106(6):508–512, 1998.

[162] A. Seiyama, J. Seki, H. C. Tanabe, I. Sase, A. Takatsuki, S. Miyauchi, H. Eda, S. Hayashi, T. Imaruoka, T. Iwakura, and T. Yanagida. Circulatory basis of fMRI signals: relationship between changes in the hemodynamic parameters and BOLD signal intensity. *NeuroImage*, 21 (4):1204–1214, 2004.

[163] D. Shattuck and R. Leahy. BrainSuite: an automated cortical surface identification tool. *Med Image Anal*, 6(2):129–142, 2002.

[164] J. Sijbers, I. Michiels, M. Verhoye, J. Van Audekerke, A. Van der Linden, and D. Van Dyck. Restoration of MR-induced artifacts in simultaneously recorded MR/EEG data. *Magn Reson Imaging*, 17(9):1383–1391, 1999.

[165] J. Sijbers, B. Vanrumste, G. Van Hoey, P. Boon, M. Verhoye, A. Van der Linden, and D. Van Dyck. Automatic localization of EEG electrode markers within 3D MR data. *Magn Reson Imaging*, 18 (4):485–488, 2000.

[166] K. D. Singh, G. R. Barnes, A. Hillebrand, E. M. Forde, and A. L. Williams. Task-related changes in cortical synchronization are spatially coincident with the hemodynamic response. *NeuroImage*, 16(1):103–114, 2002.

[167] K. D. Singh, I. E. Holliday, P. L. Furlong, and G. F. Harding. Evaluation of MRI-MEG/EEG co-registration strategies using Monte Carlo simulation. *Electroencephalogr Clin Neurophysiol*, 102(2):81–85, 1997.

[168] M. Singh, S. Kim, and T. S. Kim. Correlation between BOLD-fMRI and EEG signal changes in response to visual stimulus frequency in humans. *Magn Reson Med*, 49(1):108–114, 2003.

[169] D. A. Soltysik, K. K. Peck, K. D. White, B. Crosson, and R. W. Briggs. Comparison of hemodynamic response nonlinearity across primary cortical areas. *NeuroImage*, 22(3):1117–1127, 2004.

[170] M. Sommer, J. Meinhardt, and H. P. Volz. Combined measurement of event-related potentials (ERPs) and fMRI. *Acta Neurobiol Exp (Wars)*, 63(1):49–53, 2003.

[171] G. Srivastava, S. Crottaz-Herbette, K. Lau, G. Glover, and V. Menon. ICA-based procedures for removing ballistocardiogram artifacts from EEG data acquired in the MRI scanner. *Neuroimage*, 24(1):50–60, 2005.

[172] B. Stefanovic, J. M. Warnking, and G. B. Pike. Hemodynamic and metabolic responses to neuronal inhibition. *NeuroImage*, 22(2):771–778, 2004.

[173] A. C. Tang and B. A. Pearlmutter. Independent components of magnetoencephalography: Localization and single-trial response onset detection. In Z.-L. Lu and L. Kaufman, editors, *Magnetic Source Imaging of the Human Brain*, pages 159–201. Lawrence Erlbaum Associates, Apr. 2003. ISBN 0-8058-4511-9.

[174] A. C. Tang, B. A. Pearlmutter, M. Zibulevsky, and S. A. Carter. Blind separation of multichannel neuromagnetic responses. *Neurocomputing*, 32–33:1115–1120, 2000.

[175] A. C. Tang, B. A. Pearlmutter, M. Zibulevsky, T. A. Hely, and M. P. Weisend. An MEG study of response latency and variability in the human visual system during a visual-motor integration task. In *Advances in Neural Info Proc Sys 12*, pages 185–191. MIT Press, 2000.

[176] V. L. Towle, J. Bolanos, D. Suarez, K. Tan, R. Grzeszczuk, D. N. Levin, R. Cakmur, S. A. Frank, and J. P. Spire. The spatial location of EEG electrodes: locating the best-fitting sphere relative to cortical anatomy. *Electroencephalogr Clin Neurophysiol*, 86(1):1–6, 1993.

[177] N. J. Trujillo-Barreto, E. Aubert-Vazquez, and P. A. Valdes-Sosa. Bayesian model averaging in EEG/MEG imaging. *NeuroImage*, 21(4):1300–1319, 2004.

[178] N. J. Trujillo-Barreto, E. Martínez-Montes, L. Melie-García, and P. A. Valdés-Sosa. A symmetrical bayesian model for fMRI and EEG/MEG Neuroimage fusion. *Int J of Bioelectromag*, 3(1), 2001. URL http://www.ijbem.org/volume3/number1/valdesosa/.

[179] D. S. Tuch, V. J. Wedeen, A. M. Dale, J. George, and J. W. Belliveau. Conductivity tensor mapping of the human brain using diffusion tensor MRI. *Proc Natl Acad Sci U S A*, 98(20):11697–11701, 2001.

[180] D. Van Essen. Surface reconstruction by filtering and intensity transformations, 2004. URL http://brainvis.wustl.edu/.

[181] B. D. Van Veen, W. van Drongelen, M. Yuchtman, and A. Suzuki. Localization of brain electrical activity via linearly constrained minimum variance spatial filtering. *IEEE Trans Biomed Eng*, 44 (9):867–880, 1997.

[182] S. Vanhatalo, P. Tallgren, C. Becker, M. D. Holmes, J. W. Miller, K. Kaila, and J. Voipio. Scalp-recorded slow EEG responses generated in response to hemodynamic changes in the human brain. *Clin Neurophysiol*, 114(9):1744–1754, 2003.

[183] S. Vanni, J. Warnking, M. Dojat, C. Delon-Martin, J. Bullier, and C. Segebarth. Sequence of pattern onset responses in the human visual areas: an fMRI constrained VEP source analysis. *NeuroImage*, 21(3):801–817, 2004.

[184] R. Vigário, J. Särelä, V. Jousmäki, M. Hämäläinen, and E. Oja. Independent component approach to the analysis of EEG and MEG recordings. *IEEE Trans Biomed Eng*, 47(5):589–593, 2000.

[185] D. Vitacco, D. Brandeis, R. Pascual-Marqui, and E. Martin. Correspondence of event-related potential tomography and functional magnetic resonance imaging during language processing. *Hum Brain Mapp*, 17(1):4–12, 2002.

[186] J. Vrba and S. E. Robinson. Differences between Synthetic Aperture Magnetometry (SAM) and linear beamformers. In J. Nenonen, R. Ilmoniemi, and T. Katila, editors, *12th Int Conf Biomagnet*, 12th International Conference on Biomagnetism, Helsinki, Finland, Aug. 2000. Biomag2000. ISBN 951-22-5402-6.

[187] J. Vrba and S. E. Robinson. Signal processing in magnetoencephalography. *Methods*, 25(2):249–271, 2001.

[188] M. Wagner and M. Fuchs. Integration of functional MRI, structural MRI, EEG, and MEG. *Int J of Bioelectromag*, 3(1), 2001. URL http://www.ijbem.org/volume3/number1/wagner/index.htm.

[189] A. Waites, M. Shaw, R. Briellmann, A. Labate, D. Abbott, and G. Jackson. How reliable are fMRI-EEG studies of epilepsy? A nonparametric approach to analysis validation and optimization. *Neuroimage*, 24(1):192–199, 2005.

[190] J. Z. Wang, S. J. Williamson, and L. Kaufman. Magnetic source images determined by a lead-field analysis: the unique minimum-norm least-squares estimation. *IEEE Trans Biomed Eng*, 39(7): 665–675, 1992.

[191] S. Warach, J. R. Ives, G. Schlaug, M. R. Patel, D. G. Darby, V. Thangaraj, R. R. Edelman, and D. L. Schomer. EEG-triggered echo-planar functional MRI in epilepsy. *Neurology*, 47(1):89–93, 1996.

[192] D. Weber. EEG and MRI Matlab toolbox, 2004. URL http://eeg.sourceforge.net/.

[193] H. J. Wieringa, M. J. Peters, and F. Lopes da Silva. The estimation of a realistic localization of dipole layers within the brain based on functional (EEG, MEG) and structural (MRI) data: a preliminary note. *Brain Topogr*, 5(4):327–330, 1993.

[194] J. P. Wikswo, Jr, A. Gevins, and S. J. Williamson. The future of the EEG and MEG. *Electroencephalogr Clin Neurophysiol*, 87(1):1–9, 1993.

[195] C. H. Wolters, A. Anwander, M. A. Koch, S. Reitzinger, M. Kuhn, and M. Svensén. Influence of head tissue conductivity anisotropy on human EEG and meg using fast high resolution finite element modeling, based on a parallel algebraic multigrid solver. In T. Plesser and P. Wittenburg, editors, *Forschung und wissenschaftliches Rechnen*, pages 111–157. Max-Planck-Gesselschaft, München, 2001. URL http://www.billingpreis.mpg.de/hbp01/wolters.pdf.

[196] J. Xiong, P. T. Fox, and J. H. Gao. Directly mapping magnetic field effects of neuronal activity by magnetic resonance imaging. *Hum Brain Mapp*, 20(1):41–49, 2003.

[197] I. Yousry, T. Naidich, and T. Yousry. Functional magnetic resonance imaging: factors modulating the cortical activation pattern of the motor system. *Neuroimaging Clin N Am*, 11(2):195–202, viii, 2001.

[198] T. Yousry, U. Schmid, H. Alkadhi, D. Schmidt, A. Peraud, A. Buettner, and P. Winkler. Localization of the motor hand area to a knob on the precentral gyrus. A new landmark. *Brain*, 120 (Pt 1): 141–57, 1997.

[199] Z. Zhang. A fast method to compute surface potentials generated by dipoles within multilayer anisotropic spheres. *Phys Med Biol*, 40:335–349, May 1995.